UPPSALA
UNIVERSITET

Digital Comprehensive Summaries of Uppsala Dissertations from the Faculty of Science and Technology 393

A Treatise on the Geometric and Electronic Structure of Clusters

Investigated by Synchrotron Radiation Based Electron Spectroscopies

ANDREAS LINDBLAD

ACTA
UNIVERSITATIS
UPSALIENSIS
UPPSALA
2008

ISSN 1651-6214
ISBN 978-91-554-7095-1
urn:nbn:se:uu:diva-8463

Dissertation presented at Uppsala University to be publicly examined in Häggsalen, Ångströmlaboratoriet, Lägerhyddsvägen 1, Uppsala, Friday, March 14, 2008 at 10:15 for the degree of Doctor of Philosophy. The examination will be conducted in English.

Abstract
Lindblad, A. 2008. A Treatise on the Geometric and Electronic Structure of Clusters. Investigated by Synchrotron Radiation Based Electron Spectroscopies. Acta Universitatis Upsaliensis. *Digital Comprehensive Summaries of Uppsala Dissertations from the Faculty of Science and Technology* 393. 103 pp. Uppsala. ISBN 978-91-554-7095-1.

Clusters are finite ensembles of atoms or molecules with sizes in the nanometer regime (*i.e.* nanoparticles). This thesis present results on the geometric and electronic structure of homogeneous and heterogeneous combinations of atoms and molecules. The systems have been studied with synchrotron radiation and valence, core and Auger electron spectroscopic techniques.

The first theme of the thesis is that of mixed clusters. It is shown that by varying the cluster production technique both structures that are close to that predicted by equilibrium considerations can be attained as well as far from equilibrium structures.

Electronic processes following ionization constitute the second theme. The post-collision interaction phenomenon, energy exchange between the photo- and the Auger electrons, is shown to be different in clusters of argon, krypton and xenon. A model is proposed that takes polarization screening in the final state into account. This result is of general character and should be applicable to the analysis of core level photoelectron and Auger electron spectra of insulating and semi-conducting bulk materials as well.

Interatomic Coloumbic Decay is a process that can occur in the condensed phases of weakly bonded systems. Results on the time-scale of the process in Ne clusters and mixed Ar/Ne clusters are herein discussed, as well observations of resonant contributions to the process. In analogy to Auger *vis-à-vis* Resonant Auger it is found that to the ICD process there is a corresponding Resonant ICD process possible. This has later been observed in other systems and by theoretical calculations as well in subsequent works by other groups.

Delocalization of dicationic valence final states in the hydrogen bonded ammonia clusters and aqueous ammonia has also been investigated by Auger electron spectroscopy. With those results it was possible to assign a previously observed feature in the Auger electron spectrum of solid ammonia.

Keywords: Cluster, nanoparticle, Heterogeneous, Homogeneous, Mixed, Cluster production methods, co-expansion, pick-up, doping, Cluster geometry, radial segregation, Interatomic Coulombic Decay, ICD, Auger electron spectroscopy, AES, X-ray photoelectron spectroscopy, XPS, Ultra-violet spectroscopy, UPS, Noble gas, Rare gas, Ne, Ar, Kr, Xe, Ammonia, NH3, Sulphur hexafluoride, SF6, MAX-lab, BESSY

Andreas Lindblad, Department of Physics and Materials Science, Ångströmlaboratoriet, Lägerhyddsv. 1, Box 530, Uppsala University, SE-75121 Uppsala, Sweden

ISSN 1651-6214
ISBN 978-91-554-7095-1
urn:nbn:se:uu:diva-8463 (http://urn.kb.se/resolve?urn=urn:nbn:se:uu:diva-8463)

”Allting kan man. . . lära sig – utom ett:

Att sätta sig bredvid sig själv.

Det kan endast en *rutinerad dubbelgångare* göra, och som du aldrig blir det, förbiser jag grannlaga denna din ofullkomlighet, då jag nu, beskedliga läsare, sticker denna lyckotermometer i din av glädje bävande näve.”

Lyckans lexikon – eller mannen och kvinnan.
En kort belysning av allting.

Falstaff, fakir (1895)

Till Mina Syskon.

List of Papers

This thesis is based on the following papers, which are referred to in the text by their Roman numerals.

Main bibliography for this thesis

I **Postcollision interaction in noble gas clusters: Observation of differences in surface and bulk line shapes.**
A. Lindblad, R. F. Fink, H. Bergersen, M. Lundwall, T. Rander, R. Feifel, G. Öhrwall, M. Tchaplyguine, U. Hergenhahn, S. Svensson, and O. Björneholm.
Journal of Chemical Physics, **123** (21): 211101, 2005.

II **Radial surface segregation in free heterogeneous argon/krypton clusters.**
M. Lundwall, M. Tchaplyguine, G. Öhrwall, R. Feifel, A. Lindblad, A. Lindgren, S. Sorensen, S. Svensson, and O. Björneholm.
Chemical Physics Letters, **392** (4-6): 433–438, 2004.

III **Chemical shifts of small heterogeneous Ar/Xe clusters**
A. Lindblad, T. Rander, M. Mucke, V. Ulrich, T. Lischke, I. Bradenau, G. Öhrwall, U. Hergenhahn, O. Björneholm
in manuscript

IV **Self-assembled heterogeneous argon/neon core-shell clusters studied by photoelectron spectroscopy.**
M. Lundwall, W. Pokapanich, H. Bergersen, A. Lindblad, T. Rander, G. Öhrwall, M. Tchaplyguine, S. Barth, U. Hergenhahn, S. Svensson, and O. Björneholm.
Journal of Chemical Physics, **126** (21): 214706, 2007.

V **The geometric structure of pure SF_6 and mixed Ar/SF_6 clusters investigated by core level photoelectron spectroscopy**
A. Lindblad, M. Winkler, *et al.*
in manuscript

VI **The far from equilibrium structure of argon clusters doped with krypton or xenon.**
A. Lindblad, H. Bergersen, T. Rander, M. Lundwall, G. Öhrwall, M. Tchaplyguine, S. Svensson, and O. Björneholm.
Physical Chemistry Chemical Physics, **8** (16): 1899–1905, 2006.

VII **Preferential site occupancy of krypton atoms on free argon-cluster surfaces.**
M. Lundwall, A. Lindblad, H. Bergersen, T. Rander, G. Öhrwall, M. Tchaplyguine, S. Svensson, and O. Björneholm.
Journal of Chemical Physics, **125** (1): 014305, 2006.

VIII **The diffusion behavior of O_2 doped on large Ar clusters**
T. Rander, A. Lindblad, M. Lundwall, M. Tchaplyguine G. Öhrwall, S. Svensson, O. Björneholm
submitted

IX **Femtosecond interatomic coulombic decay in free neon clusters: Large lifetime differences between surface and bulk.**
G. Öhrwall, M. Tchaplyguine, M. Lundwall, R. Feifel, H. Bergersen, T. Rander, A. Lindblad, J. Schulz, S. Peredkov, S. Barth, S. Marburger, U. Hergenhahn, S. Svensson, and O. Björneholm.
Physical Review Letters, 93 (17): 173401, 2004.

X **Observation of resonant interatomic coulombic decay in Ne clusters.**
S. Barth, S. Joshi, S. Marburger, V. Ulrich, A. Lindblad, G. Öhrwall, O. Björneholm, and U. Hergenhahn.
The Journal of Chemical Physics, 122 (24): 241102, 2005.

XI **Charge delocalization dynamics of ammonia in different hydrogen bonding environments: free clusters and in liquid water solution**
A. Lindblad, H. Bergersen, T. Rander, W. Pokapanich, M. Tchaplyguine, G. Öhrwall and O. Björneholm
in manuscript

Reprints were made with permission from the publishers.

The following is a list of publications to which I have contributed to. They will not be covered in this thesis.
Extended bibliography

1. **First observation of vibrations in core-level photoelectron spectra of free neutral molecular clusters.**
   H. Bergersen, M. Abu-Samha, A. Lindblad, R. R. T. Marinho, D. Ceolin, G. Öhrwall, L. J. Sæthre, M. Tchaplyguine, K. J. Børve, S. Svensson, and O. Björneholm.
   Chemical Physics Letters, **429** (1-3): 109–113, 2006.

2. **Two size regimes of methanol clusters produced by adiabatic expansion.**
   H. Bergersen, M. Abu-Samha, A. Lindblad, R. R. T. Marinho, G. Öhrwall, M. Tchaplyguine, K. J. Børve, S. Svensson, and O. Björneholm.
   Journal of Chemical Physics, **125** (18): 5, 2006.

3. **A photoelectron spectroscopic study of aqueous tetrabutylammonium iodide.**
   H. Bergersen, R. R. T. Marinho, W. Pokapanich, A. Lindblad, O. Björneholm, L. J. Sæthre, and G. Öhrwall.
   Journal of Physics: Condensed Matter, **19** (32): 326101 (9pp), 2007.

4. **Enhanced surface sensitivity in AES relative to XPS observed in free argon clusters.**
   M. Lundwall, M. Tchaplyguine, G. Öhrwall, A. Lindblad, S. Peredkov, T. Rander, S. Svensson, and O. Björneholm.
   Surface Science, **594** (1-3): 12–19, 2005.

5. **Preferential site occupancy observed in coexpanded argon-krypton clusters.**
   M. Lundwall, H. Bergersen, A. Lindblad, G. Öhrwall, M. Tchaplyguine, S. Svensson, and O. Björneholm.
   Physical Review A, **74** (4): 7, 2006.

6. **Shell-dependent core-level chemical shifts observed in free xenon clusters.**
   M. Lundwall, R. F. Fink, M. Tchaplyguine, A. Lindblad, G. Öhrwall, H. Bergersen, S. Peredkov, T. Rander, S. Svensson, and O. Björneholm.
   Journal of Physics B-Atomic Molecular and Optical Physics, **39** (24): 5225–5235, 2006.

7. **Photon energy dependent intensity variations observed in Auger spectra of free argon clusters.**
M. Lundwall, A. Lindblad, H. Bergersen, T. Rander, G. Öhrwall, M. Tchaplyguine, S. Peredkov, S. Svensson, and O. Björneholm.
Journal of Physics B: Atomic Molecular and Optical Physics, **39** (16): 3321–3333, 2006.

8. **The electronic structure of free water clusters probed by Auger electron spectroscopy.**
G. Öhrwall, R. F. Fink, M. Tchaplyguine, L. Ojamae, M. Lundwall, R. R. T. Marinho, A. N. de Brito, S. L. Sorensen, M. Gisselbrecht, R. Feifel, T. Rander, A. Lindblad, J. Schulz, L. J. Sæthre, N. Mårtensson, S. Svensson, and O. Björneholm.
Journal of Chemical Physics, **123** (5): 10, 2005.

9. **Ioniclike energy structure of neutral core-excited states in free Kr clusters.**
S. Peredkov, A. Kivimaki, S. L. Sorensen, J. Schulz, N. Mårtensson, G. Öhrwall, M. Lundwall, T. Rander, A. Lindblad, H. Bergersen, S. Svensson, O. Björneholm, and M. Tchaplyguine.
Physical Review A, **72** (2): 4, 2005.

10. **Size determination of free metal clusters by core-level photoemission from different initial charge states.**
S. Peredkov, S. L. Sorensen, A. Rosso, G. Öhrwall, M. Lundwall, T. Rander, A. Lindblad, H. Bergersen, W. Pokapanich, S. Svensson, O. Björneholm, N. Mårtensson, and M. Tchaplyguine.
Physical Review B, **76** (8): 4, 2007.

11. **Experimental evidence for molecular ultrafast dissociation in O_2 clusters.**
T. Rander, M. Lundwall, A. Lindblad, G. Öhrwall, M. Tchaplyguine, S. Svensson, and O. Björneholm.
European Physical Journal D, **42** (2): 253–257, 2007.

12. **Synchrotron radiation study of chloromethane clusters: Effects of polarizability and dipole moment on core level chemical shifts.**
A. Rosso, A. Lindblad, M. Lundwall, T. Rander, S. Svensson, M. Tchaplyguine, G. Öhrwall, and O. Björneholm.
Journal of Chemical Physics, **127** (2): 5, 2007.

13. **The role of molecular polarity in cluster local structure studied by photoelectron spectroscopy.**
A. Rosso, T. Rander, H. Bergersen, A. Lindblad, M. Lundwall, S. Svensson, M. Tchaplyguine, G. Öhrwall, L. J. Sæthre, and O. Björneholm.
Chemical Physics Letters, **435** (1-3): 79–83, 2007.

14. **Final state selection in the 4p photoemission of Rb by combining laser spectroscopy with soft-x-ray photoionization.**
J. Schulz, M. Tchaplyguine, T. Rander, H. Bergersen, A. Lindblad, G. Öhrwall, S. Svensson, S. Heinasmaki, R. Sankari, S. Osmekhin, S. Aksela, and H. Aksela.
Physical Review A, **72** (3): 4, 2005.

15. **Magnetron-based source of neutral metal vapors for photoelectron spectroscopy.**
M. Tchaplyguine, S. Peredkov, H. Svensson, J. Schulz, G. Öhrwall, M. Lundwall, T. Rander, A. Lindblad, H. Bergersen, S. Svensson, M. Gisselbrecht, S. L. Sorensen, L. Gridneva, N. Mårtensson, and O. Björneholm.
Review of Scientific Instruments, **77** (3): 6, 2006.

16. **Localized versus delocalized excitations just above the 3d threshold in krypton clusters studied by Auger electron spectroscopy.**
M. Tchaplyguine, A. Kivimäki, S. Peredkov, S. L. Sorensen, G. Öhrwall, J. Schulz, M. Lundwall, T. Rander, A. Lindblad, A. Rosso, S. Svensson, N. Mårtensson, and O. Björneholm.
Journal of Chemical Physics, **127** (12): 8, 2007.

17. **Direct observation of the non-supported metal nanoparticle electron density of states by x-ray photoelectron spectroscopy.**
M. Tchaplyguine, S. Peredkov, A. Rosso, J. Schulz, G. Öhrwall, M. Lundwall, T. Rander, A. Lindblad, H. Bergersen, W. Pokapanich, S. Svensson, S. L. Sorensen, N. Mårtensson, and O. Björneholm.
European Physical Journal D, **45** (2): 295–299, 2007.

Preface

Caveat lector

Physics has great aspirations – it is the science that aims to model and understand the universe surrounding us, from the smallest thing conceivable, to the largest of dynamical processes on the smallest, to the largest time-scales[1].

This thesis considers *clusters* of atoms or molecules – objects that have sizes in the nanometer range (*i.e.* the typical length scale is 1 billionth of a meter) and a limited number of particles. The two main discernible themes of the thesis are the geometric structure of mixed clusters and electronic decay phenomena that can occur after photoionization (of pure and mixed clusters). The studied electronic decay processes occurs at a femtosecond time-scale (1 millionth of a billionth of a second). Though the scope may seem somewhat limited with respect to physics as a whole, the subject of cluster physics is interesting in both the fundamental properties of the systems and the potential applications; clusters bridge the gap between isolated particles and the condensed state.

Curiosity and the strife for ever increasing knowledge about the world have driven the field of physics since the first cave-person *(sic!)* looked at the stars and wondered about them. On that note I humbly find the fundamental physics of clusters as a good enough motivation to study them. That is not to say that applications of cluster physics are uninteresting – far from it; electronic components constructed from clusters could, for instance, allow computers to run faster; heterogeneous catalysis aided by metal nano-particles can make our environment cleaner – by converting substances destroying the environment to harmless ones or by decreasing the energy consumption of chemical processes.

A thesis is by necessity limited, and thus a compromise between brevity and completeness. The text should, however, give a reasonably complete introduction to the publications and manuscripts mentioned in the main bibliography (p. 5, *et seq.*) – with the cited references certainly doing

[1] The smallest length that can be constructed from fundamental physical constants is the Planck length which has an order of magnitude of 10^{-35} m. The radius of the observable universe is estimated to be in the order of 10^{26} m. Thus physics studies objects on size scales that covers 61 orders of magnitude. Analogously, the time-scales can be said to cover roughly 62 orders of magnitude.

so. As common references of more general character, on subjects stated, the books by Landau and Lifshitz [1] (thermodynamics and statistical physics), Messiah [2] and Sakurai [3] (quantum mechanics), Jackson [4] (classical electrodynamics), Haberland [5], Johnston [6] (cluster physics) are warmly recommended. If no citation to a publication is explicitly given in the text for, *e.g.* a formula it can almost certainly be found in one of those books.

Comments on my own participation

Teamwork is the *sine qua non* of modern experimental physics; common to all the papers presented in this thesis is that the experimental work was a cooperative effort – partly by members of the Surface physics group of the Physics department at Uppsala University and in part by people from other Universities/Institutes. Notably, in the latter category, our cooperation with the group of Uwe Hergenhahn (at the Max-Planck institut für Plasmaphysik) should be mentioned.

For the papers presented in the main bibliography denoted with Roman numerals. I took active part also in the analysis of the experimental data and to some extent helped out with the manuscript preparation. For Papers **I**, **III**, **V**, **VI**, **XI** I was the "man with the plan" for the experimental work and analysis of the data; I was also the responsible person for authoring/editing the manuscripts.

The extended bibliography (given Hindu-Arabic numerals, p. 7 and forward) is an incomplete list of publications to which I have contributed to in some sense. I feel though that my contributions to those have been much more modest, and others should be given the opportunity to discuss them; therefore I do not detail those papers in this thesis.

Contents

1. Inledning

"...på de bronsstatyer som står vid städernas portar
är ofta högra handen blank och nött av de många
som haft väg förbi och vidrört den eller kysst den.
Att de förminskas av nötningen, dessa föremål, ser vi,
men hur partiklarna flyr utan avbrott och överger tingen,
det har en ogin natur ej unnat vår syn att bli varse."

Titus Lucretius Carus, *De Rerum Natura*

Så beskriver den romerske poeten Lucretius (ca. 90-50 f. kr.) de atomer som han ansåg att allt var uppbyggt av. Att sådana är mycket små hade han förvisso rätt i – det får plats en miljard stycken på 10 centimeter om man lägger ut dem på en rad.

Hans atombegrepp var dock detsamma som de gamla grekernas: att det var alltings minsta odelbara (och oförstörbara) beståndsdelar. Att han tidvis var galen p.g.a. att han i sin ungdom druckit en kärleksbrygd var dock troligtvis inte anledningen till hans något omoderna atommodell. Först i början på 1900-talet framlades den modell av atomen som kunde förklara till exempel uppkomsten av absorptionslinjer som finns i ljuset från solen.

Denna avhandling handlar om *kluster* bestående av ett *uppräkneligt* antal atomer[1], vilket sålunda innebär att de har en begränsad storlek. Sagda storlek är en eller ett par storleksordningar större än de enskilda atomerna. Just tack vare detta har kluster speciella egenskaper. Dessa skiljer sig från både enstaka atomers egenskaper och från ämnen i fast tillstånd (som kan anses ha ett oändligt antal atomer och sakna yta). Den stora andelen atomer som sitter på ytan är en av de stora anledningarna som finns att studera sådana system och även en av de stora möjligheterna för tekniska tillämpningar.

T.ex. kan kemiska reaktioner möjliggöras på en yta även om de är mycket ovanliga (eller t.o.m. omöjliga) när atomerna och/eller molekylerna är i gas eller vätskefas. Guld reagerar vanligtvis inte med några andra ämnen. Det har dock visat sig att kluster med 20 guldatomer kan

[1] Eller lika gärna molekyler. För enkelheten skull kommer ordet 'atom' användas på ett sådant sätt i fortsättningen av detta kapitel att det kan bytas ut mot 'molekyl' annat än där det framgår explicit att så inte är fallet.

reagera med giftiga kolmonoxidmolekyler och bilda om dem till koldioxidmolekyler[2].

För att datorer skall kunna bli snabbare – av rent hårdvarumässiga skäl – så måste avståndet mellan kretsarna i processorerna krympa och även bli fler. Redan, i skrivande stund, så har många processortillverkare frångått användandet av kiseloxid som isolerande material i processorerna. Detta eftersom komponenterna nu blivit så små att effekter, som tidigare gått att ignorera, blivit så stora att nya isolerande material har varit tvungna att användas för att kunna driva utvecklingen framåt.

I ett längre perspektiv ställs stort hopp till material och elektroniska komponenter uppbyggda av endast ett fåtal atomer där egenskaperna kan finjusteras med hjälp av antalet atomer i de kluster som är byggstenarna. T.ex. så har kluster skyddade av ett lager med organiska molekyler visats kunna laddas upp med enstaka elektroner, något som motsvarar en kondensator med en kapacitans som är mindre än 1 attofarad[3].

Om allt detta varit enkelt att genomföra hade det redan varit gjort. Emellertid är klusterfysik fortfarande ett relativt ungt forskningsfält. Därför finns det mycket saker kvar att studera, även på en grundläggande nivå. Även om metallpartiklar i nanometerstorlek använts för att färga glas i hundratals år, är det först i våra dagar som det finns experimentella tekniker och teoretiska modeller som lämpar sig för att studera och förklara många av de fenomen som är specifika för kluster. Alltså finns det flera goda anledningar att studera enkla system (som kluster av ädelgasatomer) som modellsystem för mer komplexa system. Dels för att bygga upp grundläggande kunskaper om kluster, och dels för att det då går att skilja ut vad som är egenskaper som är av allmän karaktär och vad som är specifikt för enskilda system.

För att överhuvudtaget studera kluster måste vi ha några att studera. Ett av problemen associerat med (rena) kluster är att de smälter ihop när de kommer i kontakt med varandra. För att förstå varför, låt oss titta på en vätskedroppe och för enkelhets skull så kan vi betrakta den som en sfär. För resonemanget som följer är detta ingen begränsning.

Energin för en sådan droppes yta kan skrivas $E = \sigma 4\pi R^2$, där ytspänningen σ och sfärens area $4\pi R^2$ har använts (den senare given av radien R). Låt oss nu dela droppen i n stycken delar. Eftersom den totala volymen ($\frac{4}{3}\pi R^3$) rimligen bevaras kan vi skriva:

$$\left(\frac{4}{3}\pi R^3\right) = V = n\frac{4}{3}\pi r^3$$

Alltså har vi nu n stycken droppar med radien $r = \frac{R}{\sqrt[3]{n}}$.

[2] B. Woon *et al.*, "Charging Effects on Bonding and Catalyzed Oxidation of CO on Au_8 Clusters on MgO", Science 21 (2005), Vol. 307. no. 5708, pp. 403 – 407.
[3] A. C. Templeton *et al.*, Acc. Chem. Res. (2000), 33, 27–36

Den totala energin som krävs för att upprätthålla den nu mycket större ytarean hos de n stycken smådropparna kan jämföras med energin hos den ursprungliga droppen. Detta gör vi genom att ta skillnaden mellan smådropparnas energi och den större:

$$E_{\text{små}} - E_{\text{stor}} = n\sigma 4\pi \left(\frac{R}{\sqrt[3]{n}}\right)^2 - \sigma(4\pi R^2) = \left(\sqrt[3]{n} - 1\right)\sigma 4\pi R^2$$

De små dropparna har alltså en högre potentiell energi än vad den stora droppen har. Detta leder till att när sådana små droppar kommer i kontakt med varandra så kan de minska sin energi genom att slås ihop. Givetvis är just detta faktum ett problem när man vill tillverka saker genom att sätta ihop dem av kluster. Ett sätt att göra detta är att förhindra att de kommer i kontakt med varandra överhuvudtaget genom att binda molekyler till ytan som förhindrar att klusterdelarna av partiklarna kommer i kontakt med varandra.

För att utföra våra experiment så tillverkar vi klustren med hjälp av en klusterkälla där gaser kondenseras till kluster. Till och med gaser som neon, som har en smältpunkt vid -248.5 °C går att kondensera till kluster. För att åstadkomma sådana temperaturer utnyttjas, i klusterkällan, en princip som kallas *adiabatisk expansion*.

I en adiabatisk expansion, där inget utbyte av värme med omgivningen sker, går det att räkna ut sluttemperaturen om man vet initialtemperaturen och trycken i start och sluttillstånden för processen. För exempelvis en champagne-flaska är övertrycket ca. 5 atmosfärer. När korken är öppnad är trycket 1 atmosfär. Enligt Winston Churchill skall champagne vara ”Torr, kall och gratis” – så vi sätter temperaturen till 7 °C (280 Kelvin). Genom att utföra det mycket enkla experimentet att öppna flaskan ändras temperaturen enligt:

$$T_2 = T_1 \left(\frac{p_1}{p_2}\right)^{(1-\gamma)/\gamma}$$

där γ är kvoten mellan värmekapaciteterna för konstant tryck respektive konstant temperatur för luft ($\gamma \approx 1.4$). Uttrycket ovan ger en temperatursänkning med ungefär -100 grader Celcius. Detta förklarar hur det kan bli så kallt att små vattenkristaller bildas när flaskan öppnas. Naturligtvis blir det bara så kallt lokalt i flaskans öppning under en kort tid, annars skulle det exempelvis vara nödvändigt att ha vantar även inomhus på nyårsafton.

I klusterkällan så expanderas en gas adiabatiskt genom ett hål med en trattliknande öppning med ett konstant högt tryck bakom hålet in i vakuum – tryckskillnaden är således mycket större än i vårt champagneexempel ovan. Ofta så kyls även munstycket ned (med flytande kväve) vilket gör att mycket låga temperaturer kan åstadkommas.

Det som bestämmer vilka ämnen som det går göra kluster av är vilket tryck och vilken temperatur som kan användas. Andelen atomer i den lilla volym där klusterbildning faktiskt sker måste vara tillräckligt stor för att klustren skall komma över den kritiska storlek som gör att de kan överleva tillräckligt länge.

Vi kan ta till champagnen (något man ju enligt Lilly Bollinger kan göra lite närsomhelst) för att försöka förstå varför en sådan kritisk storlek finns. Då man häller upp champagnen i glas så uppstår det bubblor lite varstans i glaset. Bubblorna uppstår genom att tillräckligt många koldioxidmolekyler ansamlas på samma ställe för att kunna trycka undan tillräckligt mycket vätska för att det skall uppstå en gas-vätske yta inuti vätskan. För att en sådan bubbla skall överleva finns det ett minsta tryck som gasen måste utöva på bubblans väggar för att stå emot trycket från den omgivande vätskan och upprätthålla ytan emot den. Detta minsta tryck är $2\sigma/R$ (och fås ur Young-Laplace ekvationen). Är trycket större än så expanderar bubblan även om den håller sig på samma djup.

Tyvärr verkar denna ekvation omöjliggöra att bubblor bildas överhuvudtaget. Väldigt små bubblor skulle behöva ett extremt högt tryck för att kunna bildas. I ett champagneglas så är det de små defekterna i glaset som bryter vätskans symmetri och därmed tillåter att bubblor bildas[4].

Om vi tar en av våra ytterst små droppar, som vi gjorde genom att dela den stora droppen i inledningen, så gäller samma relation för tryckspråget över ytan. Det nya i situationen är att gasen nu är utanför vätskan. Finns det en yta mellan en vätska och en gas så finns det alltid en mängd molekyler i vätskan som har tillräckligt med energi för att gå från vätskan till gasen. Det tryck, då denna process har samma hastighet som motsvarande process har då molekyler kondenserar från gas till luft, kallas för ämnets ångtryck (vid den temperaturen)[5].

En liten droppe får alltså ett högre gastryck över ytan än en större – förs denna gas bort blir droppen mindre och mindre för att slutligen försvinnna. Dock är avdunstning en kylande process (eftersom varje partikel som lämnar droppen tar med sig energi i form av rörelseenergi) och om droppen hinner kristalliseras så sjunker ångtrycket markant.

[4] Vill du testa detta är det bara att öka antalet defekter i glaset, detta genom att t.ex. diska dåligt (vilket dock är dåligt för din champagne) eller genom att tillsätta några korn salt i t.ex. någon snåljåps mousserande på valborg. Medan personen tvättar av sig (och du spelar oskyldig) kan du passa på att charma din omgivning genom att lärt tala om bubbelbildning och symmetribrott. Det är inte nödvändigt att ange mig som källa.

[5] Är du rädd om bubblorna i din champagne skall du kyla den (ångtrycket för koldioxiden minskar med temperaturen). Vill du spara den över natten (t. ex. efter en provsmakning eller efter en mindre supé) kan du spara fler bubblor till din champagnefrukost genom att sticka ner skaftet på en tesked i flaskhalsen (eller ännu bättre en ihoprullad linneservett) – detta hindrar luftströmmar från att föra bort koldioxiden och därmed rubba jämvikten vilket gör att mer koldioxid kan lösgöra sig från vätskan.

Alltså måste gasdensiteten vara mycket hög i klusterkällans munstycke, där kondensationen sker, för att det ska bildas kluster som är tillräckligt stora för att de skall kunna kristalliseras. Det går även att tillsätta en extra gas i expansionen för att klusterbildningen skall bli mer effektiv.

En stor del av de arbeten som utgör basen för avhandlingen du just nu läser handlar om blandade kluster. Dessa kan produceras antingen genom att två gaser får expandera tillsammans eller genom att först bilda kluster av ett ämne och därefter tillsätta atomer av ett annat ämne på ytan. Dessa arbeten fokuserar främst på att försöka finna ledtrådar till sådana klusters olika strukturer genom att studera *fotoelektronspektra*.

En atom består av negativt laddade elektroner och en positivt laddad kärna (som innehåller positivt laddade protoner och neutrala neutroner). Alltså redan där fjärran från Lucretius syn på saken. Har man lika många elektroner som kärnan har positiva laddningar får man en neutral atom. Att elektronerna är bundna till kärnan via elektrisk växelverkan är lätt att sluta sig till, men vad det är som gör att inte alla elektroner kraschar in i kärnan[6] kräver en helt annan förklaring. I början av denna text noterades det att det dröjde väldigt länge mellan vår poet Lucretius och det att detta fenomen fick en förklaring.

Förklaringen bygger på att partiklar kan uppträda som vågor (mer exakt att de är både och) – och att stående vågor inte förflyttar någon energi. Det senare är t.ex. något som händer för vågor på en gitarrsträng. Om avståndet d mellan punkterna där vågen är utbredd är en jämn multipel av våglängden λ, $d = n\lambda$ för $n = 1, 2, 3, \ldots$ så förflyttar sig inte vågens noder längs strängen.

Lois de Broglie visade i början av 1920-talet att partiklar även kunde uppträda som vågor med en viss våglängd. Detta kombinerat med Niels Bohrs atommodell, där elektronerna rör sig i cirkulära banor kring atomkärnan, ger att de radier kring kärnan där elektroner kan befinna sig utan att accelereras mot kärnan blir $n\lambda = 2\pi r$ (det senare är helt enkelt banans längd). Varje sådant avstånd motsvarar en viss bindingsenergi för elektronerna. Viktigt är att dessa energier är diskreta, alltså har ett distinkt antal som är separerade från varandra.

Den *fotoelektriska effekten* kan förklaras utifrån dessa bindingsenergier. För att lösgöra en elektron från en atom med hjälp av en foton så krävs det en viss *energi* hos fotonen (intensiteten hos ljuset spelar ingen

[6] En elektron skulle accelereras in mot den positiva kärnan mycket snabbt. Inte ens en cirkulär bana *á la* månen kring jorden skulle rädda den från detta öde eftersom en cirkulär rörelse även den innebär att att en partikel måste acellereras in emot centrum (annars skulle den fortsätta rakt fram och inte böja av hela tiden). En laddning som ändrar sin rörelse sänder ut elektromagnetiska vågor – på så vis skulle elektronen hela tiden förlora energi i små portioner och komma allt närmare kärnan.

roll). Elektronen får då en energi som är skillnaden mellan foton-energin och bindingsenergin för elektronen.

Genom att mäta den kinetiska energin för elektroner för en given våglängd kan man alltså få information om bindningsenergierna i systemet. För atomer som är i kontakt med andra atomer innehåller dessa energier även information om den kemiska omgivningen. Upptäckten av att vissa typer av sådana fotoelektronspektra innehåller information om vilken atom som blev joniserad, samt hur dess kemiska omgivning ser ut, resulterade i att Kai Siegbahn belönades med Nobelpriset i fysik 1981.

Med sådana metoder har alltså klusterstrukturerna studerats i denna avhandling (artiklarna **II**–**VIII**). Det går även att studera vad som händer med det joniserade systemet genom att mäta energierna från elektroner som sänds ut för att detta skall göra sig av med överskottsenergin som tillsatts systemet genom fotojonisationen. Dessa elektroner brukar benämnas Augerelektroner. I kluster (och kondenserade material) har det även visat sig att en annan typ av process kan ge upphov till att elektroner sänds ut efter jonisation. Dessa benämns ICD-elektroner (efter Interatomic Coulombic Decay, som diskuteras närmare i kapitel 4). Denna process förutsades och observerades experimentellt relativt nyligen (1997 respektive 2003) och aspekter av denna process har studerats i rena neonkluster i artiklarna **X** och **IX** samt för blandade argon/neon kluster i artikel **IV**.

Då en Augerelektron sänds ut efter det att ett system sänt ut en fotoelektron efter en fotojonisationsprocess kan den ha högre kinetisk energi än fotoelektronen. Då den senares energi bestäms av bindningsenergin och fotonenergin kan fotoelektronens energi därför väljas (i princip) godtyckligt – medan Augerelektronens energi bestäms av energiförhållandet mellan energinivåerna i den enkel och dubbelladdade jonen. Därför finns det möjlighet för dessa båda elektroner att utbyta energi då de lämnat systemet. Denna interaktion ger upphov till effekter i fotoelektron- och Augerelektronspektra (se kapitel 4). Skillnaderna för denna interaktion i kluster kontra fria atomer diskuteras närmare i artikel **I** och kapitel 6.

Denna avhandling tar dock inte upp ett så komplicerat system som champagneexemplet ovan utgör. De studerade systemen är uppbyggda av enstaka partikelslag som kan anes utgöra modellsystem för betydligt mer komplexa diton. Därför har vi kunnat studera hur t.ex. ädelgaser och molekyler skiktar sig när de blandas – en del beter sig som saft andra som olja och vatten. Även processer som leder till att positiva laddningar sprids ut i joniserade system har också gått att studera i dessa isolerade system. Även om detta är intressant i sig så har detta även möjlighet att tillämpas på ett flertal viktiga områden. Exempel på sådana områden är givna i början av denna text samt i slutet av sista kapitlet.

2. Introduction

Imagine a slab of material having a certain set of physical and chemical properties. If one was to divide the piece of material in two, it would still behave very much like the original slab when scrutinized. Repeated sufficiently many times the division would yield free atoms which have properties which are often far from that of the solid of said substance.

In solid state physics a solid is usually considered to be built up from an *infinite* number of particles, so adding or subtracting a single atom does not have an effect on any property in this limit. Also the surface portion is said to be negligible, which is a good approximation when you have an infinite number of bulk atoms.

A finite number of atoms bound to each other constitute a *cluster* of atoms. A cluster have a large number of surface atoms compared to the number of atoms in the bulk – hence surface effects can not be ignored. Moreower, the properties of the cluster vary with size, in contrast to the infinite solid case discussed above. This size depedence can either be smoothly varying in proportion to the particle number or for smaller particle numbers oscillate wildly. Hence there is two "regimes" to talk about: a classical and a quantum regime. For instance, tin clusters consisting of ten atoms are covalently bonded to each other as opposed to bulk tin which have a (weak) metal bond – this give them a higher melting point than bulk tin[7]. Going from very large tin clusters towards smaller the melting point is instead *decreasing* compared to the bulk value following a smooth trend. Experimental melting points for both size regimes are illustrated in Figure 2.1, the larger clusters follow the experimentally determined melting point curve, the size interval for the small clusters is also indicated – the measured melting points are above the bulk melting point.

Clusters themselves thus provide the proving ground for how material properties depend on size. Intimate knowledge of this dependency is important for instance for the semi-conductor industry, since the ever growing demand for faster processors in our computers pushes the boundary for miniaturization of the circuits. Speed can be gained by having more of them to fit on a microchip and for them to become closer to each other to minimize the length that signals need to traverse. The manufacturing of semi-conductor components come ever closer to the boundary where quantum effects becomes dominating. In some respects

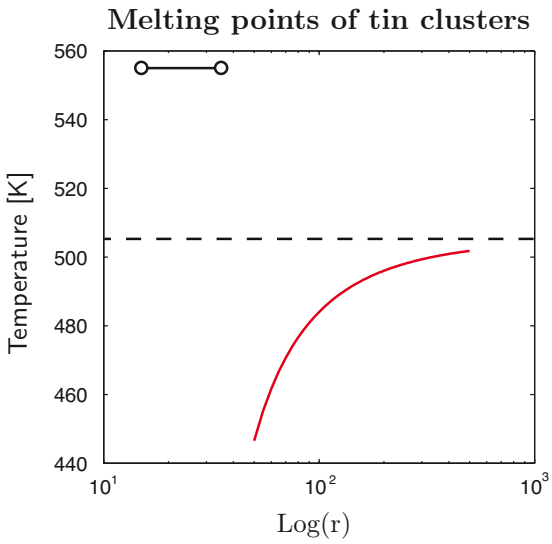

Figure 2.1: Experimentally determined melting point curve of large tin clusters and melting points for small clusters[8]. The abscissa is the logarithm of the cluster radius, the ordinate axis the measured cluster temperature. The dashed line indicates the bulk melting point's temperature.

this limit have already been surpassed – leakage currents caused by the modern (at the time of writing) 45 nm manufacturing technology have forced the switch to new insulating materials in processors.

The clusters studied in this thesis are produced from noble gases or molecules, and combinations thereof. Classification of different kinds of clusters and how they are produced are detailed in chapter 3. In that chapter a discussion about the thermodynamics of cluster production is also given. The geometrical structure of pure and mixed clusters is considered using noble gases as examples. In particular, in Paper **II** through **VIII** different mixed systems have been investigated that rely heavily on these models for the interpretation.

Photoelectron spectroscopy, an experimental technique that by the detection of the kinetic energies of emitted electrons following photoionization can give information about the geometrical and electronic properties of the system studied. Provided that the electronic levels in the system are localized, *i.e.* core levels[9, 10]. This technique is also surface sensitive owing to the finite mean escape depth of electrons emanating from inside a bulk part of atoms in a condensed phase. These factors combined makes it a very well suited technique for inquiries into cluster matters. The fundamental physics behind this technique and details of it are given in chapter 4.

Following the ionization of a core level, the created cationic core hole state is of *metastable* character. This is a state whence the system must, sooner or later, decay from since it is higher in energy than the ground-state of the ion. For heavy atoms the dominating decay channel is x-ray fluorescence – a process which by the state relaxes by the emission of a high energy photon in conjunction with an electron from the valence fills the core hole vacancy – leaving the system with one valence vacancy. There is also a non-radiative channel whereby an electron from the valence is emitted and another valence electron fills the core hole vacancy thus leaving the system with double valence vacancies. This process is called an *Auger process*; the emitted electron is, usually, referred to as the *'Auger electron'*. A model for the Auger electron spectrum of hydrogen bonded clusters are considered in Paper **XI**.

The Auger electron has a high kinetic energy owning to the highly excited core hole state which it emanates from. If the photelectron that was created in the initial core ionization process have a lower kinetic energy it will exchange energy with the Auger electron. This process is called *post-collision interaction* and a detailed account of it is provided in section 4.4 (page 51, *et seq.*). Paper **I** concerns this process in clusters *vis-à-vis* atoms.

Before the results are described and discussed in chapter 6, details about synchrotron radiation and the experimental setup are given in chapter 5.

3. Clusters

3.1 Basics of cluster physics

3.1.1 Scaling laws – the liquid drop model

Clusters, which are aggregates consisting of a *countable* number of atoms, bridge the gap between the single atom and the infinite solid. Thus physical and chemical properties of matter can be studied as a function of the number of constituent particles. The number of atoms that are a part of the surface of a cluster can be very large compared to the number of bulk atoms; for a cluster consisting of 13 atoms the surface fraction is 92%.

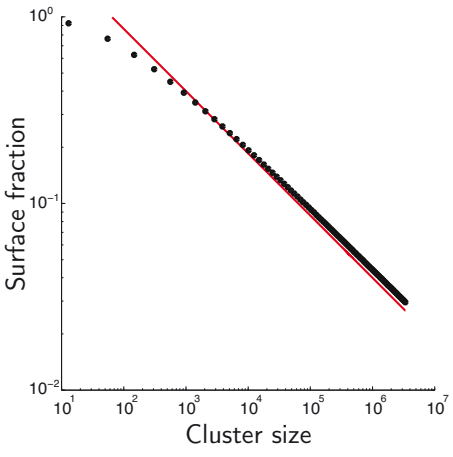

Figure 3.1: The surface fraction in the spherical cluster approximation (solid line) vs. surface fractions of icosahedral clusters at shell closings.

For larger clusters properties vary according the so-called liquid drop model; a scaling law such that the property $\chi(N) \propto N^{-\frac{1}{3}}$. A nice example of this is given by Buffat and Borel [11] who find the melting point of gold clusters to vary in this fashion. Deviations from this scaling law are often found for small and moderate sized clusters since they are often caused by quantum effects such as electronic shell closings or geometric shell closings. In Figure 3.1 the discrepancy between the surface fraction predicted by the liquid drop model and the surface fraction found at geometrical shell closings for icosahedral structures is shown. Geometric shell closings produce particularly stable cluster structures of certain sizes – these 'magical numbers' were first observed in mass spectra of xenon clusters[12]. Electronic shell closings affecting the ionization potentials of metal clusters are of a different nature. For instance in clusters of Na[13], Mg and Al[14] valence electrons can fill up orbitals that are delocalized over the whole cluster in a potential characterized by the size of the cluster and its ionic core.

3.1.2 Types of clusters

To form clusters almost any atom or molecule will do, and usually they are loosely categorized according to the intra-particle bonding mechanism. A comparison of inter-particle interactions can be found in Table 3.1.

For *metal clusters* the bonding is metallic. For the alkali and alkaline earths, *e.g. s*-block metals the bonding is purely metallic. This bond is delocalized and non-directional via the valence *s*-orbitals. For the *sp*-metals, such as aluminum, the bonding also has some covalent character and thus some directionality of the bond exist. Similarly the transition metals have a large degree of covalent bond character because of the valence *d*-orbitals. The order of magnitude for the bond strength of metal clusters is around 10 eV/atom.

Semi-conductor clusters have bonds with the same order of magnitude in the bonding strength. They have covalently bonded constituents that are either semi-conductors in the solid state *e.g.* carbon or silicon or compound substances such as GaAs.

Ionic clusters are always formed from atoms or molecules that have a very large difference in electronegativity – such as NaCl.

Noble gas Clusters are bound via van der Waals interaction between the atoms. This interaction is very weak (in the order of 0.01 eV/atom). *Molecular clusters* can, besides the aforementioned kind of interaction, also have other electrostatic contributions to their intermolecular bonding, *viz.* hydrogen bonds. They can have covalently bonded constituents but then it becomes a question of definitions whether if it is a cluster or a molecule – a discussion we shall not entertain ourselves with here.

There is also mixed clusters which are combinations of different kinds of particles that interact via one (or several) of the mechanisms outlined above.

Interaction	Potential	Typical energy [eV]
ion-ion	r^{-1}	10
ion-dipole	r^{-2}	1
dipole-dipole	r^{-3}	0.1
vdW	r^{-6}	0.01
hydrogen bond		1
covalent bond	more or less ionic	
metallic bond	more or less ionic	

Table 3.1: *Potential ranges and order of magnitudes of the interaction strength for some inter-molecular forces[15].*

3.2 Thermodynamics of cluster production

3.2.1 The laws of thermodynamics

For the discussion of *adiabatic expansion* below[1] it is convenient to first having contemplated upon the basic laws of thermodynamics.

0. *If two systems are in thermal equilibrium with a third system they, in turn, are in thermal equlibrium with each other.*

1. *The energy of an isolated system is conserved.*

$$d\mathscr{U} = đQ + đW + \sum_i \mu_i dN_i \tag{3.1}$$

i.e. the terms on the right specify how the internal energy ($\mathscr{U}$) of a closed system can be changed[2] by adding or removing heat (Q) and/or performing work (W) on the system or letting the system perform work. Mass flow is also an energy transfer mechanism, here exemplified by the sum over μdN, where μ is the chemical potential of the system. It may be necessary to specify more terms if, for instance, electric, magnetic or gravitational fields are present but for our purposes the first law as stated above will be sufficient.

2. *For a non-equilibrium isolated system the entropy (S) will increase over time and the maximum entropy is attained at equilibrium.*

$$(S =) \oint \frac{đQ}{T} \geq 0 \tag{3.2}$$

It should be noted that the equality hold for *reversible* processes only, for all other processes the integral is larger than zero.

3. If the temperature approaches zero for a system the entropy tends to a constant value.

The first and second law can be combined into to what is sometimes referred to as *the fundamental relation of thermodynamics*

$$d\mathscr{U} - TdS + pdV - \sum_i \mu_i dN_i \leq 0 \tag{3.3}$$

where $đW = -pdV$ is pressure-volume work.

[1] The derivation follows that of Harnes [16], a similar treatment can also be found in Mandl's book [17].
[2] By exchanging energy with its surroundings.

3.2.2 Adiabatic expansion

Consider a thermodynamic process where no heat (Q) is exchanged between the system and its surroundings – such a process is called *adiabatic* (or *isocaloric* or even *isoenthalpic* if the process is reversible [1]). Furthermore we assume that the number of particles in the system is constant ($dN = 0$).

The internal energy $\mathscr{U}$ is a thermodynamical state function, which can be written as a *total derivative*[3] described by a set of variables defining the state: temperature, volume, entropy, number of particles *et cetera*. Knowing this, the internal energy can be written as (considering $\mathscr{U}$ as a function of the volume and the enthropy):

$$d\mathscr{U} = \left(\frac{\partial \mathscr{U}}{\partial S}\right)_V dS + \left(\frac{\partial \mathscr{U}}{\partial V}\right)_S dV \tag{3.4}$$

where the first term is the temperature of the system and the other term the pressure with a minus sign. This is a restatement of the fundamental relation of thermodynamics (equation 3.3) for a *reversible* process.

$$d\mathscr{U} = TdS - pdV \tag{3.5}$$

It would be convenient to have the internal energy as a function of the temperature and volume and not as a function of the entropy and volume. The entropy is also a thermodynamic state function which can be written as a total differential:

$$dS = \left(\frac{\partial S}{\partial T}\right)_V dT + \left(\frac{\partial S}{\partial V}\right)_T dV \quad \underset{dV=0}{\Longrightarrow} \quad dS = \left(\frac{\partial S}{\partial T}\right)_V dT \tag{3.6}$$

using this, again together with the assumption of an *isochoric* process, equation (3.5) can be written, dividing with dT throughout:

$$\frac{d\mathscr{U}}{dT} = \underbrace{\left(\frac{\partial U}{\partial T}\right)_V}_{=C_v} = T\left(\frac{\partial S}{\partial T}\right)_V \tag{3.7}$$

Where the first identity holds at constant volume; using the definition of the heat-capacity at constant volume and the Maxwell relation $\left(\frac{\partial S}{\partial V}\right)_T =$

[3] *i.e.* the property $d\xi = \frac{\partial \xi}{\partial y}dy + \frac{\partial \xi}{\partial z}dz$ ensures that $\int_i^f d\xi = \xi(f) - \xi(i)$ *i.e.* that the value is independent of the path taken. A thermodynamic state function obviously must exhibit the properties mentioned otherwise a *perpetuum mobile* would be possible to construct: Consider a cycle such that going from state 1 to 2 by adding heat Q and returning to the same set of coordinates as characterizes state 1 by extracting work from the system. If the internal energy was not a exact differential the integral over that cycle would not necessarily be zero which would violate conservation of energy.

$\left(\frac{\partial p}{\partial T}\right)_V$ equation (3.5) can be cast as:

$$d\mathscr{U} = \mathcal{C}_v dT + T\left(\frac{\partial p}{\partial T}\right)_V dV - pdV \tag{3.8}$$

for an adiabatic process no change in internal energy takes place, thus

$$dT = \frac{1}{\mathcal{C}_v}\left[p - T\left(\frac{\partial p}{\partial T}\right)_V\right] dV \tag{3.9}$$

Seeking the change of temperature with respect to the volume at constant energy:

$$\frac{dT}{dV} = \underbrace{\left(\frac{\partial T}{\partial V}\right)_{\mathscr{U}}}_{=\mu_J} = \frac{1}{\mathcal{C}_v}\left[p - T\left(\frac{\partial p}{\partial T}\right)_V\right] \tag{3.10}$$

where the Joule coefficient[17, p. 130] have been identified. From this it is obvious that an ideal gas would not change temperature upon such an expansion[4]; the kinetic energy of an ideal gas is conserved since no internal attractions exist between the particles, and thus no forces which can perform work.

To describe the state of a real gas one must improve upon the hard-sphere *ansatz* somehow. Usually this is done by expanding the gas in terms of its density and find the coefficients of the expansion by *e.g.* fitting the resulting function to experimental data. One common equation of state is that of van der Waals,

$$\left(p + \frac{a}{\frac{V^2}{n^2}}\right)(V - nb) = nRT \tag{3.11}$$

where a is a measure of the attraction between the particles and b accounts for the volume that is excluded from V by them. Using equation 3.10 together with the definition of the molar volume $V_m = V/n$ and that $\left(\frac{\partial p}{\partial T}\right)_V = \frac{R}{V_m - b}$ when using the van der Waals equation of state one arrives at:

$$\left(\frac{\partial T}{\partial V}\right)_{\mathscr{U}} = -\frac{1}{\mathcal{C}_v}\frac{a}{V_m^2}$$

For expansion into vacuum from a finite initial volume one can consider the final volume to tend to infinity, integration gives

$$T_2 - T_1 = \lim_{V \longrightarrow \infty} \int_{V_m}^{V'} -\frac{1}{\mathcal{C}_v}\frac{a}{V} dV = \lim_{V' \longrightarrow \infty} \frac{a}{\mathcal{C}_V}\left[\frac{1}{V_m} + \frac{1}{V'}\right]$$

[4]The ideal gas law is $pV = nRT$[17] which gives $T\left(\frac{\partial p}{\partial T}\right)_V = \frac{pV}{nR}\frac{nR}{V} = p$, hence the square bracketed term in equation (3.10) is zero. This is all well since the Joule coefficient should vanish for an ideal gas [*ibid.*].

Strictly speaking one should take care that the molar volumes are different for states 1 and 2, but in this case the limit makes the second molar volume zero. We arrive at the sought relation:

$$T_2 = T_1 - \frac{a}{\mathcal{C}_v}\frac{1}{V_m} \tag{3.12}$$

normally a, V_m and $\mathcal{C}_v$ are positive quantities whence an adiabatic expansion into vacuum usually[5] leads to a cooling of a gas.

3.2.3 Critical cluster size

Condensation is an everyday phenomenon; for instance ice-crystals forming on a window, when opening champagne bottles (or beer/soda if that is the preference) and so on. The macroscopic manifestations of such processes are well understood thermodynamically, *i.e.* how much condensed vs. uncondensed phase did occur at a certain pressure, temperature (and other parameters). At a molecular level though, the understanding is not that detailed.

Condensation is a first order phase transition[6], as such it develops by initially growing seeding sites (nucleation) and subsequently growing the phase on those sites (given that growth can occur). Nucleation and growth are two separate stages each characterized by different time scales.

For a nucleation site to be created, a random thermal fluctuation of the initial system is needed. A free energy barrier exists between the phases of the system since work is needed to create an interface/surface between them. The nucleation site survives only if it can overcome the energy penalty associated with upholding the surface by the energetic advantages of being in the new phase – this occurs if the site contains a

[5] For a van der Waals gas this *caveat* is not necessary; for some particular situations though such an expansion can lead to an increase in temperature *e.g.* for an ionic gas the coulumbic repulsion stored as potential energy in the small initial volume gets converted to kinetic energy in the expansion.

[6] During such a process the system either releases or absorbs energy (the *enthalpy* of transformation). Following the derivative of the free energy with respect to a thermodynamic variable, one discovers that it is discontinuous at the transition; in contrast, second order transitions do not exhibit this behaviour.

Since the exchange of energy between the system and its surroundings is non-instantaneous, first order transitions are characterized by mixed phase regimes since not the whole system turns into one phase instantly – *e.g.* when bringing water to boil (slowly) it does not vaporize at once but liquid and vapour co-exist. If the system is brought past the phase transition point non-adiabatically (*i.e.* quicker than the "reaction time" of the system) a *metastable* state can be created which has not undergone the phase transition (yet) an example of this is *supersaturation*, *i.e.* a solution containing more dissolved material than could normally be dissolved by the solvent at the given circumstances. Nice examples of this is carbonated water and the compressed gas in a supersonic cluster nozzle.

large enough number of particles, the smallest such number is called the *critical size*.

Classical nucleation theory – the critical cluster size

Let ΔG be the difference in free energy between the phases and Δg be the free energy difference between the states per unit volume nucleus such that $\frac{4}{3}\pi r^3 \Delta g = -n\Delta\mu$ where n is the number of particles and $\Delta\mu$ the difference of chemical potentials between the phases, then:

$$\Delta G = 4\pi r^3 \Delta g + 4\pi r^2 \gamma \tag{3.13}$$

describes the competition between volumetric forces ($\propto r^3$) and surface forces ($\propto r^2$) as can be seen in Figure 3.2.

Competition between volumetric and surface forces

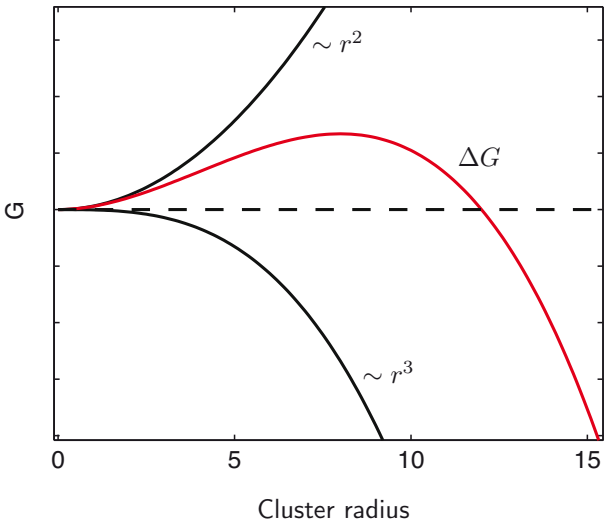

Figure 3.2: The terms to the right of the equality of Eq. 3.2 plotted both separately and as the sum which equals ΔG.

From the figure it is obvious that the criterion for a nucleation site to survive is that it should have a radius such that:

$$\frac{\partial \Delta G}{\partial r} \leq 0$$

with the equality part defining the critical cluster size: the radius that maximizes ΔG:

$$\left.\frac{\partial \Delta G}{\partial r}\right|_{r^\star} = 0$$

which for $r^\star = -\frac{2\gamma}{\Delta g}$ yields the barrier height:

$$\Delta G^\star = \frac{16\pi}{3}\frac{\gamma}{\Delta g}$$

Letting $\tilde{v}$ be the volume per molecule then using the identity $n\tilde{v} = \frac{4}{3}\pi r^3$, an expression for the critical size and barrier height can be obtained that depends on the critical *number* of molecules via the work of formation stated as:

$$\Delta G(n) = -n\Delta\mu + \gamma \mathcal{A}_1 n^{2/3}$$

Here the surface area per monomer $\mathcal{A}_1 = \sqrt[3]{36\pi\tilde{v}}$ have been used, denoting the volume per monomer in the bulk liquid as $\tilde{v}$. This expression only depends on (known) properties of the particles and measurable quantities[7]

$$n^\star = \left(\frac{2}{3}\frac{\gamma\mathcal{A}_1}{\Delta\mu}\right)^3$$

which is the "critical" parameter in the *Gibbs-Thomson equation*[8], *i.e.* small droplets have higher effective vapour pressure (higher curvature) than larger causing smaller ones to evaporate and larger ones to grow.

If the nucleation occurs at constant pressure and temperature a distribution of nuclei sizes will be created, each size with a probability $\exp\left(-\Delta G(n)/kT\right)$ where $\Delta G(n)$ is the total free energy of a nucleus with n particles.

If conditions are such that critical and supercritical clusters can form (*i.e.* the ensemble contain clusters with sizes larger than or equal to $n^\star$) and that the number of particles "feeding" the distribution from the bottom is sufficiently large (a number of particles is "lost" to critical nuclei) then the rate at which clusters attain the critical size is constant. Hence the nucleation rate depends on the distribution of subcritical clusters, which by their decay returns monomers to the bottom of the distribution. The density must therefore be high in the region where clustering occur for any clusters to survive – and be numerous enough to enable experimental inquires into their nature.

3.3 Cluster growth

3.3.1 Nucleation and condensation

By adiabatically expanding a gas through a cooled nozzle with a high backing pressure very low temperatures can be reached in the supersonic beam. A supersaturated vapour is created and the high density of atoms

[7] Since $\Delta\mu = kT\ln S_0 + p_{\text{eq}}\tilde{v}(S_0 - 1)$ is the chemical potential difference between the vapour and the liquid phases. $S_0 = p_0/p_{\text{eq}}$ is the supersaturation and p_{eq} is the vapour pressure of the bulk liquid at equilibrium at temperature T. p_0 is considered *ideal*, in classical nucleation theory, thus given by $p_0 = \frac{NkT}{V}$ – obviously this is a rather strong assumption which can be improved upon[18, 19].

[8] $p/p_{\text{eq}} = \exp\left(\frac{n^\star}{n}\right)$

make collisions a frequent occurrence which enable the creation of dimers through three-particle collisions. Enough energy can be removed from two of them by the third so that a dimer can be formed. The process is called *nucleation*.

$$A + A + A \longrightarrow A_2 + A'$$

here A' removes energy from the dimer which in turn acts as a site for further cluster growth:

$$A_N + A \longrightarrow A_{N+1}$$

Of course two clusters can merge to form a larger cluster, a process called *coalescence*:

$$A_N + A_M \longrightarrow A_{N+M-k} + kA$$

thus increasing the volume to surface ratio which lowers the energy of the system.

3.3.2 Cooling

Cluster formation is an *exothermic* process; the internal energy of the clusters increase since each atom adds its heat of condensation to the cluster. There are however cooling mechanisms that prevent disintegration of the clusters.

If a second gas B is added to the beam, which does not form clusters with A at the given set of conditions, then the clusters can be cooled by collisions with B gas atoms, thermal energy is carried away as increased kinetic energy of the B atoms. Usually B is a noble gas.

$$A_N(T) + B(E_{\text{kin}}) \longrightarrow A_N(T' < T) + B(E'_{\text{kin}} > E_{\text{kin}})$$

Thermal energy can also be converted into kinetic energy by boiling off cluster particles.

$$A_N \longrightarrow A_{N-1} + A$$

A collision can also cause *sputtering*[9]:

$$A_N + A \longrightarrow A_{N-1} + 2A$$

Radiative cooling, mentioned for completeness, is much slower than the processes described above and is hardly a factor for clusters created in a adiabatic expansion.

$$A_N \longrightarrow A'_N + \hbar\omega_{\text{ir}}$$

[9] Of course sputtering can also occur in a doping experiment (*vide infra*) but then an $A_{N-1}B$ cluster is formed.

3.3.3 Production of homo- and heterogeneous clusters

Clusters arrive at their final structure by growing to a certain size and subsequently cooling down. Upon creation the clusters are hot and liquid-like and solidify when the cluster cools down to its final temperature ($\sim$ 30 K for argon[20]). The cluster growth processes gets more complicated in the case of mixed cluster production.

For the heterogeneous cluster experiments presented in, for instance Paper **VI**, the host clusters were created by adiabatic expansion and subsequently doped with another gas[21]. Heterogeneous clusters can also be created by expanding a gas-mixture through a nozzle, this is usually referred to as *co-expansion*. Clusters created in the latter fashion are the subject of Paper **II**.

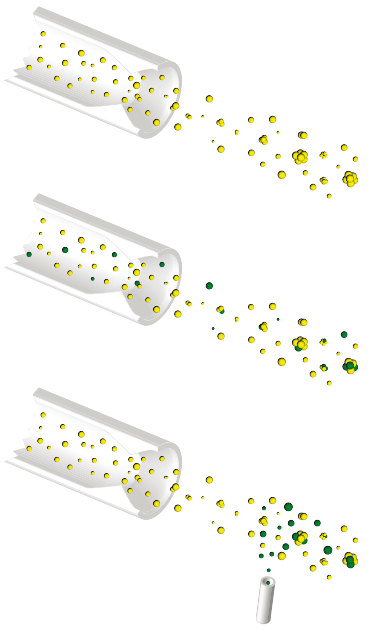

Figure 3.3: Expansion, co-expansion and doping.

The dynamics of clustering in the case of co-expansion is quite different from that of doping. In the former case a mixture of gases are adiabatically expanded and go from a hot (mixed) liquid-like state towards a cooled state whereas in the latter case cold clusters picks up atoms from a hot gas atmosphere.

3.3.4 Mean size and distribution of clusters

The mean size of the clusters in a supersonic beam is given by the cluster source's parameters, temperature, backing pressure and nozzle geometry. From the experimental data of Karnbach et al. [22] an empirical expression for the mean size can be deduced, as formulated by Buck and Krohne [23]:

$$<N>= e^{-12.83+3.51(\ln \Gamma^*)^{0.8}} \tag{3.14}$$

Equation (3.14) depends on a single parameter only[10]: Γ^* – a dimensionless parameter describing the rate of condensation in the beam. Hagena

[10] As stipulated by *Gibbs' phase rule*[1, p. 265]. The degrees of freedom in the system is the number chemical constituents (here one) subtracted by the number of distinct phases (here two, gas and clusters) plus two. For clusters created from a gas containing only one element, the number of degrees of freedom is equal to one.

[24] and Buck and Krohne [23] formulate the parameter as:

$$\Gamma^* = k\frac{p \cdot d'^{0.85}}{T^{2.2875}} \tag{3.15}$$

k is a gas specific constant proportional to the condensation probability of the expanded gas which can be calculated from the sublimation enthalpy[22]. d' is the *effective* nozzle diameter (described below) and T is the temperature.

Ref. 23 advices to use different expressions of the mean size depending on the rate of condensation. Besides Eq. 3.14 for $\Gamma^* \geq 1800$ the authors recommend:

$$\begin{aligned} <N> &= a_0 + a_1\Gamma^* + a_2\left(\Gamma^*\right)^2 + a_3\left(\Gamma^*\right)^3 && \Gamma^* \leq 350 \\ <N> &= 38.4\left(\frac{\Gamma^*}{1000}\right)^{1.64} && 350 \leq \Gamma^* \leq 1800 \end{aligned} \tag{3.16}$$

Where $[a_0, a_1, a_2, a_3] = [2.23, 7.00 \cdot 10^{-3}, 8.30 \cdot 10^{-7}, -12.83]$

The concept of 'equivalent nozzles' [24] (and references therein) take the geometry of the nozzle into account. Since a given cluster mean size can be produced by a multitude of source conditions, a relation between the opening angles and nozzle diameters can produce an *effective diameter* for a certain geometry by comparing with $\theta_0 = 35.7°$ which is half the opening angle of a molecular beam from a flat nozzle.

He	Ne	Ar	Kr	Xe
3.85	185	1646	2980	5554

Table 3.2: Values of the constant k for the noble gases He-Xe from Karnbach et al. [22]. Valid if in Equation (3.15) the pressure is given in mbar, the temperature in Kelvin and the equivalent nozzle diameter in μm.

$$d' = d\frac{\tan\theta_0}{\tan\theta} \tag{3.17}$$

The distribution of cluster sizes around the mean size is not generally known for neutral noble gases since mass spectroscopic measurements causes the clusters to fragment. The width of the distribution is usually taken to be half the mean size (as is done by Buck and Krohne [23]).

3.4 Geometrical struture of noble gas clusters

3.4.1 Structure vs. size in homogeneous clusters

The total binding energy of a cluster can be divided into surface and bulk parts as a function of the number of particles[25]:

$$\mathscr{E}_b = aN + bN^{\frac{2}{3}} + cN^{\frac{1}{3}} + d \tag{3.18}$$

The linear term is the volume (bulk) contribution to the energy, the second is the surface, the third describes edge contributions and the constant defines the energy origin. The constants $\{a, b, c, d\}$ for ichosahedral and fcc cluster structures can be found in [26]. As mentioned in Chapter 2 the surface part of a cluster remains substantial even for clusters containing hundreds of thousands of atoms. The minimal energy structure of a cluster, at a certain size, is a compromise between the cost of having atoms on the surface and minimizing the bulk energy. The energy difference between a free atom and an atom in the solid state is called the *cohesive* energy. It is instructive to consider the energy difference between a crystalline infinite solid and a finite cluster at a certain size normalized to the approximate number of surface atoms:

$$\Delta\mathscr{E} = \frac{\mathscr{E}_b - N\mathscr{E}_{\text{cohesive}}}{N^{\frac{2}{3}}} \tag{3.19}$$

Noble gases (except He) in the solid state have an fcc crystal structure[27]. If one, to minimize the surface energy with respect to the bulk energy, forms an as spherical cluster as possible from such a crystalline structure then $a = \mathscr{E}_{\text{cohesive}}$ and $\lim_{N\to\infty} \Delta\mathscr{E} = b$. The deviation from the solid is, in principle, the cost of having a surface which becomes smaller the larger the cluster gets.

If one instead tries to minimize the surface energy by maximizing the mean number of neighbours of the surface atoms then, $a - \mathscr{E}_{\text{cohesive}} \geq 0$. This is because a close packed surface inevitably introduces a strain in the bulk of the cluster since the interlayer distance is different from the

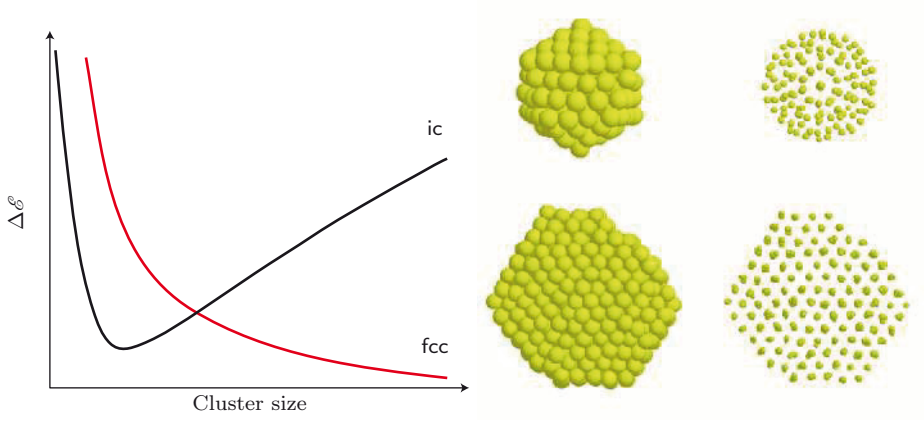

Figure 3.4: The icosahedral structure minimizes the surface energy at the cost of introducing a bulk strain; the fcc structure minimizes the bulk energy at the cost of increased surface energy. Typical structures of large (fcc) and small (icosahedral) van der Waals clusters.

interatomic distances within each shell. For larger clusters $\Delta\mathscr{E}$ for such structures diverges as $N^{\frac{1}{3}}$, but in the limit of small clusters the energy for such structures, *e.g.* icosahedral, is smaller than that of fcc clusters of the same size since the surface fraction can be very large.

Examples of icosahedral and fcc cluster structures can be found in Figure 3.4. In the same figure the quantitative behaviour of Eq. 3.19 is plotted for both types of structures considered here. The curves cross which indicate that a transition from one phase to the other takes place at a certain size which is dependent of the kind of cluster constituent. For argon the transition size is determined from electron diffration study to be $N \approx 750$ by Farges et al. [28]. Kakar et al. [29] put this transition at $N \approx 200$, and in the references mentioned in that paper theoretical values from 1500 to 10000 can be found. The transition from an icosahedral structure to defect fcc structures and $N \approx 500$ has also been suggested[30].

3.4.2 Modeling intra-molecular forces

To model clusters it is necessary to have an expression for the interparticle potential energy (the resulting force is a function of gradient of that potential). For systems that only interact with van der Waals forces[11] the interaction strength is inversely proportional to the separation to the sixth power ($\propto r^{-6}$).

Provided that the particles do not form a chemical bond (*e.g.* covalent, ionic, metallic) – then when the particles are moved closer to each other the overlap of their electron clouds cause a repulsive force. This force is a manifestation of the Pauli exclusion principle (see *e.g.* [2, 3]). This repulsive force grows very quickly with decreasing distances – the strength is proportional to an exponential, be^{-ar}, where b and a are constant atomic properties[33]. Lennard-Jones put it as being proportional to the 12^{th} power of the interparticle distance[34] and this approximation usually very well produce experimental data.

The Lennard-Jones potental can thus be formulated as:

$$\mathscr{U}(r) = 4\epsilon\left[\left(\frac{\sigma}{r}\right)^{12} - \left(\frac{\sigma}{r}\right)^{6}\right] \tag{3.20}$$

Where ϵ is the minimum of the interaction energy and σ the equilibrium distance.

The combination of Lennard-Jones potential parameters for two different gases (A and B) can be done using the Berthelot-Lorentz combination rule. This have been done in, *e.g.* Ref. 35. The rule simply stipulates that the well depths are combined with the geometric mean $\epsilon_{AB} = \sqrt{\epsilon_A \epsilon_B}$ and

[11] Also referred to as London dispersive forces since they are due to interaction between induced dipoles[31, 32].

that the equilibrium distances are to be combined with their geometric mean $\sigma_{AB} = (\sigma_A + \sigma_B)/2$. This rule tends to overestimate the strength of the interaction between the particles[36] – but it is often used for calculations since all one needs to know is the potential parameters for the constituents (for more involved methods see *e.g.* Refs. 37 and 38).

Figure 3.5 depicts the Lennard-Jones potentials for the systems considered in this thesis. That is where Eq. 3.20 reasonably describe the interparticle interaction, *e.g.* not ammonia.

The potentials for the pure cases increases in both depth and equilibrium distance as the polarizability of the particles increase. The van der Waals attraction increases with increasing polarizability. The latter is related to the number of electrons in the system – more electrons, higher polarizability.

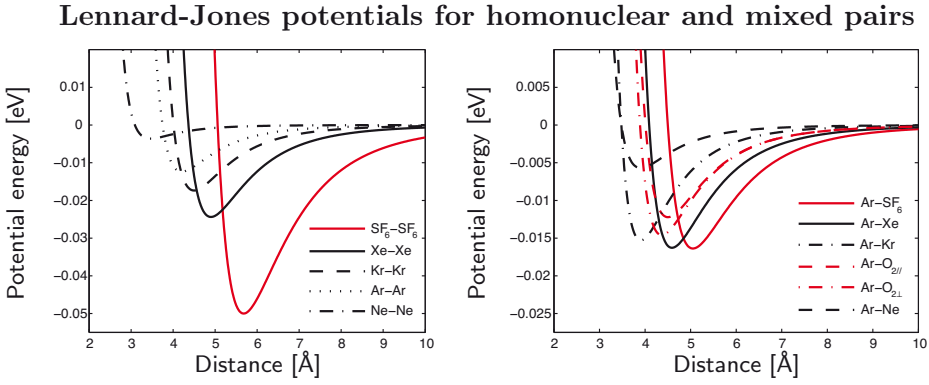

Figure 3.5: Potential curves for pure and mixed noble gas/molecular pairs. All plotted using parameters from Tang and Toennies [37], except argon-oxygen[39] and the pairs involving SF_6[40].

3.4.3 Heterogeneous cluster structure

By creating clusters from a gas mixture, additional degrees of freedom are added to the system: the mixing ratio between the species, bonding distances and strengths between the species and their cohesive energies. This means for example that the mean size of the clusters created in an adiabatic expansion no longer can be described with one parameter only as outlined above for single component clusters.

The cohesive energy

To find the equilibrium structure of a mixed cluster, one can assume that if the constituent species have enough mobility for long enough time, they become distributed in such a fashion that the species with the highest cohesive energy is found in the bulk and the lowest on the surface.

The cohesive energy can be formulated as the lowering of the total energy for an ensemble of atoms in the solid state compared to the energy of the same number of free atoms spaced infinitely far apart. The amount of cohesive energy per atom is related to the strength of the interatomic bonds in the solid (remember that the bonding strength of the noble gases increase with atomic number).

	$\mathscr{E}_{\text{cohesive}}$ [eV]
Ne	0.02
Ar	0.08
Kr	0.116
Xe	0.16

Table 3.3: Bulk cohesive energies per atom at (1 atm. and 0 K) taken from[27].

A two-component system can minimize its surface energy by surface enrichment by the component with the lowest cohesive energy. The atoms with the highest cohesive energy stay in the bulk where the coordination number is highest. The system will strive towards this structure as long as the temperature is high enough to permit the atoms to move around freely.

Lennard-Jones interactions in mixed systems

A comprehensive molecular dynamics study on the structure of mixed rare gas clusters (denoted A and B below) has been done by Clarke et al. [41]. They show that more elaborate conclusions about the structure can be made if both binding energy ϵ and distance σ is taken into account instead of just the cohesive energy. If A has the highest binding energy five cases can be discerned for the *equilibrium* structures:

1. $\epsilon_{AB} \simeq \epsilon_{AA} \simeq \epsilon_{BB}$
   Uniform mixing favoured because of the similarity between A and B.

2. $\epsilon_{AB} < \epsilon_{AA} \sim \epsilon_{BB}$
   The limit of large AB interaction is the previous case. In the other limit the cluster fragments into an A and a B cluster. Between the two limits, constellations with an A rich part and a B rich part separated with a more or less diffuse interface layer (for larger AB interaction strengths the layer gets more diffuse).

3. $\epsilon_{BB} < \epsilon_{AB} \sim \epsilon_{AA}$
   A core of A particles is covered by a coat of B particles separated from each other. The B surface grows together from regions with high A-B coordination.

4. $\epsilon_{AB} \sim \epsilon_{BB} < \epsilon_{AA}$
   Favors island formation of B on top of A core. In contrast to the

preceding point the surface grows from parts with high B-B coordination.

5. $\epsilon_{AB} \ll \epsilon_{AA}$
   B evaporates from a core of A particles. This is nothing but collisional cooling as described previously.

Increasing the temperature enhances mixing (and fragmentation if AB interaction is weak). Differences in bond length σ enhance tendencies to segregate.

Excellent examples of the latter mechanism is found in the work by Tchaplyguine et al. [42] and in Paper **II** on Xe/Ar and Kr/Ar cases respectively; argon is found at the surface of both xenon and krypton cores but with different radial distributions. In Chapter 6 the other systems considered are discussed.

The Ar-Ar and Ar-Kr parameters are similar (Figure 3.5), especially the bond distances. Experimentally it is found that the Ar concentration decrease with increasing proximity to the cluster centre. A perturbation from the equilibrium structure, argon on top of krypton can be expected to be due to the similarity of bonding parameters (case 1). However, the mixture should remain partly segregated considering that the difference in cohesive energies still makes it energetically favorable for the cluster to put argon on its surface.

Looking at the potentials of Ar-Ar, Ar-Xe and Xe-Xe it can be concluded that those correspond more closely to case 4 above, with a high degree of segregation because of the difference in bond lengths between all the dimer interactions in question. Ar/Xe clusters created in a coexpansion have highly segregated structures with argon on the surface and xenon in the bulk, and as seen in Ref. 42 and Paper **III** even the interface between the core and surface part of the cluster can be observed.

Here the discussion have been on how pure and mixed equilibrium cluster structure may be explained by the cohesive energy and/or by using Lennard-Jones parameters of the system. Thereby the implicit assumption is made that the clusters are hot (liquid) upon creation so that the lowest energy structure can be attained by diffusion processes inside the cluster. In chapter 6 it is shown that mixed cluster structures also depend on the way that the clusters were produced. Both equilibrium structures and structures far from equilibrium can be achieved.

4. Electron Spectroscopy

4.1 The electronic structure of matter

An atom consists of one or several electrons surrounding a nucleus. The light electron is a negative particle; the proton(s) in the heavier nucleus is positively charged. Coulombic forces trap the electrons in a potential surrounding the nucleus. How this system can be stable is explained with quantum mechanics.

Using classical electrodynamics it is not be possible to find a solution that would allow a system of a positive and a negative charge to be stable. The Coulombic attractive force would accelerate the electron in a spiral toward the proton until they crash together as in Figure 4.1. An electron in a circular orbit is accelerated towards the center; the electron would then lose energy by emitting electromagnetic radiation (γ) with a frequency inversely proportional to the radius. Classically the energy remaining in the system which separate the charges will then decrease continuously. Hence, the radius of separation will decrease and the frequency of the radiation increase. The predicted electromagnetic spectrum of such a system would be a continuous one over a broad range of frequencies (*i.e.* cyclotron radiation).

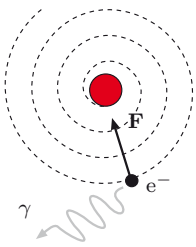

Figure 4.1: A classical atom meets its destiny.

However, early works[1] in the field of spectroscopy showed a discrete spectrum of energies for the hydrogen atom. A new theory had to be developed to explain this discrepancy of electrodynamics and experimental observations.

4.1.1 Quantum mechanics of atoms

Quantum mechanics was developed in the beginning of the 20$^{\text{th}}$ century by physicists like Max Planck (introduced energy 'quanta'), Niels Bohr (the solution to the Hydrogen atom), Erwin Schrödinger (the fundamental wave equation of quantum mechanics), Werner von Heisenberg (the uncertainty relation(s)) and many more[43].

[1] G. Kirchhoff, A. J. Ångström in separate works in 1859 about the Fraunhofer solar spectrum.

4.1.2 The hydrogen system

For the simplest atom, hydrogen, the Schrödinger wave equation $\mathscr{H}|\Psi\rangle = E\Psi$ can be solved analytically. The Hamiltonian is the total energy operator of the system which can be written:

$$\mathscr{H} = -\frac{\hbar^2}{2m}\nabla^2 - \frac{e^2}{4\pi\varepsilon_0 r}$$

The solutions are usually called *orbitals* and the derivation can be found in any textbook on modern physics (*e.g.* Sakurai [3]). The energy of an electron in hydrogen can be described by the main quantum number n only[2]. However, to fully describe the state of the electron we also must specify the spin s and orbital angular momentum ℓ and their directions m_s, m_ℓ. For $n = 1, 2, 3, \ldots$ we have $\ell = 0, 1, \ldots, n-1$ which is sometimes denoted with lower-case letters $s, p, d, f, \ldots$.

The energy levels of hydrogen E_n are $2n^2$ fold degenerate; each electron *shell* $(K, L, M \ldots)$ have *sub-shells* characterized by the orbital quantum number ℓ. For a certain n the degeneracy is partly lifted because of *spin orbit interaction*:

$$E = E_n + E_{\text{so}}$$

where the last term is a perturbation of the energy that depends on if the angular momentum are parallel or anti-parallel to the spin. For example, below it can be seen that the atomic argon $3p$ feature is spin-orbit split into two peaks in the spectrum shown in Figure 4.4.

4.1.3 Many electron atoms

If more than one electron is present in the system the interaction between the electrons needs to be taken care of, besides interaction between the electrons and the nucleus. Proper attention needs to be paid to the fact that the total wave function must be asymmetric – the electron is a fermion and as such cannot have the same set of quantum numbers as any other electron in the system.

This is usually done, in textbooks, by perturbation theory using linear combinations of hydrogenic orbitals and energies as starting point. But calculating the energy of the levels can be a quite formidable endeavor[44]. Noble gases have a particularly simple electron configuration, since all the shells are filled, *e.g.* the electron configuration of argon is $1s^2 2s^2 2p^6 3s^2 3p^6$.

[2]Sometimes n are represented by capitals K,L,M... for $n = 1, 2, 3 \ldots$

4.2 The Photoelectric effect

That electromagnetic radiation can ionize atoms, was discovered by Heinrich Hertz in 1886. Maxwell's theory of electromagnetism, that had been published in 1865[3], predicted that light was electromagnetic waves which moved at the speed of light. Hertz (and others) performed experiments designed to investigate this electromagnetic radiation.

The apparatus Hertz used was a high voltage induction coil to create a discharge between two pieces of brass and a piece of copper wire with a brass sphere on one end and on the other a sharp point directed towards the sphere. The basic idea is that the charges in the discharge oscillate back and forth thus emitting electromagnetic radiation; if the emitted light would create another spark between the tip of the wire and the brass sphere light would then be proven to be electromagnetic waves.

During 1886, Hertz carried out a series of experiments with his apparatus showing that electromagnetic waves were reflected through prisms, that it was polarized etc., just the same properties as light waves. The only snag was that it sometimes were very hard to see the tiny spark created at the wire tip[4], to improve this Hertz enclosed the wire in a dark casing – which *reduced* the intensity of the spark. He soon found out that if the part of the casing shielding the discharge were removed the intensity was not reduced and that glass reduced the intensity but not quartz (quartz being transparent to ultra-violet light).

By using a quartz prism to disperse the electromagnetic waves it was also found that the greatest intensity of the detected spark was obtained in parts of the dispersed light which were above the visible range. Hertz reported his observations in *Annalen der Physik* 1887 (**33**, 983) but offered no explanations of the phenomena[5].

In 1899, J.J. Thompson observed that negative particles were emitted when a metal surface was exposed to ultra-violet light. Later, in 1902, P. von Lenard observed that the emitted particles' kinetic energy[6] did depend on the color (frequency) of the light and *not* on the intensity of the light.

---

[3] The equations that are named after Maxwell were first published in the paper *"A Dynamical Theory of the Electromagnetic Field"*, Philos. Trans. R. Soc. London, **155**, 459 (1865).

[4] As one remedy it was suggested that a suitably prepared frog's leg would serve equally well as a detector.

[5] The spark in the detector was enhanced by charges knocked out from the material in the detector by photons from the ultra-violet parts of the spectrum emitted from the discharge.

[6] More exactly he measured the stopping potential of the emitted electrons. He performed the experiment by, in essence, shining light on the positively charged plate of a parallel plate capacitor and observing the potential that causes the, by the light, induced current to become zero.

In one of his *annus mirabilis* (1905) papers Einstein gave a mathematical description of the photoelectric effect[45]. The ionization was described to be caused by the absorption of a 'light quantum' and that different materials had different onset frequencies f_0 for electron emission was explained by that the size of the energy packet needed to be large enough to overcome the first ionization potential of the material.

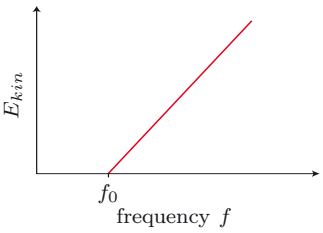

Figure 4.2: A minimum frequency of the photons are required to ionize a material.

For this work he was awarded the Nobel prize of physics 1921 *"for his services to Theoretical Physics, and especially for his discovery of the law of the photoelectric effect"*.

The use of *quantized energy-levels* was used in 1900 by Max Planck to explain the distribution of radiation from a black body. To avoid the *ultra-violet catastrophe* of classical electrodynamics, *i.e.* that the radiation energy distribution tends to infinity for short wavelengths, he assumed that the energy of the emitting oscillators was quantized. By stating that light consists of discrete energy packets, Einstein could formulate an equation that explained the photoelectric effect:

$$\varepsilon_{\text{kin}} = \hbar\omega - \phi$$

where the kinetic energy of the photoelectron is related to the frequency of the light and the work needed to escape the material. $\hbar$ is Planck's constant (divided by 2π) and $\omega = 2\pi f$ is the angular frequency of the light. The slope of the line in Figure 4.2 is thus Planck's constant.

4.3 X-ray and UV Photoelectron Spectroscopy

For atoms *in vacuo* the work needed to remove an electron from a certain level is equal to the binding energy ε_i of that level. The process can be written:

$$\hbar\omega + \text{A} \longrightarrow \text{A}^+ + e^-$$

and the relationship between the kinetic energy of the photoelectron and the photon energy then becomes:

$$\varepsilon = \hbar\omega - \varepsilon_i \qquad (4.1)$$

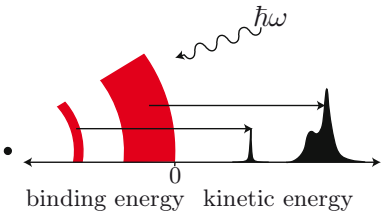

Figure 4.3: X-ray and UV photons probe different parts of a system. The zero on both scales is called the vacuum level.

The relationship between the kinetic- and binding energy scales is outlined in Figure 4.3.

If the photon has an energy in the order of tens of electron-volts, the energy is sufficient to ionize valence levels of atoms. Photoelectron spectroscopy using such UV-photons is usually referred to as UPS[7]. A photoelectron spectrum (taken at a photon energy of 61 eV) of argon clusters is presented in Figure 4.4 where features of both the atomic $3p$ levels are resolved as well as the cluster $3p$ feature.

The valence levels usually have a large spatial extent; the overlap of such orbitals between neighboring atoms can cause valence electrons to be shared between several atoms – the basis for chemical bonding.

X-ray photons are energetic enough to probe deeper lying electronic states (*core* levels) of the system studied. Those levels tend to be localized, *i.e.* their spatial overlap with eventual neighbours is negligible but their energy is still sensitive to the chemical surrounding of the atom[9].

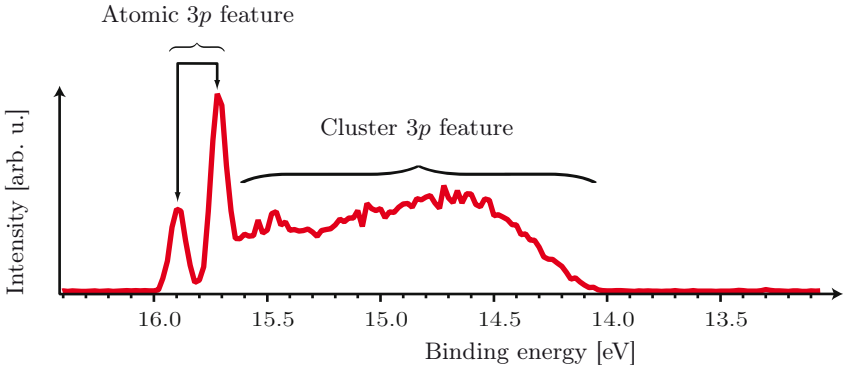

Figure 4.4: UPS spectrum of a beam containing both free argon atoms and argon clusters. The sharp features pertain to the argon $3p$ level which is split, due to spin-orbit interaction, into two states: $3p_{1/2}^{-1}$ and $3p_{3/2}^{-1}$. The corresponding cluster feature(s) is/are shifted towards lower binding energies.

4.3.1 Atomic core-level lineshapes and positions

The energy position of a certain atomic level is given by the energy difference between the initial neutral and core-ionized final states of the system. The initial energies are determined by the exchange and Coulomb interaction between the electrons and the Coulomb interaction between each electron and the nucleus. The final state energies are in addition affected by the contraction of the outer orbitals due to the increase of the effective charge of the nucleus by +1, since the core electrons no longer screens the nuclear charge as effectively.

Because of the finite lifetime of the core ionized state, the observed energy is inevitably recorded within an uncertainty such that $\Delta E \Delta t \leq \frac{\hbar}{2}$.

[7] Ultraviolet Photoelectron Spectroscopy.

Alternatively this is stated as:

$$\Gamma\tau = \hbar \tag{4.2}$$

where Γ is the FWHM width of the state and τ the core-hole lifetime.

Intensities are given by the transition dipole moments obtained from *Fermi's golden rule*

$$I \propto |\langle \Psi_f | \boldsymbol{\mu} | \Psi_i \rangle|^2$$

If stated as a function of kinetic energy of the photoelectron, we get the *Lorentzian* lineshape:

$$P(\varepsilon_{kin}) = \frac{\Gamma}{2\pi} \frac{1}{\frac{1}{4}\Gamma^2 + \varepsilon_{kin}^2} \tag{4.3}$$

Consequently the spectral resolution is limited by this *life-time broadening*. In practice other broadening mechanisms also contributes to limit the resolution, *e.g.* the monochromaticity of the photons and spectrometer instrumental broadening. The total lineshape is therefore modeled with a Lorentzian convoluted with a Gaussian – a so called Voigt lineshape. Under certain circumstances, to be specified below in Section 4.4, an energy shift caused by interaction between the photoelectron and secondary electrons make the lineshape asymmetric.

To sum up what has been covered so far: an atomic level is characterized in spectra by a *lineshape* at a certain binding energy ε_i (or kinetic energy $\varepsilon_{\text{kin}} = \hbar\omega - \varepsilon_i$). This lineshape has: a Lorentzian part $\mathscr{L}$, characterized by its life-time width; a Gaussian part $\mathscr{G}$ that takes into account experimental broadening due to, *e.g.* the limited photon energy and spectrometer resolutions; an asymmetric part $\mathscr{A}$ that effects the Lorentzian part with a shift and a distortion. Said distortion is determined by the relation between the excess kinetic energy of the photoelectron and the "nominal" Auger electron kinetic energy for the level in question.

4.3.2 Cluster core-level lineshapes and positions

The cluster core-level lineshape will be considered here as a perturbation of atomic lineshapes owing to *polarization screening* of the positively charged ion in the final state of photo ionization which introduces a chemical shift of the binding energy and a broadening[46], and affected by the surface sensitivity inherent in any photoelectron spectroscopy experiment[47]. Postcollision interaction effects ($\mathscr{A}$) on the cluster lineshape are covered in Paper **I** and will therefore be discussed in Chapter 6.

In contrast to ionization of valence orbitals, where de-localization of the final state charge is a significant factor, the charges remain localized on the ionized atom in the case of core level ionization. As a result, the lifetime of the corehole can be expected to be essentially equal that of

the free atom – the Lorentzian broadening part $\mathscr{L}$ of the lineshape is preserved.

This is true in most of the systems considered here. A notable exception being the study of the Ne $2s$ inner valence level of neon clusters studied in Paper **IX**. The lifetime of the free neon atom Ne $2s$ ionized state differs considerably from the lifetime of the same level when studied in pure neon clusters (picoseconds vs. femtoseconds). The lifetime is even different for the surface and the bulk parts of the cluster spectra in that case. The lifetime difference is cased by a process called Interatomic Coulombic Decay, which is discussed in the last section of this chapter.

This leaves the Gaussian part $\mathscr{G}$ of the cluster lineshape to be investigated further.

Polarization screening

The formulae dictating the influence of polarization screening of the XPS final state will be reviewed and subsequently, in the following parts, how they are influenced by factors listed here.

- Different atoms have different *coordination numbers* which depends on the clusters' geometrical structure.
- Distribution of cluster sizes (hence different abundances of atoms with specific coordination) since the clusters are produced in an adiabatic expansion.
- Different kinds of atoms or molecules, such as: Ar, Kr, Xe... have different polarizabilities.

The field of the positive ion polarizes the surrounding atoms. Hence a part of the energy of the final state in the ionization process is stored in the induced dipole field.

Following Björneholm et al. [46], the ionization potential of an atom situated at $\mathbf{r}$ in a cluster can be expressed as the sum of the atomic ionization potential and the polarization energy:

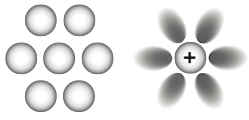

Figure 4.5: Charge induced dipoles.

$$\mathscr{I}_N(\mathbf{r}) = \mathscr{I}_1 + \mathscr{U}_N(\mathbf{r})$$

Let $\mathbf{E}(\mathbf{R}_i)$ be the electric field of the ion, then the polarization energy can be written:

$$\mathscr{U}_N(\mathbf{r}) = -\frac{1}{2}\sum_{i=1}^{N}\mathbf{p}_i \cdot \mathbf{E}(\mathbf{R}_i)$$

The induced dipole moment $\mathbf{p}_i$ of atom i depends on the field of the ion as well as the field of all other induced dipoles. The interaction between

the induced dipoles is given by the tensor $\mathbf{M}_{\mu\nu} = (\delta_{\mu\nu}R^2 - 3R_\mu R_\nu)/R^5$. Consider the interaction energy between two dipoles, $\mathbf{p}_1$ and $\mathbf{p}_2$, it is a product of the dipole strength of dipole 1 and the field created by dipole 2. Expressing the field as the gradient of the potential $\mathbf{E} = -\nabla\phi$ and using $\phi(R) = \frac{\mathbf{p}_2\cdot\hat{\boldsymbol{r}}}{R^2} = \nabla\left(\frac{\mathbf{p}}{r}\right)$ we get:

$$\mathbf{p}_1 \cdot \mathbf{E}(\mathbf{R}) = -\mathbf{p}_1 \cdot \boldsymbol{\nabla}\phi(R) = -\mathbf{p}_i \cdot \boldsymbol{\nabla}\left[\nabla\left(\frac{\mathbf{p}_2}{R}\right)\right] = \mathbf{p}_1 \cdot \boldsymbol{\nabla}\left(\nabla R^{-1}\right)\mathbf{p}_2$$

where the last term can be simplified:

$$\boldsymbol{\nabla}\left(\nabla R^{-1}\right) = -\boldsymbol{\nabla}\left(\frac{\mathbf{R}}{R^3}\right) = \frac{\nabla\mathbf{R}}{R^3} - 3\frac{\hat{\boldsymbol{r}}\hat{\boldsymbol{r}}}{R^3} = \frac{\mathbf{1}}{R^3} - 3\frac{\mathbf{RR}}{R^5}$$

The unit tensor is defined as $\nabla\mathbf{R} = \mathbf{1}$ and the expression for the energy becomes[4]:

$$\frac{\mathbf{p}_1\mathbf{p}_2}{R^3} - 3\frac{(\mathbf{p}_1\cdot\mathbf{R})(\mathbf{R}\cdot\mathbf{p}_2)}{R^5}$$

If we instead have an assemblage of N dipoles interacting the straightforward generalization of the interaction energy is:

$$\frac{1}{2}\sum_{i,j=1}^{N}\mathbf{p}_{i\mu}\frac{(\delta_{\mu\nu}R^2 - 3R_\mu R_\nu)}{R^5}\mathbf{p}_{j\nu} = \frac{1}{2}\sum_{i,j=1}^{N}\mathbf{p}_{i\mu}\mathbf{M}_{\mu\nu}\mathbf{p}_{j\nu}$$

where summation over the greek indices representing coordinates are taken to be implicit. The total polarization energy $\mathscr{U}_N(\mathbf{r})$ includes the term discussed above, a term attributing to the ion-dipole interaction and a term which corrects the free field $\mathbf{E}$ for the presence of the dipoles. Through the latter term $\mathbf{p} = \alpha\mathbf{E}$ the *atomic polarizability* enters the formula for the cluster ionization potential.

$$\mathscr{U}_N(\mathbf{r}) = \frac{1}{2}\sum_{i,j=1}^{N}\mathbf{p}_{i\mu}\mathbf{M}_{\mu\nu}\mathbf{p}_{j\nu} + \frac{1}{2}\sum_{i=1}^{N}\frac{|\mathbf{p}_i|^2}{\alpha} - \sum_{i=1}^{N}\mathbf{p}_i\cdot\mathbf{E}(\mathbf{R}_i)$$

The individual dipole moments must be calculated from a system of equations stipulated by the variational condition $\frac{\partial}{\partial p_{\mu i}}\mathscr{U}_N(\mathbf{r}) = 0$.

4.3.3 Shifts and broadening – site abundance effects

Polarization screening of the final state gives rise to a chemical shift of the cluster ionization potential. The magnitude of this shift for an individual atom depends on the cluster geometry, which dictates the distances to and number of neigbours, and the atomic polarizability, which determines the strength of the individual dipoles. Since the number of neighbours is different for the bulk part of the cluster compared to the surface part it

can be expected that the cluster feature should have a bulk and surface part.

The broadening of the cluster features – surface and bulk – depends mostly on the cluster geometry and size distribution effects. In chapter 3 it is mentioned that clusters are created around some mean size $<N>$ in an adiabatic expansion, which also contributes to the broadening since polarization shifts vary with size.

In spectra this is manifested by a broadening since the abundance of different sites differ for different sizes. Usually this size distribution is taken to be Gaussian with a full width at half maximum as $\frac{<N>}{2}$.

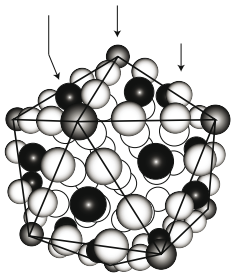

Figure 4.6: An icosahedral cluster. Arrows indicate different surface sites. Bulk atoms are unshaded.

As indicated above, the number of neighbours separates the bulk from surface. A bulk atom has 12 neighbours in an icosahedral cluster this determines the main part of the shift. The broadening of the bulk stems from that the polarization from the surrounding is slightly different in different parts of the clusters. Surface atoms have a varying number of neighbours, for that reason the surface feature is wider.

At least for homogeneous clusters this is true. The surface feature of krypton in mixed Kr/Ar clusters can be less broad than the bulk feature of pure krypton clusters if the mixed cluster is created by doping with low doping pressure. The krypton atoms tend to end up in highly coordinated surface sites leaving argon at sites with lower coordination[8]. If the geometry of the cluster is *a priori* known (or assumed) a lineshape which takes this broadening into account explicitly can be calculated[49]. Otherwise it is usually taken to be of Gaussian nature.

4.3.4 The cluster lineshape

Before summing up this section we note that the relative intensity of the surface and the bulk features varies with the photon energy. This is due to the surface sensitivity inherent in any photoelectron spectroscopy experiment, caused by that the electron mean free path varies with the kinetic energy of the photoelectron. For a detailed discussion about this phenomenon in clusters, see Tchaplyguine *et al.*[50]; moreover, Lundwall *et al.* [47] have examined, in detail, differences between surface sensitivity in XPS and Auger spectra of clusters.

A cluster feature is chemically shifted with respect to the monomer of the constituents, the magnitude of the shift is, for non-conducting

[8]This is the main result of Paper **VII**. It have also been observed in mixed Ar/Kr clusters created by a co-expansion[48].

species[9], determined by polarization screening; because of different coordination numbers, and thus different screening strengths, a surface and bulk feature can be discerned. The shift is also affected by the kind of atoms surrounding the ionized atom; this is evident in the spectra of mixed clusters presented in Chapter 6. The broadening of the cluster features are thus composed of (excluding atomic contributions to the lineshape): a Lorentzian part $\mathscr{L}$ – with a life time width given by the core hole lifetime that can be effected by, *e.g.* Interatomic Coulombic Decay. A Gaussian part $\mathscr{G}$ – reflects the abundance of different coordination numbers and the distribution of sizes in the beam. And an asymmetry $\mathscr{A}$ which effects the Lorentzian part of the surface and bulk differently owning to post-collision interaction[10] between the Auger and photoelectrons.

[9] The screening for metallic systems is much more effective since the charge get delocalized over the whole system very rapidly.
[10] *C. f.* below, in chapter 6 and in Paper **I**.

4.4 Postcollision interaction

4.4.1 Introduction and semiclassical theory

A core hole created upon photoionization is, within femtoseconds, filled by an electron from an outer laying orbital. The excess energy in the system is released either via X-ray emission (radiative channel) or by emission of an *Auger* electron from one of the outer shells (non-radiative channel). The emission of the electron via the non-radiative channel leaves the system in a doubly ionized state, which can be studied via the Auger electron.

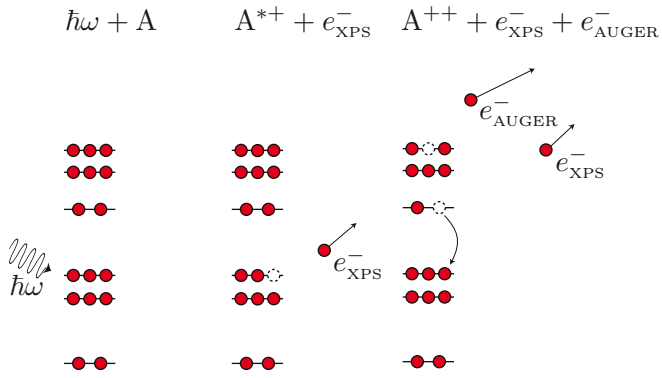

Figure 4.7: Non-radiative (Auger) decay of the XPS final state (in the middle) leaves two electrons in continuum states – enabling postcollision interaction phenomena.

In a two-step picture, *i.e.* the ionization creates a core-hole which subsequently decays via a radiationless channel. The Auger process can be written as:

$$\hbar\omega + A \longrightarrow A^{*+} + e^-_{\mathrm{XPS}} \longrightarrow A^{++} + e^-_{\mathrm{Auger}} + e^-_{\mathrm{XPS}}$$

where the photon energy $\hbar\omega$ is assumed to be above the core ionization threshold of the system A. The intermediate state A^* has a finite lifetime τ. If the kinetic energy of the photoelectron is larger than that of the Auger electron, the observed lineshape P will be a Lorentzian with a width Γ reflecting the corehole lifetime via the relation $\Gamma\tau = 1$ as above but here in atomic units.

If the kinetic energy of a photoelectron is lower than the kinetic energy of the Auger electron then an energy exchange between the two electrons in the continuum occurs; this is referred to as *postcollision interaction* (PCI). Stating the problem is quite simple – in a classical picture the XPS electron moves in a potential $-1/r$ until it gets passed by the Auger electron, after which it travels in the $-2/r$ potential of the Auger final state. The time it takes to pass the XPS electron for the Auger elec-

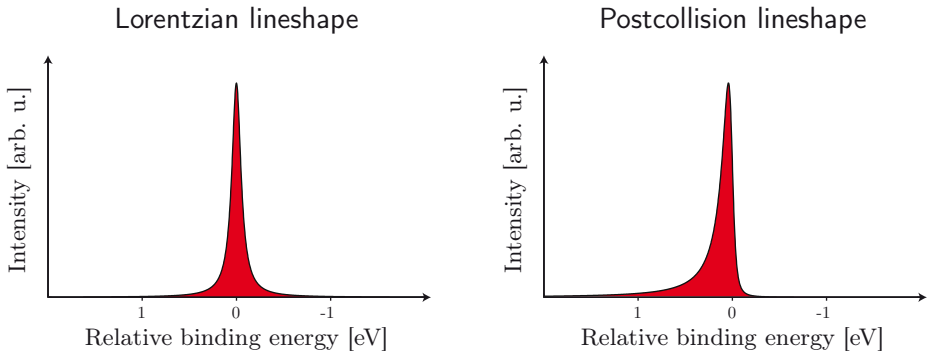

Figure 4.8: Compared to a Lorentzian a PCI line-shape, of a photoelectron line, is shifted towards higher binding energy and it is asymmetric with a tail stretching out towards higher binding energies.

tron is $\tau_a + t$, the actual core-hole lifetime of the observed single decay process plus the time it takes for the Auger electron to catch up with the photoelectron. The passing occurs at some radius R and, by energy conservation, the energy gained by the Auger electron is $1/R$ which is equal to the energy lost by the photoelectron. Thus, the kinetic energy of the photoelectron is reduced and it appears to have a higher binding energy.

Obviously this energy shift is not of discrete nature: it is inversely proportional to the passing radius R which is a function of time – more precisely of $\tau_a + t$ – the Auger initial state decays exponentially with a time-constant τ, hence some photoelectrons will travel far and thus are passed "late" but the majority will be passed "early". Examining the Coulombic potential, we find that for small passing radii (early passes) the energy shift changes rapidly, whereas for large radii the energy shift does not change as rapidly with R; shifts towards higher binding energies are large but have lower probability than smaller shifts. The line can then be expected to extend a tail towards higher binding energies and to be steeper on the lower binding energy side than a corresponding Lorentzian[11]. A plot of a Lorentzian (Eq. 4.3), and a PCI line-shape (Eq. 4.5, van der Straten et al. [51]) is shown in Figure 4.8.

Most PCI theories start out within the framework of time-independent quantum mechanical scattering theory. The lineshape, given by Fermi's golden rule, depends on the overlap of the electrons' continuum orbitals of the initial $|\Psi_i\rangle$ and final states $|\Psi_f\rangle$.

$$P(\varepsilon_{\text{KIN}}) = \frac{\Gamma}{2\pi} |\langle \Psi_f | \Psi_i \rangle|^2 \tag{4.4}$$

[11] This is the line-sharpening often mentioned in connection to PCI phenomena, it is thus rather sharpening of half the line with the other smeared out since the intensity must be constant.

The choice of wave functions and level of sophistication exerted whilst evaluation the overlap integral differs between theories. A review (and criticism) of different semi-classical approaches has been made by Russek and Mehlhorn [52]. Eq. 4.5 is an analytical PCI line-shape, derived by van der Straten et al. [51] using the semi-classical JWKB-approximation to compute the integral in Eq. 4.4.

$$P_{\mathrm{PCI}}(\varepsilon_{kin}) = \frac{\Gamma}{2\pi}\frac{1}{\frac{1}{4}\Gamma^2 + \varepsilon_{kin}^2}\frac{\pi C \exp\left[2\frac{C}{v_1}\arctan\left(\frac{2\varepsilon_{kin}}{\Gamma}\right)\right]}{v_1 \sinh\left(\frac{\pi C}{v_1}\right)} \tag{4.5}$$

Here v_1 is the *classical* asymptotic speed of the photoelectron (*i.e.* the speed when $r \longrightarrow \infty$: $\sqrt{2\varepsilon_{\mathrm{XPS}}}$). In the theory of van der Straten et al. [51] C enters as a parameter that corrects the energy shift by accounting for the time it takes for the Auger electron to overtake the photoelectron.

$$C_{\mathrm{ISO}} = \begin{cases} 1 - \sqrt{\frac{\varepsilon_{\mathrm{XPS}}}{\varepsilon_{\mathrm{AUGER}}}} & \varepsilon_{\mathrm{XPS}} \leq \varepsilon_{\mathrm{AUGER}} \\ 0 & \text{otherwise} \end{cases} \tag{4.6}$$

C is tagged with 'ISO', for *isotropic*, since it is integrated over all angles. Strictly speaking the momenta of the electrons should be taken into account, nevertheless angular effects are ignored here; our experiments are performed in the magic angle[12] (57.4°) to minimize anisotropic effects.

We shall see below (and also in chapter 6) that C has a much more elaborate interpretation: it enters the quantum mechanically derived line-shape/cross section as a charge via the Coulombic wavefunctions used to describe the electrons in the final state of the system.

[12] Anisotropic emission of the photoelectrons should be expected since the electrons may carry away some part of the angular momentum imparted by the photon. Within the dipole approximation the differential cross section of electron emission after photon absorbtion can be written [53]:

$$\frac{d\sigma}{d\Omega} = \frac{\sigma}{4\pi}\left(1 + \frac{\beta}{2}\left[3\cos^2\Theta - 1\right]\right)$$

where σ is the angle integrated cross section and Θ is the angle between the emitted electron and the electric field vector. The angular part of the cross section is plotted in Figure 4.9 for the possible beta values -1, 0, 1, 2 (in the figure they can be distinguished by their orientation, -1 vertical, 0 symmetrical and 1 and 2 horizontal, the latter being the outermost.). Upon photoionization of an p electron by a photon (which has angular momentum $\ell = 1$) the outgoing electron wave has angular momentum $\ell = p \pm 1$ consequently the outgoing wave is a superposition of an s-wave and a d-wave. In the magic angle, the intensity distribution of the analyzed electrons is independent of the wave character of the outgoing electrons.

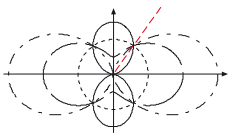

Figure 4.9: The angular part of the differential cross section. The magic angle is defined by the straight line and the abscissa.

4.4.2 Quantum theory of postcollision interaction

"I've got a feeling we're not in Kansas anymore..."

Judy Garland in *The wizard of Oz*

A fully quantum mechanical treatment of postcollision interaction has been done by G. B. Armen, J. Tulkki and coworkers which can be found in Refs. 54 and 55. In the latter a comparison between the analytical semi-classical lineshape and the quantum mechanical 'Coulomb lineshape' is made; it is found that the line-shapes agree excellently if $\varepsilon_{\mathrm{XPS}} \gtrsim \sqrt{\Gamma \varepsilon_{\mathrm{A}}}$. The quantum mechanical formalism is based on the concept of *shakedown* transitions in the continuum, either to a lower continuum state for one of the electrons (ordinary PCI) described in [54, 55] or to a bound state (photoelectron recapture) which is covered in [56]. The mutual screening of the ion by the electrons in the final state is taken care of by a *dynamic* charge Q which differ from unity because of the final state interaction; Q is defined by an expression identical to that of C used in the van der Straten lineshape.

Perhaps the most aesthetic way to express the lineshape (which is the derivative with respect to the energy of the total cross-section: $\frac{d\sigma}{d\varepsilon}$) is to use the radiationless resonant Raman scattering formalism (see Armen and Levin [56], and references therein). Considering excitation following absorption of an X-ray photon *i.e.* processes such that a hole is created at the i^{th} core-level (designated $[i]$) by excitation of the electron to an orbital $x\ell$ – which can be a bound $(m\ell)$ or a continuum $(\varepsilon\ell)$ orbital – leaving the system in a valence two-hole final state $[f, f']$ after the decay of the core hole. The two hole final state can be composed in two ways[13]:

$$A + \omega \longrightarrow A[i]x\ell \begin{cases} \longrightarrow & A[f,f']n\ell + e_s^- \qquad (1) \\ \longrightarrow & A[f,f'] + e_x^- + e_A^- \qquad (2) \end{cases}$$

Either the intermediate state $|\tau\rangle$ decays leaving an electron in a bound orbital $|n\ell\rangle$ and emitting a "spectator" electron (a spectator resonant Auger decay) as in Eq. 1, or it decays by an Auger decay with two electrons in continuum orbitals $|\varepsilon\ell\rangle$ (Eq. 2). If $\Gamma_{i-ff'}$ is the Auger transition rate into a certain final state, the total cross section for the creation of the $[f, f']$ state can be written as a sum of both contributions, keeping in mind that the cross section for the Auger decay must be the differential cross section at a certain energy for the electron already in the continuum. Using atomic units and α as the fine structure constant:

$$\sigma_{[f,f']} = \sigma^+_{n\ell} + \frac{d}{d\varepsilon}\sigma^{++} = \frac{2}{3}\pi\alpha\omega\Gamma_{i-ff'}\left(|\langle n\ell|\ \tau\rangle|^2 + |\langle \varepsilon\ell|\ \tau\rangle|^2\right) \qquad (4.7)$$

[13] *NB!* That throughout the "direct" part – double photoionization of the valence without the creation of a core-hole – is ignored throughout the discussion here.

As of yet, we have not derived any expression for the intermediate state wavefunction $|\tau\rangle$. It is formed by absorption of a photon which induces an excitation in the atom from its ground state $|0\rangle$ creating a core hole in the process. We can formulate this as an inelastic scattering problem: a photon scatters the ground state into a channel such that the photon is absorbed with the accompanying excitation of an electron from shell i into orbitals $x\ell$.

A photoexcitation amplitude can be written $\langle [i]x\ell|\,\boldsymbol{\mu}\,|0\rangle$, where $\boldsymbol{\mu}$ is the dipole operator. However the intermediate state contains both bound and free waves, paraphrasing Ref. 57 we write it as a solution to the Lippman-Schwinger equation:

$$|\tau\rangle = \sum_m \frac{|m\ell\rangle\,\langle [i]m\ell|\,\boldsymbol{\mu}\,|0\rangle}{\omega - \varepsilon_i + \tau_{ml} + i\Gamma/2} + \int_0^\infty d\tau \frac{|\tau\ell\rangle\,\langle [i]\tau\ell|\,\boldsymbol{\mu}\,|0\rangle}{\omega - \varepsilon_i - \tau + i\Gamma/2} \tag{4.8}$$

when inserted into Eq. 4.7 we get the total cross section (with $\varepsilon_{\text{kin}} = \omega - \varepsilon_i$):

$$\sigma_{[f,f']} = \mathscr{C}\left(\sum_m \frac{|\langle [i]m\ell|\,\boldsymbol{\mu}\,|0\rangle|^2}{(\varepsilon_{\text{kin}} + \tau_{ml})^2 - \Gamma^2/4} + \int_0^\infty d\tau \frac{|\langle [i]\tau\ell|\,\boldsymbol{\mu}\,|0\rangle|^2}{(\varepsilon_{\text{kin}} - \tau)^2 - \Gamma^2/4}\right) \tag{4.9}$$

where $\mathscr{C} = \frac{2}{3}\pi\alpha\omega\Gamma_{i-ff'}$ have been used. The sum term, being the spectator part, has a positive binding energy shift τ_{ml} in the denominator. The integral term has a negative energy shift τ which is the asymptotic kinetic energy of the continuum orbitals. Γ is the total width of the intermediate state.

Postcollision interaction shifts intensity from the continuum channels toward the bound states, and if the PCI energy shift is large enough a photoelectron can loose its kinetic energy and end up in a bound state – photoelectron recapture[58]. This process gets increasingly more important the closer the photon energy is to the ionization threshold of the system. Semi-classical theories for the postcollision interaction fail to explain this, which partly explains why there is a limit to the applicability of the semi-classical approach.

Tulkki et al. [54] and Armen et al. [55] have shown that if the overlap between the intermediate state $|\tau\rangle$ and the final state $|\varepsilon\rangle$ is evaluated in a way that takes the change of potential for the electrons in the final state into account, then, if integration also includes summing over bound states, a 'Coulomb lineshape' can be expressed as:

$$P_Q(\varepsilon) = \frac{\Gamma_i}{2\pi}|\langle \varepsilon|\,\tau\rangle|^2 \tag{4.10}$$

where a number of simplifying assumptions has been made, *e.g.* that the dipole matrix element is constant. The overlap describes shakedown

transitions in the continuum because of the change of potential – the intermediate state has a single positive charge, the final state two – the ionic charge in the final state is partly screened, from any electron's point of view, because of the interaction between the two electrons. By writing the overlap as:

$$\langle \varepsilon | \tau \rangle = \int_0^\infty d\tau' \frac{\langle \varepsilon | \tau' \rangle}{\omega - \varepsilon_i - \tau' + i\Gamma_i/2} \tag{4.11}$$

it is possible to calculate the lineshape as a function of the excess energy of the photoelectron using only the constant lifetime width (Γ_i), the Auger electron energy and the dynamic charge Q. The latter is defined by the boundary conditions imposed on the states which are described with Coulombic wavefunctions[14]. Q is defined as $1-\sqrt{\varepsilon/\varepsilon_{\mathrm{A}}}$ if the photoelectron has lower excess energy than the Auger electron's kinetic energy, otherwise $Q = 0$.

The lineshape is a distorted Lorentzian – since the overlap can be written:

$$\langle \varepsilon | \tau \rangle = \sqrt{\frac{\Gamma_i^2}{2\pi}} \int_0^\infty d\kappa' \frac{2\mathscr{A}(\kappa, \kappa')}{\kappa'^2 - (2\varepsilon + i\Gamma_i)^2}$$

the function $\mathscr{A}$, whose explicit form (see Appendix I, of Armen et al. [55]), describes the overlap between the states at a given κ'. If none of the charges in the final state screen each other ($Q = 0$), $\mathscr{A}$ turns into a delta function. For energies sufficiently[15] high above the threshold the quantum mechanical postcollision lineshape is thus a distorted Lorentzian built up from a (continuous) series of Lorentzians at energies reflecting the shake-down energies of the photoelectron.

It is important to stress that what classically is described as "a passage of a slow electron by a faster one after some time" is here an intrinsic *property* of the stationary wavefunction of the final state if the charge of the electrons is described as partly screened by Q.

[14] Coulombic wavefunctions used by Armen et al. [55] to compute the lineshape defined by Equations (4.10) and (4.11) have the form:

$$|\varepsilon\rangle = \tfrac{1}{r}\sqrt{\tfrac{2}{\pi\kappa}} \sin\left(\kappa r + \tfrac{Q}{\kappa} \ln 2\kappa r + \arg\Gamma_i \left[1 - i\tfrac{Q}{\kappa}\right]\right)$$
$$|\tau\rangle = \tfrac{1}{r}\sqrt{\tfrac{2}{\pi\kappa'}} \sin\left(\kappa' r\right)$$

The electron energies enter through the wave numbers $\tau = \frac{\kappa'^2}{2}$ and $\varepsilon = \frac{\kappa^2}{2}$

[15] Sufficiently here means that both electrons remain unbound in the final state, *i.e.* the spectator part of the cross section is insignificant. As a rule-of-thumb[55] this is true when the excitation energy is larger than, or in the order of, $\sqrt{\Gamma\varepsilon_{\mathrm{A}}}$ (≈ 5 eV for Ar $2p$). At least for the argon $2p$ threshold the recapture probability is below 10% already at 2.25 eV excess energy[59].

4.5 Interatomic Coulombic Decay

The Auger process, as discussed above, is only energetically allowed if the double ionization threshold of the system is lower in energy than the singly ionized state. For a valence or inner valence ionized state this is often not the case; the only available relaxation path for the metastable cationic state is then a fluorescent decay (photon emission). This is the case for the lone particle (M) in Figure 4.10.

In a condensed system the situation can be different. A doubly ionized system with valence vacancies on two *different* sites can lie lower in energy than an inner shell ionized state located on a single atom. This state can be reached by that the other particle emit an electron – enabled by a transfer of energy from the ionized atom to the neighbour. This process is depicted for the hypothetical $M \cdot M$ dimer system in the figure.

The existence of such a process (*Interatomic Coulombic Decay*) was theoretically predicted by Cederbaum and co-workers for small hydrogen bonded clusters, pure[60] and mixed[61]. The cases considered first were decays following F $2s$ and O $2s$ ionization of HF and H_2O clusters. It was later also predicted for van der Waals bound systems[62, 63].

An experimental verification of the existence of such a process occurring after Ne $2s$ photoionization in neon clusters were made by Marburger et al. [64]. They observed the low kinetic energy electrons that are a fingerprint of the ICD process. In Paper **IV** (presented in chapter 6) this kind of "ICD electrons" are observed in mixed argon/neon clusters.

The photoelectron spectrum of the inner valence level contains information about the lifetime of the initial single vacancy. The opening of the additional decay channel give rise to a life time broadening of the Lorentzian part of the cluster spectral features *vis-à-vis* the monomer spectra (Paper **IX**). A photon energy dependent study of the effect in neon clusters did show that ICD can have resonant contributions. That is discussed below and in Paper **X**.

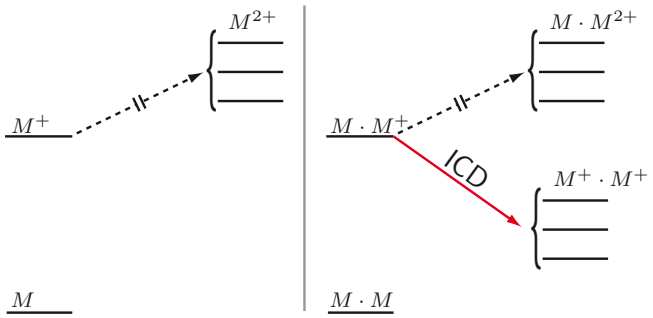

Figure 4.10: A schematic depicting Interatomic Coulombic Decay for a monomer (right) and a dimer system (left). The energy axis is vertical.

5. From electrons to photons – and back

5.1 Synchrotron radiation

– electrons to photons

Synchrotron radiation is as old as the stars in the universe. It can be observed from relativistic electrons bending in magnetic fields, *e.g.* the light from the crab nebula consists of such radiation. On earth the first observation of manmade synchrotron light was made at General Electric Research Laboratory in Schenectady, New York, on April 24, 1947[65]. At first the light produced was considered a curiosity and a nuisance since it caused the accelerated particles to lose energy. But the high polarization and intensity of the light caused the development of electron accelerator rings dedicated to produce light in bending magnets (2^{nd} generation sources). The rings built today are equipped with insertion devices such as *wigglers* and *undulators* to produce light of even higher intensity (3^{rd} generation, *e.g.* MAX II).

The development in the field is fast and, the 4^{th} generation sources, both new rings and so called *Free Electron Lasers* will outclass the current facilities by orders of magnitude in brilliance and photon flux.

5.1.1 Bending magnets, wigglers and undulators

Considering only the case where the acceleration is perpendicular to the direction of motion, the radiated power per unit solid angle for an electron in its rest frame ($\mathcal{S}^\star$) can be written[4], if θ is the angle between the observation point and the velocity vector:

$$\frac{dP}{d\Omega} = \frac{e^2|\dot{\mathbf{v}}|^2}{16\pi^2\varepsilon_0 c}\sin^2\theta \tag{5.1}$$

This is the same distribution we would obtain for a slowly moving particle (*i.e. Cyclotron radiation* which corresponds to the $\frac{v}{c} = \beta \approx 0$ case in Figure 5.1). If the particle is relativistic the expression above needs to be modified in the observers frame of reference ($\mathcal{S}$); Eq. 5.1 needs to be transformed to take into account that signals sent out from $\mathcal{S}^\star$ is not instantaneously received in $\mathcal{S}$. If the observer is in the plane of the orbit

we then get:

$$\frac{dP}{d\Omega} = \frac{e^2|\dot{\mathbf{v}}|^2}{16\pi^2\varepsilon_0 c}\frac{(1-\beta\cos\varphi)^2 - \left(1-\beta^2\right)\sin^2\varphi}{(1-\beta\cos\varphi)^5} \tag{5.2}$$

This equation describes the instantaneous power of a relativistic charge in circular motion[66]. In Figure 5.1 this equation is plotted for very slow electrons and electrons at 9/10 the speed of light. The above equation describes the case of an electron in a bending magnet, and it shows that synchrotron radiation has a very attractive quality: an intense directed light beam from a (nearly) point-like source[1].

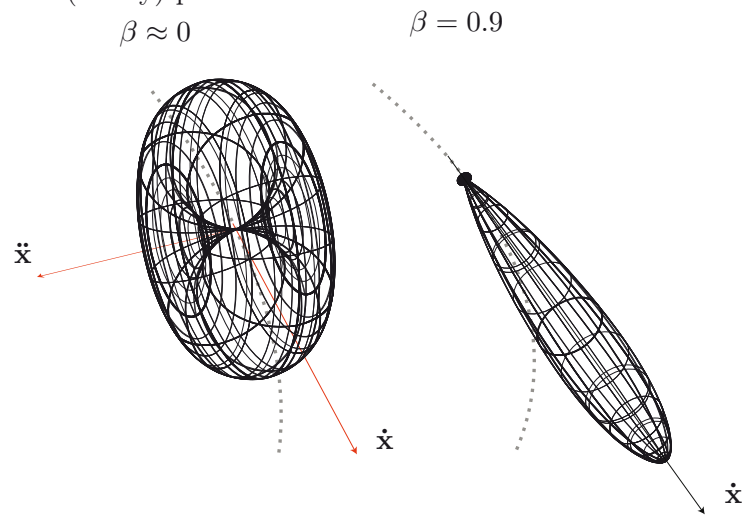

Figure 5.1: Radiated power per unit angle for an electron in circular orbit. To the right the dipole radiation field of a non-relativistic ($\beta \approx 0$) electron is shown. This is also the radiation field in the rest frame of the relativistic electron. In the laboratory frame of the electron moving at relativistic speeds the emitted radiation is heavily focused in the forward direction of the electron motion. The picture do not take into account the difference in magnitude of the emitted power – which is orders of magnitude higher for the synchrotron radiation case.

To improve upon the characteristics for a dipole magnet the path is obvious: make the electron turn more (either sharper turns or many)! If we would let the electron pass through a periodic magnetic structure *i.e.*, an array of dipoles as in Figure 5.2a, we would get more photons emitted per meter. Such a structure is either called a *wiggler* or an *undulator*. The magnetic field in a dipole is set by the demands of the storage ring, *i.e.* the electrons should move in a circular orbit; A wiggler (or undulator) can use a much higher field since in the periodic structure of them the electron returns to its proper circular path. In Figure 5.2b expressions for

[1] Intensity, point-likeness and directionality taken together is called *brilliance*.

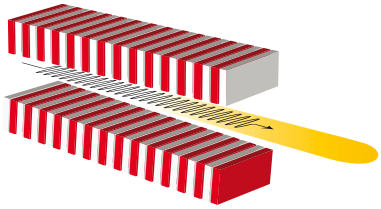

a Electron trajectory through an undulator.

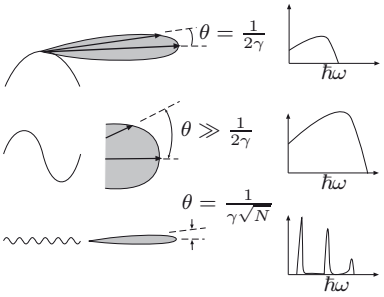

b Angular divergence and power structure of bending magnet, wiggler and undulator radiation.

Figure 5.2: Insertion devices and their properties regarding forward focusing and the spectrum of the emitted radiation.

the how the opening angles of the radiation cones emitted from different magnetic structures depend upon $\gamma = \frac{1}{\sqrt{1-\beta^2}}$ and the number of turns in the lattice N. Typical intensity versus photon-energy spectra are also depicted.

The wiggler is sometimes called a wavelength shifter, since its short path with few, but strong, magnets increase the brilliance by mainly enabling the use of a much higher magnetic field which leads to higher main frequency of the photons.

An undulator on the other hand is built up from many magnets in such a way that constructive and destructive interference occur between the wavefronts created, which increases the brilliance by sharpening the light cone and concentrating the radiated power into a number of allowed wavelengths (harmonics).

5.1.2 What does a synchrotron provide?

Synchrotron light is used for a variety of experiments by a multitude of different scientific disciplines, from biology to physics. Such a diversity is (partly) explained by the main properties of the synchrotron light:

1. The photon energy is *tunable*.
2. The photon flux is high from the far IR into the hard X-ray region.
3. The high brilliance of the source.
4. The extremely high degree of light polarization achievable.
5. Time structure that, *e.g.* allows for coincidence measurements.

5.2 Beamline I411 at MAX-lab

– photons to electrons

5.2.1 MAX-lab

MAX-lab is the national Swedish laboratory for synchrotron radiation studies. The laboratory started with the MAX I 500 MeV electron storage ring in 1986 and the MAX II 1.5 GeV electron storage ring, a 3rd generation synchrotron equipped with several undulator and wiggler beamlines[2], was opened to users in 1997.

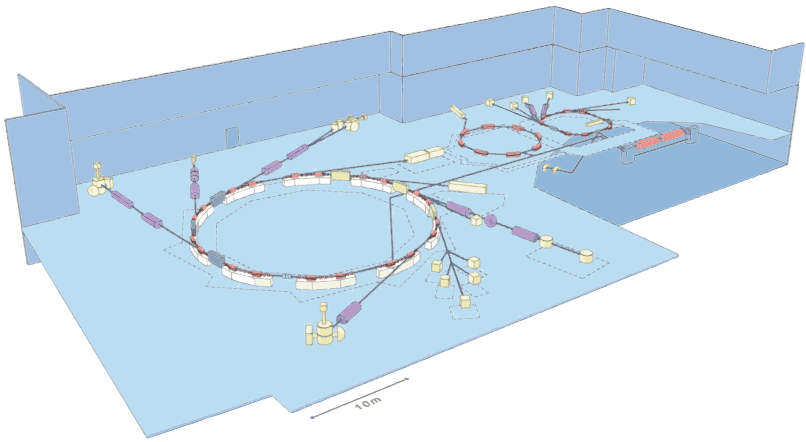

Figure 5.3: The MAX-laboratory. The large ring is the MAX II electron storage ring, MAX III is in the middle and MAX I rightmost.

5.2.2 Beamline I411

Our experiments have been performed at beamline I411 [67, 68] which was constructed mainly for photoelectron spectroscopies of matter in various states, *i.e.* gases, liquids, clusters and solids. The beamline is supplied with light from an 88 pole undulator[3] which produces photon energies in the region of 50-1500 eV.

The light passes a monochromator, which narrows down the photon bandwidth, then enters the experimental end station equipped with a Scienta R4000 electron spectrometer which can be rotated in a plane perpendicular to the photon beam. For more details concerning the beamline consider Figure 5.4 which is taken from [67].

[2]The light transported from the storage ring to the experimental station via a "beamline".
[3]$\lambda_u = 58.85$ mm and the minimum gap is 23 mm.

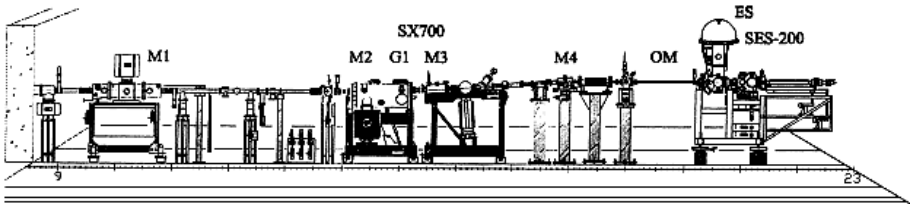

Figure 5.4: Layout of the beamline. M1 is the horizontally focusing pre-mirror. The M2 mirror, the plane-grating monochromator G1 and the focusing mirror M3 are all inside the Zeiss SX-700 monochromator. M4 is a refocusing mirror before the one-meter section OM. At the end station (ES) the Scienta SES-200 electron analyzer was situated. Nowadays the ES is equipped with a Scienta R4000.

5.2.3 The electron energy analyzer

In Figure 5.5 a hemispherical electron analyzer is illustrated. The basic idea behind it is simple enough: photoelectrons from the ionized sample are accelerated in the electric field between the two hemispherical electrodes and are spatially dispersed in proportion to their kinetic energy when they have traversed the approximately 180° of the analyzer[4]. Only electrons with a kinetic energy (within a tolerance) such that their trajectory coincide with the radius of the spectrometer will hit the detector.

An electron lens system which decelerates or accelerates the electrons to a fixed energy is mounted prior to the hemispheres. This is done to achieve constant resolution, independent of the initial kinetic energy of the electrons. The resolution of the analyzer, to the first order, can be written[69]:

$$\frac{\Delta E}{E} = \frac{s}{2r} = \mathrm{C}$$

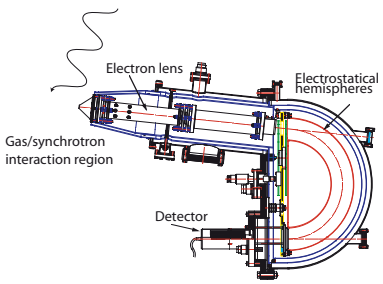

Figure 5.5: A hemisperical electron energy analyzer.

where s is the entrance slit width and r the radius of the analyzer. If the electrons were unretarded we would get $\Delta E = C \cdot E_{\mathrm{kin}}$ meaning that the resolution would vary with the kinetic energy. If the electrons were retarded to a certain energy E_p, the resolution is *fixed* to $\Delta E = C \cdot E_p$. This can also be a vast improvement on the resolution if $E_p < E_{\mathrm{kin}}$.

The energy E_p is usually called the *pass energy* and determines the resolution of the spectrometer at a given slit width.

[4] Because of fringing fields at the entrance slit the angle between the entrance slit and the exit slit is slightly less than 180°.

5.2.4 The cluster source

For the cluster experiments an in-house built cluster source has been used, see [70] (and references therein) for details. It operates on the adiabatic expansion principle. The sample gas is led into the system at pressures around 1-5 bars. The gas enters the expansion chamber through a cooled[5] conical nozzle with an opening angle of 20° and 150 μm diameter. The majority of the atoms passing through the nozzle never end up in a cluster, therefore the expansion chamber needs a high pumping capacity; two large turbo pumps keep the pressure in the 10^{-3} mbar range.

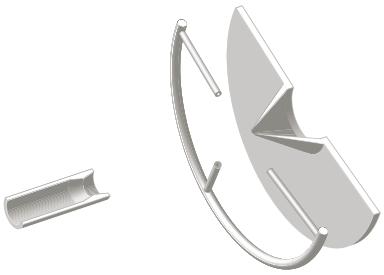

Figure 5.6: The cooled nozzle, doping needles and the skimmer. Before entering the analyzer chamber the cluster beam is skimmed off, hence a low enough pressure can be kept to allow the electron spectrometer to operate properly

In the analyzer chamber synchrotron light ionizes the cluster beam and the subsequently emitted electrons are analyzed. This chamber is separated from the expansion chamber with a conical skimmer, since the pressure must be kept under 10^{-5} mbar for the well being of the electron spectrometer.

A doping stage can be added to the expansion chamber, consisting of four thin needles mounted perpendicular to the cluster beam before the skimmer. With this it is possible to add atoms or molecules (that are gases) to the clusters produced by the cluster source.

Additionally the beamline is also equipped with a liquid beamsource that allow the study of liquids in vacuum[71]. There is also a resistively heated oven source that can be used to produce clusters from liquids, *e.g.* water. A combined gas aggregation oven source, as well as a sputtering source for metal cluster production have recently also been taken into operation[72].

[5] With liquid nitrogen or water as a coolant.

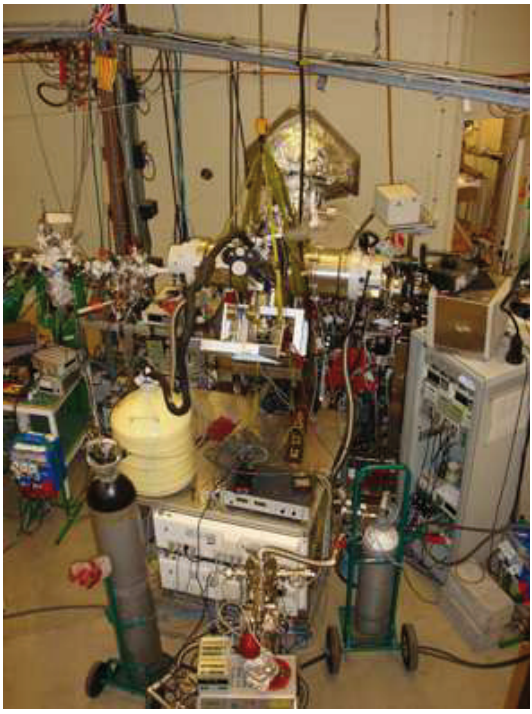

Figure 5.7: The experimental setup in real life which obviously can be very different from schematic illustrations. The mushroom shaped object covered in aluminum foil is the electron spectrometer.

6. Results

6.1 Postcollision interaction in clusters

To extract reliable quantitative information, *e.g.* binding energies, about a system from curve fitting, the lineshapes used to perform the fitting must take into account the basic physics of the system. A Lorentzian, for example, takes into account the finite lifetime of a state. In Paper **I** an extension of the existing models for the postcollision interaction lineshape is made to include the effects of finite assemblages of atoms and infinite solids.

Chapter 4 explains how polarization screening in clusters lower the energy of the final state. In the same chapter, a detailed description of the postcollision interaction effect, which is attributed to an exchange of energy between the photoelectron and Auger electron, is described. How accentuated the effect is depends on the relative energies of the electrons, the difference in ionic charge and the delay time between photoelectron and Auger emission (if we consider a two-step process). It is possible to describe the final state interaction with the aid of a *dynamic* charge[55]:

$$Q = \begin{cases} 1 - \sqrt{\frac{\varepsilon_{\mathrm{XPS}}}{\varepsilon_{\mathrm{AUGER}}}} & \varepsilon_{\mathrm{XPS}} \leq \varepsilon_{\mathrm{AUGER}} \\ 0 & \text{otherwise} \end{cases} \tag{6.1}$$

Q differs from 1 because of the mutual screening of the ion in the final state by the two electrons. This expression is identical to that defining the C_{ISO} parameter in the van der Straten lineshape (see Equations (4.6) and (4.5) respectively). The predictions for semi-classical models – such as those presented by Russek and Mehlhorn [52] and van der Straten et al. [51] – have been shown to coincide with those of the quantum theory[55] if the condition $\sqrt{\Gamma\varepsilon_{\mathrm{AUGER}}} \leq \varepsilon_{\mathrm{XPS}}$ is fulfilled. This is convenient since the semi-classical van der Straten lineshape is an analytical function – in other cases (often) exhaustive computation of integrals are needed which lessens the appeal, if the intended use is curve fitting.

6.1.1 A bulk model

As a starting point we can consider postcollision in an infinite piece of a dielectric medium. All charges considered are polarization screened. If we write the energy exchange caused by the potential change, in atomic units, as a function of the separation R we obtain for a free atom $-\frac{1}{R}$.

Approximating the solid as a linear isotropic medium with permittivity ϵ the potential change becomes $-\frac{1}{\epsilon R}$.

Knowing that Q is a charge, we expect it to be screened as well; to fit the spectrum from an infinite solid:

$$Q' = \frac{Q}{\epsilon}$$

should be used instead of C in Equations (4.5) and (4.6).

Indeed a smaller PCI asymmetry is observed for the bulk part of cluster spectra in argon, krypton and xenon. This is most evident in the argon $2p_{1/2}$ spectra in the lower panel of Figure 6.2.

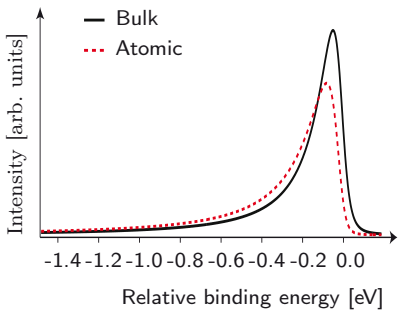

Figure 6.1: Lineshapes drawn using Equation (4.5). Note the shift and broadening of the atomic line compared to the bulk solid line.

6.1.2 A cluster model

If instead the piece of material we consider is finite, we can no longer rely on the fact that the charges are *always* partly screened. We know however that as long as the passage of the electrons occur *within* the material that the charges are screened just as in the bulk case. Hence if the Auger electron swiftly passes the photoelectron we can expect the passing to occur *inside* medium. However if the photoelectron is *outside* the material the exchange of energy is equal to that of a free atom: the total charge inside a sphere containing the medium and the ion is the same independent of ϵ by Gauss' law for the electric field.

A photoelectron from a surface atom has a much larger probability to be passed outside the cluster than one emitted from a bulk atom. Thus postcollision interaction for photoelectrons emanating from surface atoms can approximately be considered as equal to that of the free atoms.

	ϵ
Ar	1.61
Kr	1.9
Xe	2.23

Table 6.1: Relative permittivities for the noble gases considered.

6.1.3 Experimental results

The naïve approach of fitting a cluster feature by setting the PCI asymmetry parameter equal to that of an atom and just adjusting kinetic energy of the Auger and photoelectrons caused by the cluster chemical shift has a much larger residue than a fitting done with the considerations of the presented model for the surface and bulk peaks. The error – in a least square sense – is 40% smaller in the latter case for the argon spectrum in the lower panel of Figure 6.2.

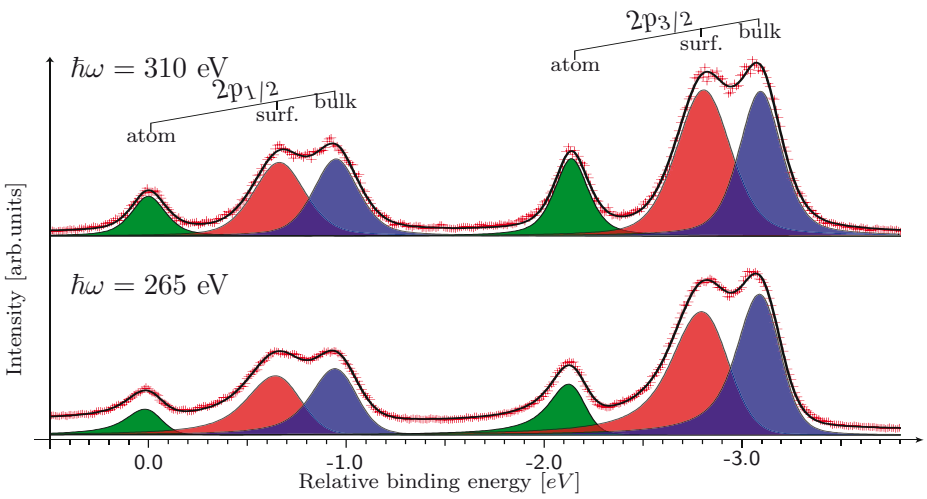

Figure 6.2: Photoelectron spectra of argon clusters $<N>\approx 1600$. The energy scale is relative to the binding energy of the atomic $2p_{1/2}$ level. Shaded areas mark the results of a least square fit employing the model described in the text.

To examine the dependence of the postcollision parameter on the permittivity a series of measurements on clusters composed of argon, krypton and xenon respectively was performed. The permittivities are listed in Table 6.1. The photon energies were chosen in each case to give one spectrum with negligible postcollision interaction effects and one spectrum with an atomic asymmetry such that $C_{\mathrm{ISO}}/\sqrt{2\varepsilon_{\mathrm{xps}}} \approx 0.6$. In Figures 6.2 and 6.3 the XPS spectra of the different clusters for the different situations can be found. For each case the effect is most pronounced for the cluster bulk feature with the highest binding energy (corresponding to lowest photoelectron kinetic energy).

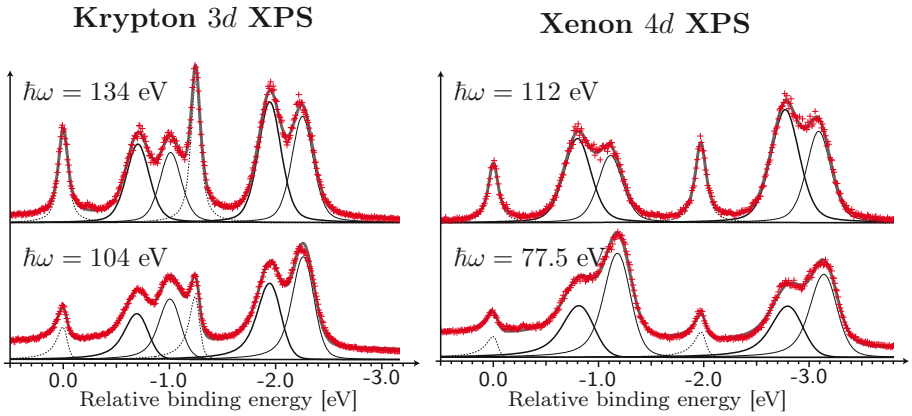

Figure 6.3: Spectra of krypon and xenon clusters with $\langle N \rangle \approx 1600$.

6.2 Doped vs. co-expanded cluster structure

6.2.1 Co-expanded clusters: radial mixing vs. segregation

In chapter 3 the structure of mixed noble gas clusters was discussed from an equilibrium point of view. If the cluster starts out from a 'hot' liquid state – implying high mobility of the particles – then, considering only the difference between cohesive energies a separation should occur with the species having lowest cohesive energy on the surface. The detailed work of Clarke and co-workers with regard to this are summarized on p. 39, *et seq.*

Paper **III** presents a study of mixed argon/xenon clusters produced by a co-expansion of the gases – both with respect to mixing ratio of the primary mixture (2.5, 5 and 9%) and the stagnation conditions. In Ar $2p$ and Xe $4d$ core photoelectron spectra from a previous study spectral features from the surface, interface and bulk parts of the mixed clusters was identified[42]. By varying the stagnation conditions our later study contain core level spectra of mixed clusters with similar chemical shifts and intensity distributions as seen before *and* mixed clusters with smaller chemical shifts and with a very small bulk feature (hence smaller clusters). The width and shape of the cluster feature in the Xe $4d$, for the 2.5 and 5% mixtures, allows for the identification of surface, interfacial and bulk Xe – and in one case a fourth component. Via a calculation of the polarization shifts of a xenon atom on top of and inside a model cluster consisting of a Xe core, covered with a monolayer of argon. The fourth component of the spectral feature was thus interpreted as being photoelectrons from Xe atoms with small argon coordination in the surface and even on top of the mixed Ar/Xe cluster. For the same system, this kind of sites have also been observed with fluorescence spectroscopic methods[73].

Because of the narrow photon energy range of the beamline where the experiments were carried out the valence photoelectron spectra (Ar $3p$ and Xe $5p$) were used to confirm that mixed clusters were indeed produced. The argon and xenon parts of the valence spectra were in all cases observed to be different from that of pure clusters. This is taken to be an indication of mixed cluster production.

For the 9% mixture only the lower stagnation pressure produce a spectral feature in the valence corresponding to Ar cluster production. The high pressure spectrum shows, basically, a flat line in the same region. For both pressures of this mixture. a surface and bulk part were observed in the Xe $4d$ core level spectra. In this case, argon goes from taking part in mixed cluster formation, as a constituent of the final cluster configuration, towards being a buffer gas facilitating the Xe cluster formation[1].

[1] *I.e.* the cooling gas co-expansion considered on page 34.

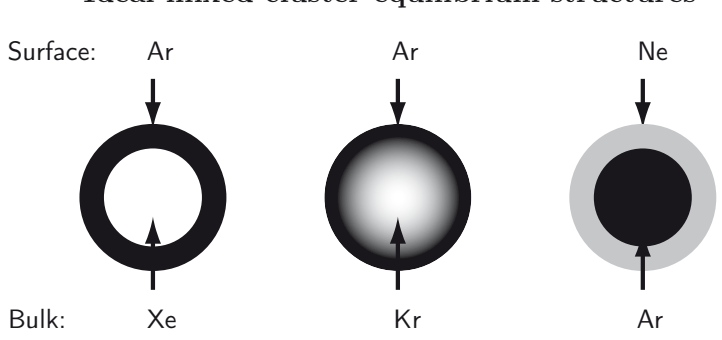

Figure 6.4: Illustrations of the structures predicted by equilibrium considerations. Those are *idealizations* of the mixed cluster structures produced in co-expansion experiments. The mixed cluster structures from a co-expansion of Ar/Xe is discussed in Paper **III**, Ar/Kr in Paper **II** and Ar/Ne in Paper **IV**.

Similar structures are found for mixed Ar/Ne clusters created by the co-expansion technique; in Paper **IV** a Ar/Ne mixing ratio dependent study (at constant stagnation conditions) was carried out. Those spectra can also be found in Figure 6.5. That mixed clusters actually were produced was monitored by direct measurement of electrons from the Interatomic Coulombic Decay emanating from a mixed Ar/Ne environment. Observation of electrons at the kinetic energy specific for Ar/Ne coordination is a very strong indication of that production of mixed clusters indeed occurs. A more detailed discussion on this mixed cluster ICD can be found below (pp. 86 *ff.*)

By analyzing the cluster spectral features of Ne 2*s* and the Ar $2p_{3/2}$ levels as a function of this a number of observations can be made. At low argon percentages there is only one argon peak in the cluster spectra. In the Ne 2*s* spectra, the cluster feature contains both a surface and a bulk part – the latter being very much broader, and shifted towards lower binding energy compared to the pure neon cluster case. Argon has a higher polarizability than neon, thus if neon is coordinated to Ar a better screening of the core ionized state gives it a lower binding energy than the pure bulk neon. The two peaks in Ne 2*s* are thus interpreted as surface neon (with neon coordination) and interfacial neon (with both neon and argon coordination). With the same argument it can be concluded that argon with neon coordination is less efficiently screened and will thus have a smaller chemical shift than argon with only argon neighbours, compared to the monomer. This suggest that the single peak Ar cluster feature in the Ar core level spectra of the 1 and 2% mixtures corresponds to a (very) small argon core surrounded by neon atoms. The calculations made of the induced polarization of atoms ionized at different sites on

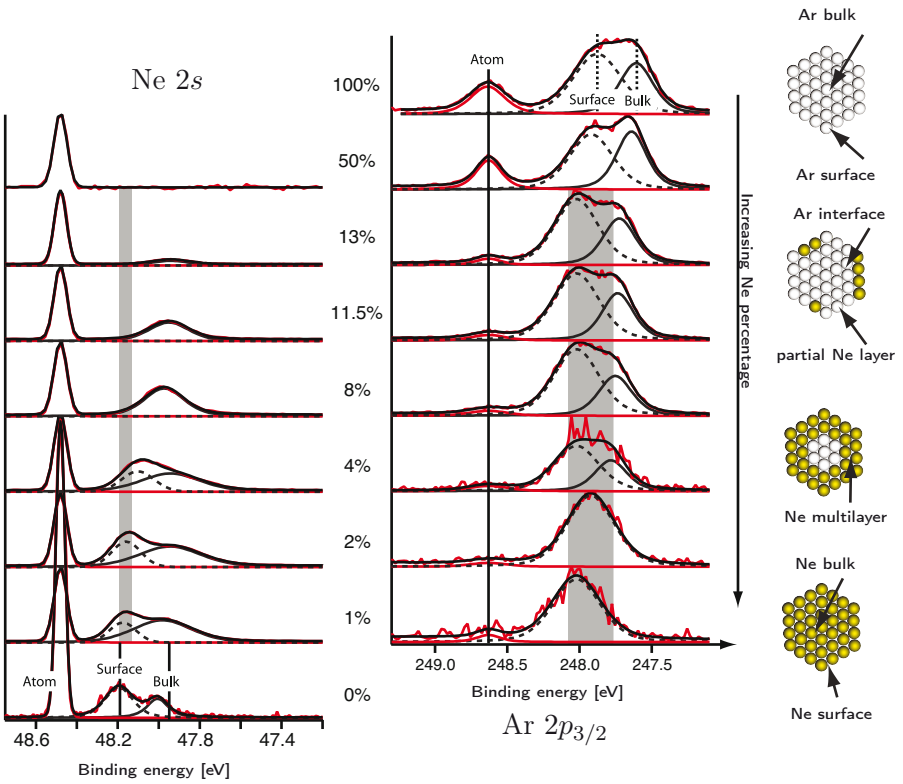

Figure 6.5: The shaded areas indicate calculated shifts for different sites on and within a model system consisting of an argon cluster covered with a neon monolayer.

a model argon cluster covered with a monolayer of Ne atoms support this. The shaded areas in Figure 6.5 indicate where the shifts end up for ionized neon and argon at different positions.

With increasing Ar percentage in the primary mixture the most obvious development is the gradual disappearance of the neon interface peak in the neon spectra, and the gradual appearance of something that ultimately develops into an argon bulk feature in the argon spectra. The chemical shift of the argon interface peak also gradually converges toward the Ar surface shift, suggesting that the number of argon atoms on the surface with mixed argon/neon coordination diminishes.

With 50% Ar in the mixture no neon cluster features can be seen in the Ne 2*s* core level spectra. Neon thus functions as a buffer gas for the Ar cluster process and no mixed clusters are produced.

If the constituent atom kinds have similar bond lengths and strengths (Ar/Kr) the deviation from this ideal structure is larger than if they are dissimilar (Ar/Xe, Ar/Ne). The sharpness of the interface between the

different constituents can be related to the equilibrium bond distance in the Lennard-Jones potential – a big difference gives a sharp interface; conversely, a small difference gives a diffuse mixing gradient.

The results of investigations on the Ar/Xe co-expanded system by Tchaplyguine *et al.*[42] and those presented inPaper **III**, and the Ar/Kr system (Paper **II**), are also vindicated by direct measurement of the cluster geometries by electron diffraction[74, 75].

6.2.2 Doped clusters

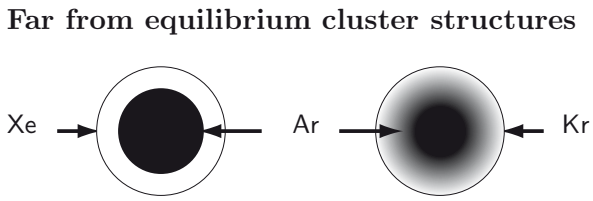

Figure 6.6: Illustrations of the structures observed for Ar host clusters doped with Kr and Xe (Paper **VI**).

So far we have only considered the co-expansion case for production of mixed clusters. But what happens if we add particles to an already formed cluster as in the doping case?

Consider an already formed cluster A_N. Adding hot particles B to the cluster adds a certain amount of energy per added atom. If the addition rate of guest atoms is low, the host cluster can accommodate the energy by transferring it to internal degrees of freedom (*e.g.* vibrations) or by evaporation of either A or B particles. If the rate of cooling is similar to the rate of heating mixed clusters are produced. How far the B particles penetrate into the host clusters depends, in this case on what happens *locally*, for a short time diffusion is effective for the dopant. Obviously what 'low' rate means depends on the size and type of the host cluster – larger clusters can absorb larger amounts of energy due to their larger number of internal degrees of freedom, clusters composed of particles with higher binding energy have higher melting point. The cluster to the right in Figure 6.6 depicts one extreme case; the host cluster stays intact and the dopant just adsorbs on the surface of the host.

High doping rates cause larger parts of the host cluster to heat up. This allow dopant molecules to move deeper into the cluster. The other limiting case – where the cluster still stays heterogeneous[2] – is when the doping rate is so high that the host cluster becomes liquid and the

[2]Evaporation predominantly occurs for the species with lowest cohesive energy. It is even possible to create pure clusters consisting of dopant particles only, so-called *cluster aggregation*[76].

subsequent cooling would result in a structure close to that of the equilibrium[3].

Doped argon/krypton clusters

The first part of Paper **VI** contains a comparison between the structure of krypton doped argon clusters and their co-expanded relatives. In Figure 6.7 the Ar $2p$ and Kr $3d$ spectra of pure clusters are compared with those of heterogeneous clusters of both kinds. Included are curve fits done with three components: monomer, surface and bulk. For the argon spectra the modified van der Straten lineshape discussed above was used to take postcollision interaction effects into account; for krypton a Voigt lineshape was utilized throughout.

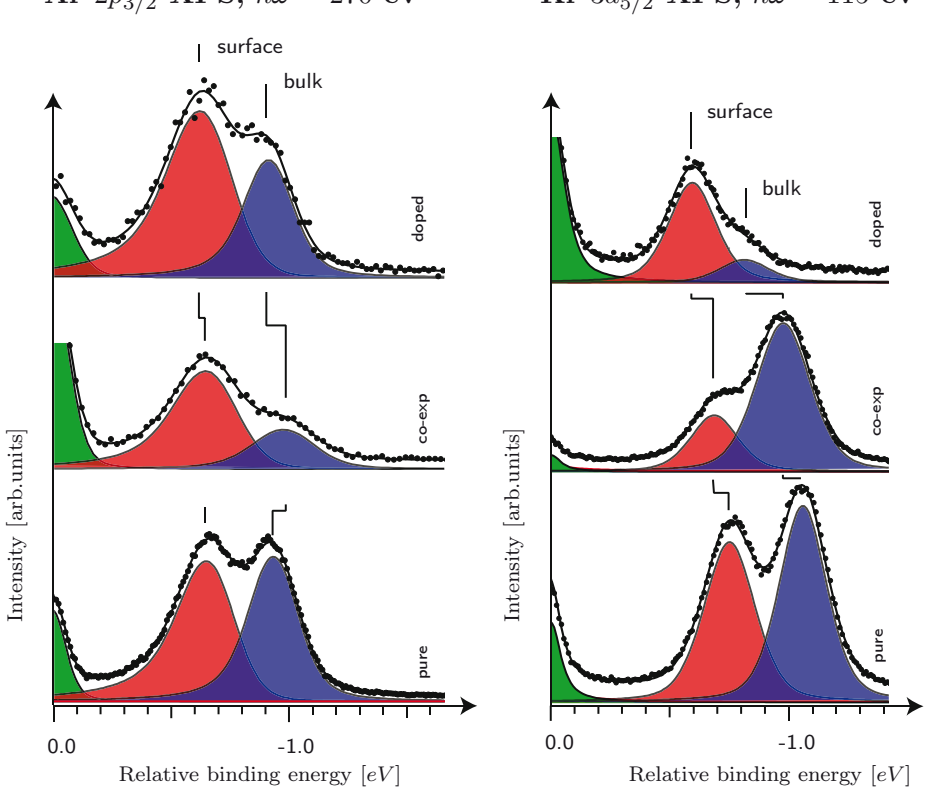

Figure 6.7: XPS spectra of the argon $2p_{3/2}$ and the krypton $3d_{5/2}$ core levels, for different situations, *i.e.* pure clusters, clusters formed in co-expansion and doped clusters. The vertical lines in both panels mark the positions of the surface and bulk features. The monomer feature is put at 0 eV in all spectra.

In the argon spectra of the heterogeneous clusters, the surface component is larger in both cases, for the co-expanded clusters this is more

[3] *I.e* like the structures found for co-expanded clusters (Figure 6.4).

pronounced. A large difference can be found in the krypton spectra; the ratio of the surface component area and the bulk component area is 81% in the doped case compared to 25% for the co-expanded. From this it can be deduced that the structure of doped clusters is far from that of co-expanded – the element with the highest cohesive energy is found at the surface and not in the bulk.

The host clusters had a mean size of $<N>\approx 7000$ which seems to be enough, at the doping pressure in question, to effectively hinder the diffusion kinetics that would allow the dopant to penetrate deeper into the host.

Paper **VII** presents a series of data where both the doping pressure and the Ar host cluster size are varied. The smallest host clusters were the ones most heavily doped, the largest host clusters was treated the lowest doping pressure. An examination of the chemical shifts of the doped clusters reveals that the Kr atoms have high argon coordination and that they reside on the surface of the cluster. The surface feature in all Kr $3d$ spectra was at higher binding energies relative to the surface (and bulk) features of pure Kr clusters. A further support of this conclusion is the high surface intensity compared to the bulk intensity.

A close look at the Gaussian widths, obtained from least square fits to the data, revealed that the width of the krypton surface peak was smaller than the bulk peak for the middle and largest sized host clusters (and correspondingly decreasing doping pressures). This is unexpected since the abundance of different sites (and thus different polarization screening, implying different chemical shifts) on the surface should make it broader than the bulk, where the coordination number is constant.

Doping is expected to, if anything, *increase* this width; the number of different coordination number should increased since not only one kind of atom participate in the polarization screening. Other broadening mechanisms, *e.g.* the size distribution in the beam, vibration in the clusters can not explain this difference. The remaining option is that the number of different sites that the Kr atoms occupy on the Ar host surface is limited. The dominating contribution to the chemical shift for an atom in a van der Waals cluster comes from the polarization screening from the nearest neighbours[46]. Thus, if only few of the conceivable possibilities of coordination are actually populated the intensity in the core level spectra should pile up at (more or less) the same chemical shift.

Provided that the cluster core does not melt due to the doping, the way for the cluster as a whole to lower its energy is to place the atoms with the highest cohesive energy at high coordination sites. Calculations of the polarization screening of a single Kr on different sites in/on large argon cluster and a calculation of Kr in an Kr island on top of an argon cluster, makes it possible to identify the sites when the computed shifts

are compared to the spectra. Computed shifts for 8 and 9 coordinated Kr, for both situations, cover the binding energy range where the surface part of the Kr cluster feature is observed in the Kr $3d_{5/2}$ core level spectra for the mixed clusters.

This kind of *preferential site occupancy*, of the atoms with the highest cohesive energy, of a mixed cluster have also been observed for Ar/Kr mixed clusters created with the co-expansion technique[77].

Mixed argon/xenon clusters

The second part of Paper **II** contains a similar analysis as was done for the argon/krypton case and a study on the structure as a function of Xe doping pressure. The argon host cluster size was chosen to be very large, *i.e.* $<N> \approx 30000$.

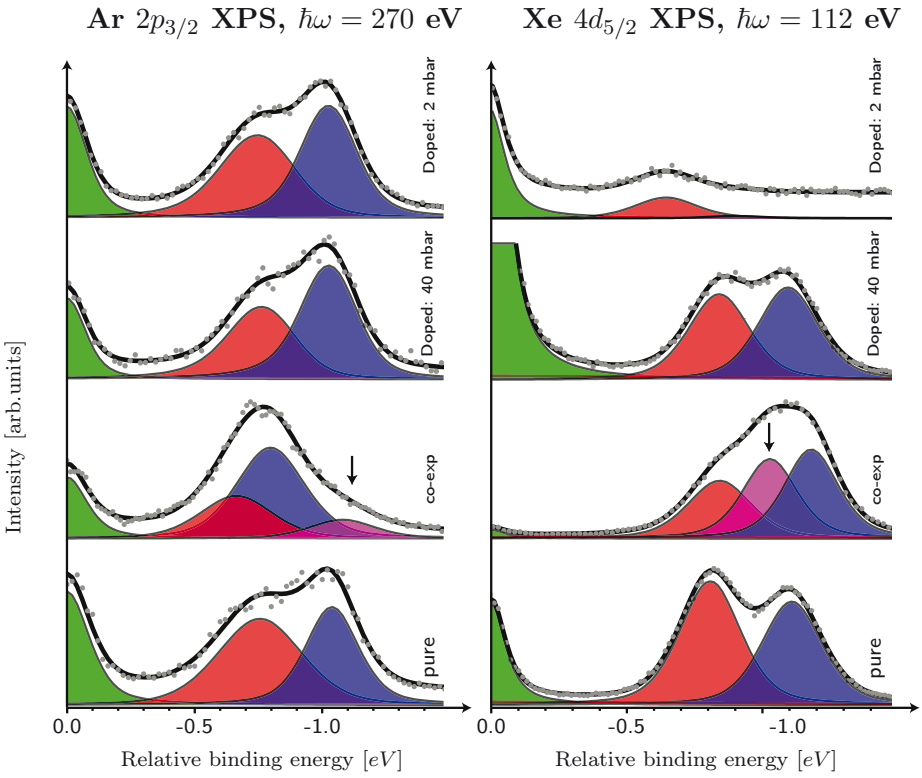

Figure 6.8: XPS spectra of argon $2p_{3/2}$ and xenon $4d_{5/2}$ for different xenon doping pressures. Spectra of pure argon and pure xenon clusters are included for comparison. The clusters formed in co-expansion were produced from a mixture of 3.2% Xe in Ar. The doped clusters were created with ∽40 or 2 mbar Xe doping pressure. In the Ar and Xe spectra the energy positions of both bulk and surface features coincides with that of pure clusters for the 40 mbar doping case. The arrow indicates the energy position of the interfacial feature of the co-expanded clusters. The monomer feature is put at 0 eV in all spectra.

Co-expanded argon/xenon clusters have been found to have a layered structure with argon on the surface and xenon in the cluster bulk. In the co-expanded spectra in Figure 6.8 a third structure is discernible which has been assigned to stem from the interface between the argon and xenon by Tchaplyguine et al. [42].

We have compared those spectra to those of very heavily doped and very gently doped clusters. Firstly, no interfacial feature is needed to get a reliable fit of the spectra. In both cases the surface and bulk features in the argon spectra are similar to those found for pure clusters. Again the larger differences is found in the spectra of the dopant. The xenon XPS for the heavily doped clusters displays similar spectral features to pure xenon; the spectra corresponding to low doping pressures display no such similarity: the surface part dominates the spectrum completely (surface to bulk ratio: 95%).

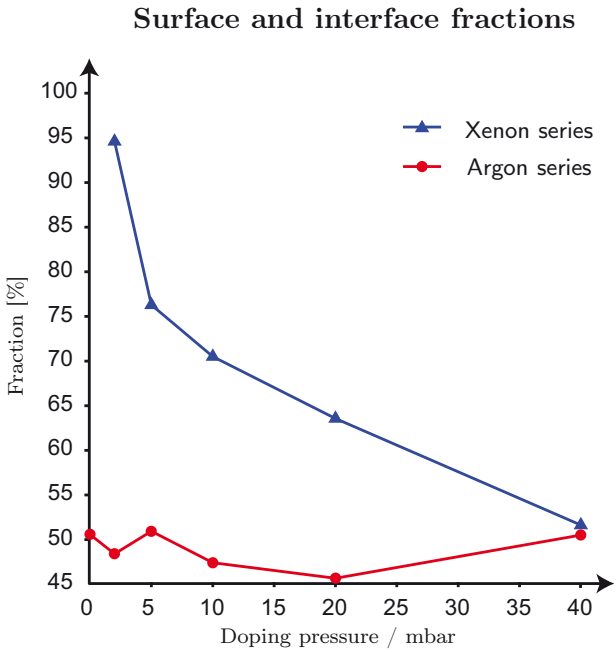

Figure 6.9: Surface fractions from the XPS spectra of argon $2p_{3/2}$ and xenon $4d_{5/2}$ for different xenon doping pressures. The surface fraction for pure argon clusters are included for comparison (at 0 mbar doping pressure).

The surface to bulk fractions in spectra taken at different doping pressures can be found in Figure 6.9. The argon part is only slightly perturbed by the doping whereas the Xe surface to bulk ratio decrease with increasing doping pressure suggesting that the Xe-Xe coordination increases. With increasing doping pressure, the energy shifts for both Xe cluster features approach those of the pure xenon cluster.

This is consistent with a structure where Xe atoms with increasingly higher xenon coordination resides on top of (and ultimately inside the surface layer) of a cluster which still retains large parts of pure argon surface and a pure argon bulk. A schematic of the clusters for low and high doping pressures can be seen in Figure 6.4. Geometries similar to this are found in molecular dynamics simulations of Xe doped Ar clusters [35, 78] for low doping rates.

6.2.3 Argon hosts with molecular dopants; O_2, SF_6

In Paper **VIII** and **V** represent a (modest) broadening of the scope; still using the – by now well known – argon cluster as host molecular dopants are used, oxygen and sulphur hexafluoride. Both molecules were studied with respect to doping pressure. Oxygen by its valence photoelectron spectrum and SF_6 via the sulphur $2p$ core level photoelectron spectrum. For the latter molecule results on the pure molecular cluster were also recorded.

The oxygen molecule proves to be a serendipitous case – the outermost valence state remain localized in the clusters. Even in the cluster features of the valence spectra, the vibrations of the molecules can be seen. For the host size ($N \simeq 8000$), and doping pressures considered, no band formation of the molecules can be seen[4]. Thanks to the local character of the outermost valence state (from here on refered to as the X-state of the oxygen molecule) and that broadening from life-time contributions is extremely small (at least from an photoelectron spectroscopic point-of-view) together with the resolution achievable at photon energies around $\hbar\omega = 60$ eV the Ar/O_2 system can be studied in great detail. The oxygen X-state of the clusters can be accurately reproduced with a least squares fit to the experimental spectrum using shifted and broadened molecular progressions, using only one fails to reproduce the cluster valence lowest binding energy feature. This procedure is similar to the one used for determining the surface and bulk chemical shifts of noble gas cluster core levels.

Naïvely we could, stretching the analogue to the noble gas core level case, assign those features "surface" and "bulk" oxygen molecules on and inside the argon cluster. However, if there were such an arrangement the intensity of the different features should vary with the photon energy since thus the kinetic energy of the photoelectrons is changed[5]. No such

[4] In contrast to the valence spectra of *e.g.* Ar/Kr, [77], where the valence bands were used to confirm that mixing occured.

[5] With higher photon energies, the kinetic energy of the photoelectrons are increased proportionately (the photoelectric effect). Since electrons have a limited escape depth (typically in the order of Ångströms) photoelectron spectroscopy is surface sensitive[9] – something which indeed is observed in the Ar $2p_{3/2}$ spectrum.

intensity variation are observed in the cluster part of the oxygen X-state spectrum (figure 4. in the paper). Given that two components are needed to accurately account for the cluster spectral features a series of calculations of polarization shifts were carried out. Each site were weighted to account for the relative abundance of different sites.

The conclusion from the calculation is that for low doping pressures the overwhelming majority of the oxygen molecules end up on the surface or in the first layer beneath it. With increasing doping pressures the growth of features corresponding to oxygen molecules in the Ar bulk increases. The Ar/Xe doped series in Paper **VI** presents a similar trend for Xe – the dopant penetrates into the bulk for high doping pressures and stays in the surface layer for low. An important difference is that information about the geometry of the clusters could be extracted from the valence spectra of the molecule. Provided that the valence state remain local and that little, or close to no, life-time contribution to the state blurs the valence a very sensitive probe on the geometrical structure exists.

Repeatedly, the use of simple energy arguments in terms of Lennard-Jones parameters and/or cohesive energies, taken together with the relative size of the constituting atoms/molecules has proven to provide a simple and robust explaination for structures of mixed noble gas clusters.

The sulphur hexafluoride SF_6 is an inert molecule with octahedral symmetry. It possesses a small hexadecapole moment. Its Lennard Jones equilibrium distance (considering the molecule as a hard sphere) is 1.162 times that of argon. Thus the energy penalty of introducing it in an argon matrix should be severe. Paper **V** contains S $2p$ core level photoelectron spectra of pure sulphur hexafluoride clusters – as a reference for a pressure dependent study of mixed Ar/SF_6 clusters. The host clusters had a mean size of about 3600 atoms in the experiments and the doping pressure was varied between 1400, 500 and 250 mbar.

In Figure 6.10 it can be seen that the changes in the argon core level spectra are small. A detailed analysis show them to broaden and that the surface to bulk ratio increases with higher doping pressure, indicating that the clusters get smaller. This is to be expected because of the higher doping rate.

In the sulphur spectra – for the mixed clusters – it can be seen that, for the all doping pressures the shift of the cluster feature is in between the surface and bulk features of the pure spectrum. A tendency to shift towards the bulk value for the chemical shift with increasing doping pressure can also be discerned. The feature also becomes wider at the same time.

Argon has a lower polarizability than sulphur hexaflouride which is reflected in the shallower Lennard-Jones potential, in Figure 3.5, p. 38.

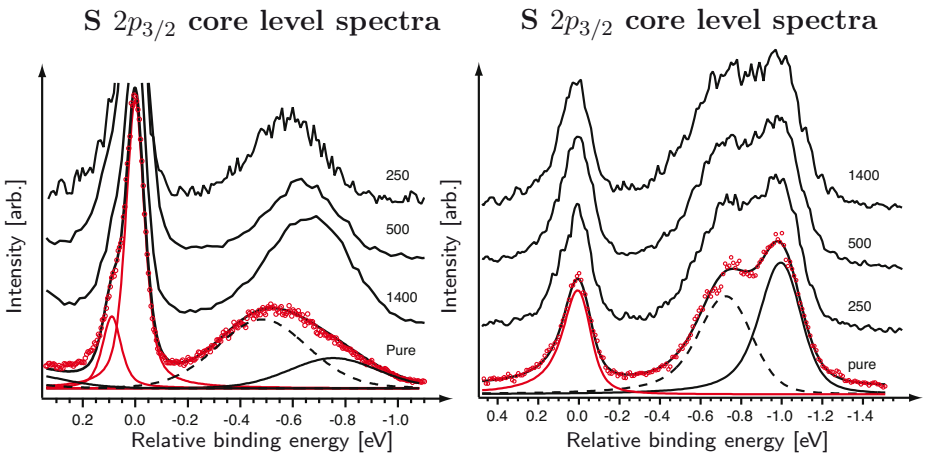

Figure 6.10: S $2p_{3/2}$ core level photoelectron spectra of pure clusters (at bottom) with results from the curve fitting procedure included. The spectra from the doping experiments have their doping pressures indicated (in mbar). The binding energy scale is relative to that of the monomer. The surface component of the cluster component (dashed, bottom) have -0.48 eV chemical shift relative to the monomer, the bulk component (full, bottom) is found at -0.76 eV.

The mixed Ar-SF_6 pair potential is similar to that of the Ar-Xe one. By the arguments of used in Paper **III** and in Ref. 42 a core-shell structure should be expected with a strong segregation.

Indeed, the shift of the cluster feature in the sulphur spectra shows neither the same shift as the bulk SF_6 (*i.e.* with full coordination), nor a shift resembling that of a SF_6 surface (*i.e.* low, but still coordination to other SF_6). Furthermore, the width of the SF_6 line is smaller than that found for the cluster feature of the pure clusters. This points to that the SF_6 molecules have large coordination with argon atoms in the mixed case – otherwise a bulk or surface shift would be discerned in the S $2p$ spectra.

If an argon atom with very large SF_6 coordination were ionized, the polarization screening would be more efficient than in the pure Ar bulk case – new features should then be clearly discernible in the low binding energy part of the argon cluster feature (as is observed in co-expanded Ar/Xe for instance). An argon atom on the surface with high SF_6 coordination should also be shifted towards lower binding energies. In the argon spectra we observe that the shifts stay the same and that the cluster features broaden somewhat with increasing doping pressures.

An structure that explains the observations made is that a part of the argon cluster core stays intact and that the SF_6 molecules have high argon coordination but still leaves most of the surface part of the cluster intact.

How can such a structure be realized with the Ar-Xe and Ar-SF_6 pair potentials being so similar? We remember that the argument for the argon/xenon case's sharp segregation built upon the differences in size between the atoms. SF_6 is much larger than the Xe atom, thus the segregation could be expected to be even more sharply defined in this case. However, simulations of SF_6 in an argon matrix show that the molecule, by substituting two argon atoms in the crystal nearly leaves the bond distances in of the closest argon atoms and their neighbours intact[40]. Hence, by occupying such a *matrix state* the molecule introduces very little strain in the crystal.

The cluster core stays intact for all the doping pressures considered, but with higher doping pressures a larger part of the cluster surface melts which allow the SF_6 molecules to gain higher SF_6 coordination, though still with substantial Ar coordination as seen in the shifts.

6.3 Interatomic Coulombic Decay

6.3.1 Manifestations of ICD in Ne_N inner shell spectra

ICD provides an additional decay channel for the metastable singly ionized state of an atom in a cluster, besides the fluorescence and Auger channels – the only ones available for the monomer. If present, it should manifest itself with an additional Lorentzian lifetime broadening of the *cluster* spectral features in comparison to the monomer feature. In Paper **IX**, the $2s$ inner shell spectra of neon clusters are investigated in this respect.

Direct observation of low kinetic energy electrons emanating from an interatomic columbic decay process was first made in neon clusters[64, 79]. Figure 6.11 is an illustration of the process for both the free and condensed neon case. The $2p^4$ state is neither energetically allowed in the free, nor in the condensed phases. However, a dicationic state can be reached in the condensed phase that has two vacancies on different atoms. The Coulombic repulsion between the two holes is lowered by their separation lowering the double ionization threshold sufficiently to make the process energetically allowed.

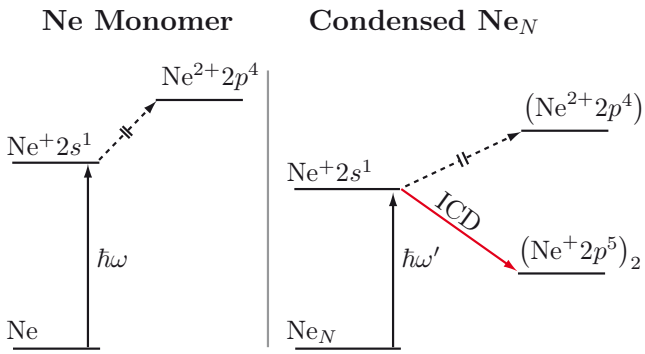

Figure 6.11: A schematic of dicationic states and radiationless decays for the neon atom in free and condensed phases, for the excited states only atoms which participate in the process is shown. The radiative fluorescence decay path is not shown. Since no Auger decay path exist for the Ne $2s$ state, Interatomic Coulombic Decay is the only channel giving rise to the additional life-time width of condensed neon.

Neon proves to be a nearly ideal test case for this process, since the $2s$ level of the isolated neon atom can not decay via the Auger channel; thus the ionized state can only have fluorescent decay, *i.e.* by emitting a photon. The Ne $2s$ state is thus very long lived in the monomer, the life-time is in the order of pico-seconds[80], and the Lorentizian broadening is correspondingly small – in the order of μeV (Eq. 4.2). The life-time in neon clusters of the $2s^1$ state was predicted to be *ultrafast*, *i.e.* in the

order of femto-seconds[81, 82]. This corresponds to a Lorentzian broadening of the spectra in the order of a hundred meV – something which should be discernible in ordinary photoelectron spectra.

Paper **IX** contains a size dependent investigation of the Ne 2*s* inner valence level. The mean cluster sizes considered are 100, 250, 600, 900 and 1100 atoms. The 900 atom spectrum is presented in Figure 6.12. In contrast to the case of Ar 3p (also presented in the paper) that has no ICD channel open, a fit only using Gaussian components for the monomer, surface and bulk components does not reproduce the intensity distribution of the Ne 2*s* cluster features. By including a Lorentzian component of both the surface and bulk components – *i.e.* using a Voigt function to represent each component of the cluster feature – the spectral features are satisfactorily reproduced. By letting the widths be independent of each other in the least squares fitting procedure the life-times of the surface and bulk of the clusters can be extracted.

The strength of the Interatomic Coulombic Decay channel depends on the number of neighbours. For the bulk part a lifetime of 6 ± 1 femto-seconds was found; the lifetime of the surface is a considerably longer 30 femto-seconds. Both numbers is on par with what has been predicted by *ab initio* methods for small neon clusters[81, 82].

6.3.2 Resonant Interatomic Coulombic Decay

A detailed excitation energy dependent study of the 0-35 eV electron kinetic energy region for photon energies around the neon 2*s* ionization threshold, are presented in Paper **X**. The photon energy was increased in steps of 0.2 eV between 37 and 52 eV. The Ne 2*s* has an ionization energy of about 48.475 eV[*ibid.*] (labeled IP_{2s} in the spectra, in Figure 6.13).

The experiment was carried out at BESSY (Berliner Elektronenspeicherring - Gesellschaft für Synchrotronstrahlung, Berlin, Germany) using a cluster setup[6] with three pairs of Helmholtz coils around the experimental chamber to compensate for external magnetic fields. The ICD electrons from neon clusters typically show up around 1.2 eV kinetic energy[64] and thus any external magnetic fields would have a large impact on their trajectories.

With the setup used, a temperature of -230 °C and a stagnation pressure of 428 mbar yields a mean cluster size of approximately 70 atoms (using the scaling laws discussed previously). At photon energies above the Ne cluster 2*s* ionization potential the finger print signal of Ne ICD can be observed around 1.2 eV electron kinetic energy. This feature stays constant in kinetic energy when the photon energy is changed. The Ne 2*s* photolines can be seen at 4 eV kinetic energy for $\hbar\omega = 52$ eV, the cluster

[6] 80 μm nozzle diameter, 30° opening angle. Cooled with liquid helium.

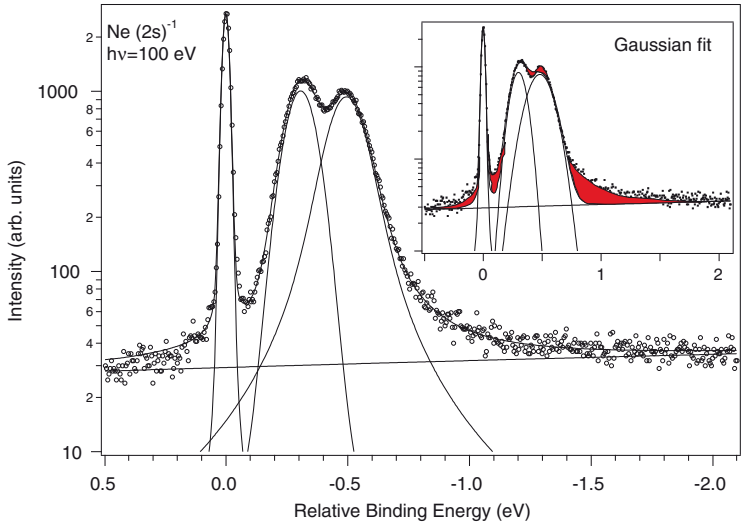

Figure 6.12: Photoelectron spectrum of the Ne 2*s* inner valence level. The cluster mean size for this experiment was 900. The inset contains a fit using only Gaussian components – obviously not accounting for the intensity that is shaded. In the large spectrum a Lorentzian component was added to the surface and bulk features. The instrumental broadening was determined by the monomer Gaussian width of 30 meV. The ordinate axis is logarithmic to emphasize the tails of the distributions.

feature at sligthly higher kinetic energy. A feature that disperses with the photon energy is also easily seen in the spectrum, its energy corresponds to a $2p^{-1}$ ionization accompanied by the creation of an exciton[7], creating a state which can, for instance, be written:

$$\mathrm{Ne}_{N-2}\mathrm{Ne}(2p^{-1}3p)\mathrm{Ne}2p^{-1}$$

This have been measured previously for slightly larger ($\sim$ 300 atoms) neon clusters[84]. The authors report a binding energy of approximately 39 eV for the first excitonic feature (or 17.6 eV energy loss w.r.t. the neon $2p$ line).

At two photon energies resonant enhancement of the low kinetic energy part of the spectrum occurs at slightly different kinetic energies. At a photon energy of 47.5 eV the resonance occurs between 1-3 eV kinetic energy, for $\hbar\omega = 47.1$ eV the resonantly enhanced part of the spectrum is between 1.5-4 eV. The $2s \rightarrow 3p$ excitons for bulk and surface neon have

[7] An *exciton* is a metastable electron hole pair created in the condensed state[27]. It is an energy loss mechanism by which an outgoing photoelectron excites an atom on the way out, thus loosing energy. In contrast to inelastic scattering this loss mechanism is discrete in nature and give rise to distinct features in photoelectron spectra.

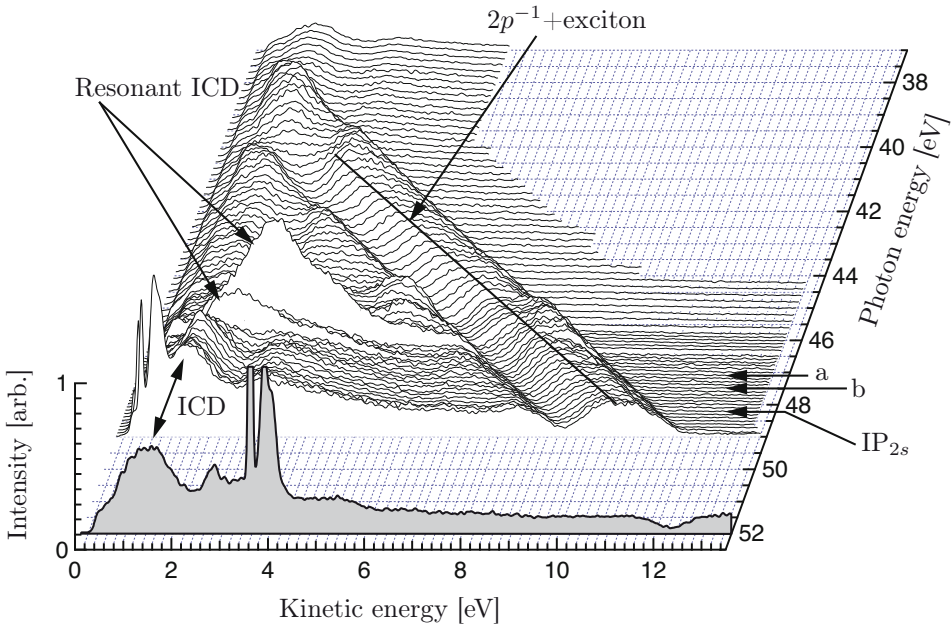

Figure 6.13: Below the Ne 2*s* ionization threshold two photon energies (a & b) can be noted – one with resonances in the 1-3 eV kinetic energy region and one with a resonance in the 1.5-4 eV region. Above the 2*s* threshold, the region around 1.2 eV displays a sizable peak constant in kinetic energy – a hallmark of ICD electrons (*vide supra*). The spectrum is adapted from Ref. 83, and used with the kind permission of Silko Barth.

been measured by electron yield and ion desorption from condensed Ne at 46.9 and 46.4 eV respectively[85]. These values are slightly lower than the ones measured[8], they can be used to assign the features in our spectra as being cluster versions of the same process which enable an ICD decay.

$$\mathrm{Ne}_{N-1}\mathrm{Ne}(2s^{-1}3p) \longrightarrow \mathrm{Ne}_{N-2}\mathrm{Ne}(2p^{-1}3p)\mathrm{Ne}3p^{-1} + e^-_{\mathrm{ICD}}$$

The kinetic energy of the electrons is slightly higher than that of "ordinary" ICD electrons. This can be explained by the better shielding of one of the final-state vacancies by the excitation process.

[8]Both the solid $2s \rightarrow 3p$ and the cluster dito are blueshifted compared to the atomic Ne 45.5443 eV[86]. The blueshift of the excited levels can be understood from the negative electron affinity of the Ne solid (E_a =-1.3 eV[85], which causes a blueshift of the excited levels (the Rydberg series converge to the bottom of the conduction band which can be found -E_a above the vacuum level). The upward shift (and level compression) is somewhat reduced by the screening of the ion core. This explains the difference in shifts between the surface and bulk parts of the spectra – the lower coordination of the surface atoms is reflected in the smaller shift compared to the atom. Excitons in noble gas clusters (and solids) are detailed, in depth, in the Ph.D. thesis of Joppien[87].

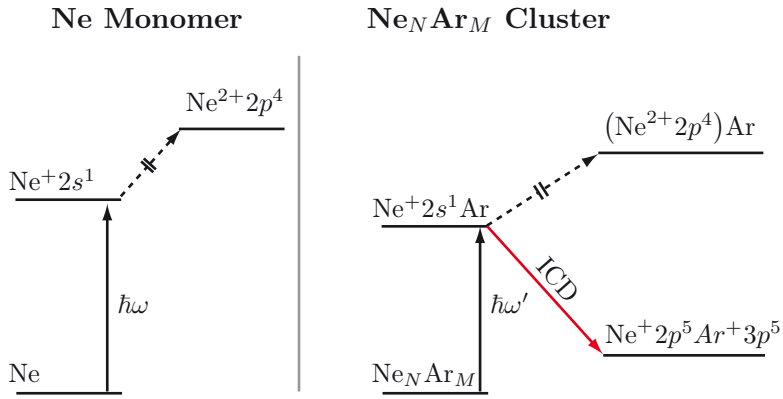

Figure 6.14: A schematic of dicationic states and radiationless decays following inner shell ionization of free neon atoms and of mixed argon/neon clusters. The radiative fluorescence decay path is not shown. Since no Auger decay path exist for the Ne 2*s* state, Interatomic Coulombic Decay is the dominant decay of the inner shell hole state for mixed argon/neon clusters.

6.3.3 ICD in co-expanded Ar/Ne clusters

Interatomic Coulumbic Decay have also been observed experimentally in mixed argon/neon clusters created from a co-expansion of a mixtures thereof. The ICD rate depends strongly on the distance r between the participating atoms ($\propto r^{-6}$[88]). Thence mixed system ICD processes can be used to gain information about the structure of the mixed clusters. The energies of the electrons emanating from an ICD process involving both the valence orbitals of an neon and an argon atom (*c.f.* Figure 6.14)

$$\mathrm{Ar}_M\mathrm{Ne}_{N-1}\left(Ne^+2s^{-1}\right) \longrightarrow \mathrm{Ar}_{M-1}\mathrm{Ne}_{N-1}\left(Ne^+2p^{-1}\right)\left(Ar^+3p^{-1}\right) + e^-_{\mathrm{ICD}}$$

was used in in paper Paper **IV** to confirm the mixed nature of the Ar/Ne clusters. The ICD electrons from this process have been shown to appear at $\backsim$7.8 eV kinetic energy in spectra[89][9]. The predicted value for the vibrationally unexcited NeAr dimer system from calculations is 7.1 eV[90].

Figure 6.15 shows electron spectra of kinetic energy region where the ICD electrons from the mixed ArNe ICD process are expected to occur. The spectra are taken with different amounts of argon in the primary gas mixture (as discussed above on page 70). The ICD feature is situated

[9]They also find a second, much weaker, structure at about 9 eV kinetic energy. Scheit *et al.* have, by including vibrations for the ArNe dimer predicted such a peak at higher kinetic energy as being the ICD decays with accompanying ν =1 and 2 vibrational excitations. In Ref. 83, S. Barth have indicated that combining the predicted vibrational distribution of the NeAr ICD electrons[90] with experimental ICD spectra[89] and by using Boltzmann statistics that it is possible to extract the temperature of some mixed clusters.

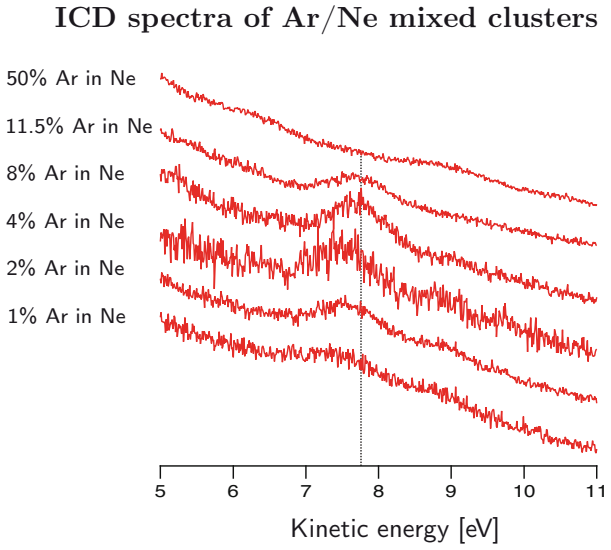

Figure 6.15: The kinetic energy region of where ICD electrons from the Ar/Ne mixed ICD process manifest themselves. The previously measured kinetic energy of such electrons are indicated by the dotted vertical line.

on a broad background coming from the zero kinetic energy edge. It is however no problem to discern the feature on top of this background.

In the spectrum from clusters with a primary mixture[10] of 1% Ar in Ne contains a very small ICD feature. With increasing Ar percentage up to 8% the intensity of the electrons with kinetic energies around 7.8 eV eV increases. With higher mixing ratios the intensity lowers, to disappear completely (*i.e.* becoming non-detectable in the spectrum) for the 50% mixture.

This intensity variation with the mixing ration can be attributed to different compositions of the mixed clusters. With a small percentage of atoms, only a fraction of the Ne atoms in the mixed cluster have any contact with an argon atom – thus the low efficiency at small primary mixing percentages. Besides, in such a situation the Ne-Ne ICD channel competes efficiently with the mixed ICD. Increasing the amount of Ar in the clusters also increase the number of sites with mixed Ar-Ne coordination, allowing a larger number of Ne atoms to decay via the mixed ICD channel. Since no Ar-Ne mixed ICD intensity is found for the 50% mixture, it can be concluded that no mixed clusters are produced under the used experimental conditions.

[10]This percentage should not be confused with the *final* percentage of Ar in the clusters. The final (mean) percentage in the clusters can be estimated via the areas of the spectral components for the monomers and clusters, and the known ionization cross sections for the valence levels. For instance the mixture prepared with 50% Ar in the primary mixture ends up having an estimated 68% of Ar in the clusters.

6.4 Delocalization in cluster Auger spectra

Paper **XI** is an investigation on how the hydrogen bond affects Auger spectra of ammonia. The Auger decay from the molecule is studied both in pure clusters and solvated in liquid water. The liquid experiment used a setup that allows for a liquid beam to be studied *in vacuo* (described in Ref. 71).

For solid rare gas films[91] and argon clusters[92], additional shifted and a broadened copies of the atomic Auger spectrum encompasses all features in the total spectrum[11]. This Auger decay path is denoted C-VV (core-valence valence) in Figure 6.16. Such states correspond to decays where both valence vacancies remain localized on the monomer unit that was core ionized.

The strength of the polarization screening is proportional to the charge squared. Thus knowing the core level binding energy shift $\Delta\mathcal{E}_{\text{xps}}$ we can predict where such localized states should appear in the spectra. The screening of the Auger final state is four times that of the core level's (dicationic *vs.* cationic). The difference in the resulting Auger electron kinetic between those states are thus three times the core level binding energy shift:

$$\Delta\mathcal{E}_{\text{Auger}} = 2^2\Delta\mathcal{E}_{\text{xps}} - \Delta\mathcal{E}_{\text{xps}} = 3\Delta\mathcal{E}_{\text{xps}} \tag{6.2}$$

The Auger electron spectra for water clusters and solid ice have been shown to contain additional intensity at high electron kinetic energies that can not be ascribed to a shift and broadening of the molecular features. The stronger inter-molecular interaction (compared to *e.g.* van der Waals bound systems) between the water molecules allow for a *delocalization* of the two final state valence vacancies. Hence, the Coulomb repulsion between the holes in the dicationic state are lowered and more energy becomes available for the kinetic energy of the Auger electrons[94]. These states are indicated as C-VV' in Figure 6.16.

The Auger spectra, following the decay of the N 1*s* core ionized state, of pure ammonia clusters, aqueous ammonia (and solid ammonia[95]) all contain such high kinetic energy features as was observed in the water case. The spectra can be seen in Figure 6.17.

The measured N 1*s* binding energy shifts are $\sim$2 eV and $\backsim$1.1 eV for the clusters and the liquid solution respectively. The Auger electron spectral features from ammonia in clusters and solution are most easily observed in the high kinetic energy part of the spectra (where no monomer features overlap). At 11.9 eV above the highest kinetic energy feature of the monomer a shoulder can be seen – apart from the one at 6 eV. Compar-

[11] That is provided that the kinetic energy of the photoelectron is sufficiently high, otherwise recapture of that electron cased by postcollision interaction distort the Auger spectra in the high kinetic energy part, as shown in a photon-energy dependent study of the argon LMM Auger done by Lundwall and co-workers[93].

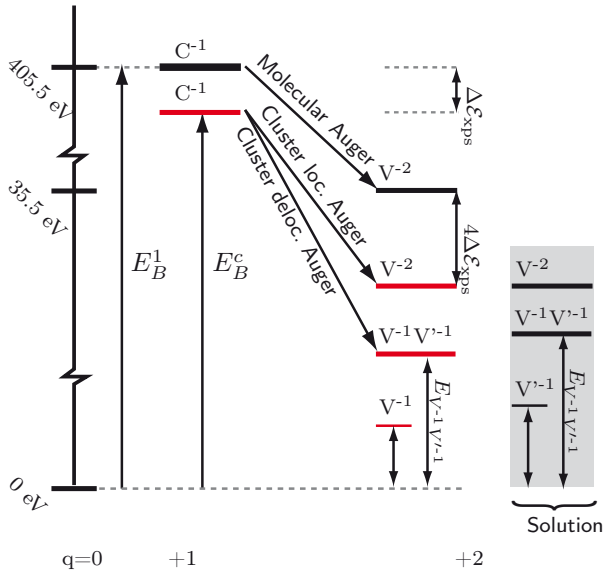

Figure 6.16: Schematic energy level diagram for different cationic states of the ammonia molecule in gas-phase and in cluster-phase. The final dicationic states of the solvated molecule are shown to the right.

ing a least squares fit to the data where only a shifted and broadened molecular spectrum was used, to a fit where this additional feature were included it can be concluded that the feature at highest kinetic energy accounts for 5% of the total Auger intensity. In the Auger spectrum of solid ammonia, published by Larkins and Lubenfeld (Ref. 95) a similar feature is reported – denoted as "satellites".

By using Eq. 6.2 the additional observed Auger features – at about 11.9 and 10 eV Auger electron kinetic energies respectively – N 1*s* binding energies at 4 and 3 eV relative to the monomer core level, *i.e.* about twice the observed chemical shift. No such feature exist in any of the N1*s* spectrum which would correspond to a (very) large relaxation of the singly ionized state. If the final state vacancies were *delocalized* to include one vacancy in the valence of a neighbouring molecule (analogous to the water case) the binding energy of that Auger final state would be lower – thus yielding Auger electrons with higher kinetic energy (The C-VV' channel in Figure 6.16). A calculation of where the Auger energies would be in the clusters – (using experimental valence photoelectron binding energies), indicate that delocalized states would end up in the vicinity of the observed feature.

Calculations of the Auger spectrum of the ammonia monomer and dimer systems[12] are included as stem diagrams in Figure 6.17a. The calculations of the dimer contain features that correspond to delocalized final state vacancies that are facilitated by the hydrogen bond.

In the water solution of ammonia the hydrogen bond pattern is obviously different from that of the clusters. The $H_2O\cdots NH_3$ hydrogen bond is stronger than that between two ammonia molecules. The binding energies of the outermost valence orbital of water is higher than that of ammonia, thus it is plausible that the Auger electrons from a state with one valence vacany on a water molecule and one on the core ionized ammonia molecule would end up at lower kinetic energy than if both vacancies were on different ammonia molecules (as in the cluster). The shaded area in Figure 6.16 depicts this situation in the solution.

The valence features from water and ammonia (both from monomer and the liquid) overlap in the valence, which disallows a straightforward estimate of the Auger energies as were done for the clusters. However, an approximate calculation, using the cluster shifts for the ammonia valence and those of liquid water (more exactly water with KCl solvated into it[13]) puts such delocalization features at about the same energies as the observed high kinetic energy feature in the Auger spectrum of the liquid solution (Figure 6.17b). The valence shifts for the ammonia are almost surely overestimated with this "model" (the coordination number of ammonia in the liquid is smaller than in the clusters), a calculation using the gas phase values (*i.e.* putting the shift to zero) does also put the delocalization features around those features observed in the spectra.

The delocalized states are double vacancies in the valence, situated on different monomer units. Such states can thus be created via direct doublephotoionization, inner shell ionization (ICD) and by Auger decay. Owning to the general nature of the two decay processes, this kind of delocalization should be a common feature in spectra of condensed phases, *i.e.* liquids, solids, clusters. In the Ammonia case those states account for, at least, 5% of the total Auger yield, in water that percentage is higher due to the stronger hydrogen bond (and therefore larger overlap of the valence).

[12] Here a small *caveat* should be given. This calculation is by no means a representation of the Auger spectrum for the whole cluster. What the calculation *does* show is that delocalized states exist for the dimer and that they have a lower binding energy when compared to the calculations of the monomer. Similar calculations on hydrogen fluoride dimers and small clusters[96] and water dimers, as well as liquid water[97] also contain said features.

[13] In aqueous solution KCl is solvated as K^+ and Cl^- ions. In those measurements, delocalization features were observed in the Auger spectrum following the decay of K^+ $2p$ core hole state[98].

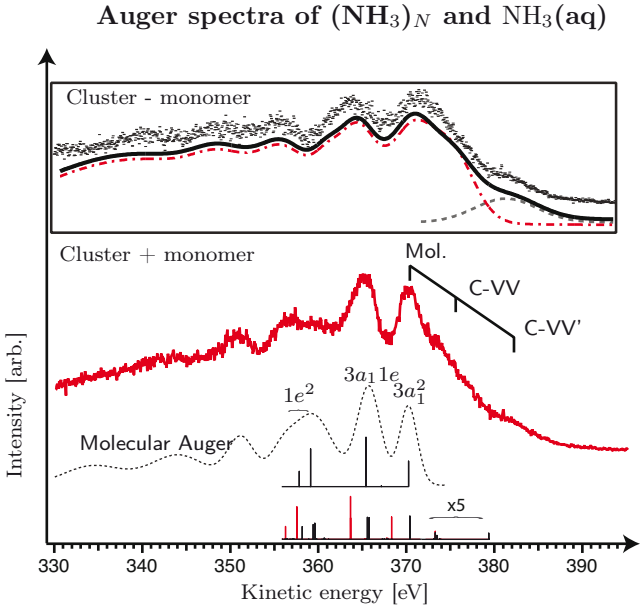

a Molecular (thin dashed line) and Cluster Ammonia Auger. Below the spectra, bar spectra from the calculations discussed in the text are included. The inset shows a the same cluster spectrum, but with the molecular contribution subtracted. Below the subtracted spectrum least squares fit of a shifted and broadened molecular spectrum (dash–dotted) and a fit that include features from delocalized states (bold black line).

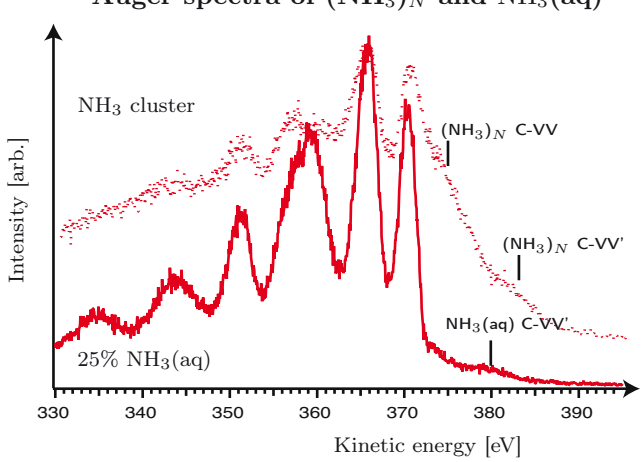

b The liquid Auger spectrum compared to that for the clusters. Vertical bars indicate localized C-VV and delocalized C-VV' states.

Figure 6.17: Auger spectra of ammonia in clusters and in aqueous solution from Paper **XI**. With the exception of the spectrum in the inset (where the monomer contribution has been subtracted) all spectra contain Auger spectral features from both condensed and uncondensed ammonia molecules.

6.5 Outlook & Discussion

In this chapter both an outlook of cluster physics as a whole, and of synchrotron based electron spectroscopy studies of clusters are discussed.

The experimental results presented in this thesis are rather inquires of fundamental nature – of phenomena associated clusters in general and to the techniques used to produce and investigate clusters in particular – than searching for applications of cluster physics.

Though applications of cluster physics indeed are very interesting and promising, there is still a vast number of unanswered questions – of very fundamental nature – that we have yet to find an answer to (or even know how to formulate). For instance, why is the estimate of the nucleation rate in a cluster beam off by 24(!) orders of magnitude[14], when compared to experiment?

An intimate knowledge of model systems (such as rare gas clusters) allow detailed study of general phenomena in a more "sterile" environment, void of the additional complexity of much more complicated systems that, perhaps, we desire to study. Thus it is possible to discern which aspects of a given system is of general nature and which are particular for that system. Case in point is the localization/delocalization features of cluster Auger spectra, from the argon LMM spectra the shifted and broadened atomic spectrum worked well – for water and ammonia this was proven to be insufficient to assign the whole spectrum and the model were generalized to include de-localized dicationic states as well (which in turn helped assign the aqueous ammonia spectrum).

The Interatomic Coulumbic Decay process was predicted in the late 1990's by Cederbaum and co-workers and confirmed experimentally by Marburger *et al.*. Those works have inspired a lot of subsequent experimental (and theoretical efforts) investigating the nature of this phenomenon. It has been shown recently that the dicationic Auger final state of neon and argon in clusters can decay, in a step subsequent to the Auger decay, via ICD creating a triply cationic state, Ref. 100, (and references therein). It remains to be studied how much this affects the life time broadening of the cluster Auger line.

S. Barth (in Ref. 83) has used the ICD decay of mixed Ar/Ne clusters to (tentatively) assign a temperature of mixed clusters. This is very interesting since very few such estimates for cluster temperatures are published; most referenced are the works of Farges *et al.*, who have determined cluster temperatures via electron diffraction measurements[28, 101, 102].

[14] If you predict the speed of a garden snail, who runs about at 0.01 m/s[99] – an all in all reasonable number (for a snail) – to be that of 10 000 billion times the speed of light, you are off by the same order of magnitude.

The study of mixed systems of more applied character – in both free, deposited and bulk form[15] – such as mixed metal clusters, surface stabilized metal/semiconductor clusters[103] – is certainly important for the field as such. The ability of tailoring material properties by their size, for instance band gaps (for *e.g.* solar cell technology), electrical conductivity, capacitance and so forth – will become very important in the future since the size of the components in the processors of our computers (in the time of writing ∼45 nm) are rapidly approaching (and in some respects already passed) the limit of bulk material behaviour. A very good example of this is that a haffnium alloy with a very high dielectric constant is used in modern day transistors in computer processors since the previously dominating SiO_2 insulator when shrunk allows for too high leakage currents which could impair even the device operation totally (see, *e.g.* Ref. [104]).

Selfassembly of nanosized surface stabilized/functionalized nanoparticles have attracted a lot of interest within the chemistry community[103, 105] and spectroscopic investigations on such systems with respect to different ligands should prove very interesting.

With the advent of synchrotron radiation sources with orders of magnitude higher brilliance, such as free electron lasers and new electron storage rings, the number of systems (and aspects thereof) that can be studied with electron spectroscopies are increased. Either by utilizing the increased photonflux – which could allow, *e.g.* mass selected free clusters to be studied or by increased resolution that could enable specific geometric sites.

A higher photon flux would also allow for more dilute systems to be studied, for example chemical reactions on cluster surfaces – possibly even followed in time via pump probe experiments.

Non-linear phenomena such as multiphoton multiionization in the VUV / X-ray regime also becomes available to study – in free electron laser pulses it has been shown that a Xe cluster with 1500 atoms looses, on average, 2-3 electrons *per atom*[106] obviously causing a Coulomb explosion of the cluster, a level of ionization hitherto unexplored with synchrotron radiation methods. Molecular dynamics simulations of such cluster explosions of *e.g.* deutarated methane (CD_4) have pointed towards the possibility of that such an explosion creates deuterons with sufficiently high energy to create a fusion reaction – something that may, at least allow for the study of fusion processes involving heavier nuclei[107].

[15] *i.e.* materials built up from clusters, thus being intermediate to crystalline and amorphous solids.

In summary, the experimental works presented can be divided into two categories; mixed heterogeneous clusters and electronic decay processes (Auger decay and Interatomic Coulombic Decay).

Electronic decay processes in clusters are of fundamental interest but also of interest for applications since Auger spectroscopy is often used to characterize materials (as is core level photoelectron spectroscopy). Particularly the delocalization phenomena is very intriguing. It would be very interesting to find a "better" mixed system than the ammonia/water liquid that would allow a more detailed picture to emerge for the Auger delocalization.

For pure argon clusters the LMM Auger spectrum is photon energy dependent – this was tentatively described as recapture of the photoelectron into a bound unoccupied state caused by (back)scattering of that electron by the neighbouring atoms, thus affecting the intensity of the Auger electrons through the resonant nature of the scattering process[108]. Naturally it would be interesting to see if this intensity variation can be seen in other systems to see if it is of general nature.

Resonant decay processes can offer information on the time-scales on which ultrafast phenomena – such as electron transfer – occur[109]. Processes can be investigated by this technique in the femtosecond – like the electron transfer from an adsorbated molecule into an semiconductor substrate[110], and even in the attosecond domain – as demonstrated for sulphur chemisorbed on a Ruthenium substrate[111] can be investigated.

When I started my Ph. D. studies our group had just begun to do the first mixed cluster experiments with noble gases, and even that added complexity compared to just singel component noble gas clusters proved to contain a rich plethora of things to study – fruits are still there to pick, we just have to find them. Of course mixed molecular, mixed metal, mixed metal/molecular clusters are of particular interest in the areas of catalysis, material physics (alloying, impurity dynamics), surface physics (adsorption, chemisorption, catalytic activity) because of the potential applicability of those systems and all of these systems are within reach with our current experimental equipment. Certainly the new generation light sources provide an even greater opportunity to study those systems in great detail.

7. Acknowledgments

Svante who always have a minute to spare. Without him, I guess that I wouldn't have had the opportunity to go to MAX-lab as a last year engineering student and study accelerator physics – something which sparked an interest which will last for life. For this I am ever grateful.

My supervisors – Olle, Gunnar and Maxim – who have patiently taught me so much along the way, not just about physics. My collegues that I tought hours of mechanics–laborations with in the mechanics lab, and of course all "my" students that I was privileged to instruct there.

Torbjörn, that I have shared office with from the start of my Ph. D., nearly to the very end, travelled with and spent endless hours with talking about everything important in life. Marcus, that I shared a fantastic week in Rio de Janeiro with, together we learned almost what is worth knowing about the art of making (and drinking) Caipirinhas.
Ricardo and Denis for matters regarding caipirinhas, vine and cheese.

The other, current and former, Ph. D. students and post-docs in the surface physics group who I have had the pleasure of having lunch and coffee with: Florian, Karoline, Raimund, Cecilia, Henrik, Wandared, Niclas, Ioana and Sebastien.

Leif Sæthre and Knut Børve who let me visit Kjemisk institutt in the beautiful town of Bergen. Velaug, Maria, Alf, Jarle, Mattias and Mahmoud for the friendly reception on the Bergen visits and the "Norwegian beamtimes".

Uwe Hergenhan and his merry group at Bessy without whom our wonderful times in Berlin might not have happened at all.

Without my friends in Teknologspexet, Snerikes nationsspex (and other societies), the time in Uppsala would have been infinitely more dull and gray. Especially the avantgardistic ℌℜℱ (Humorkollektivet Fistlarne & Skrekkorkestern), Filip, Ivar, Jonas and Torbjörn deserves a special homage – writing comedy for the stage and performing with you will always be the hardest, easiest and most enjoyable experience one can have as an author/actor. Even if we do not really care, they will someday understand.

Rebecka, without your love (and sometimes patience) there is no way that this work could have been completed. I am so happy that we live together and I love you with all my heart.

8. Bibliography

[1] L. D. Landau and E. M. Lifshitz, *Statistical Physics* (Pergamon, 1994), 3rd ed.

[2] A. Messiah, *Quantum mechanics*, vol. I and II (Dover Publications, New York, 1999).

[3] J. J. Sakurai, *Modern Quantum Mechanics* (Addison Wesley Longman, New York, 1994).

[4] J. D. Jackson, *Classical Electrodynamics* (Wiley, 1998), 3rd ed.

[5] H. Haberland, ed., *Clusters of Atoms and Molecules I & II*, Springer Series Chemical Physics Vol. 52 (Springer, Berlin, 1994–1995).

[6] R. L. Johnston, *Atomic and molecular clusters* (Taylor & Francis, London, 2002).

[7] K. Joshi, D. G. Kanhere, and S. A. Blundell, Phys. Rev. B **66**, 155329 (2002).

[8] S. L. Lai, J. Y. Guo, V. Petrova, G. Ramanath, and L. H. Allen, Phys. Rev. Lett. **77**, 99 (1996).

[9] K. Siegbahn, C. Nordling, A. Fahlman, R. Nordberg, K. Hamrin, J. Hedman, G. Johansson, T. Bergmark, S.-E. Karlsson, I. Lindgren, et al., *ESCA Atomic, Molecular and Solid State Structure Studied by means of Electron Spectroscopy* (Almquist and Wiksells, Uppsala, 1967).

[10] K. Siegbahn, C. Nordling, G. Johansson, J. Hedman, P. F. Hedman, K. Hamrin, U. Gelius, T. Bergmark, L. O. Werme, R. Manne, et al., *ESCA – Applied to Free Molecules* (North Holland: Amsterdam, 1969), 1st ed.

[11] P. Buffat and J.-P. Borel, Phys. Rev. A **13**, 2287 (1975).

[12] O. Echt, K. Sattler, and E. Recknagel, Phys. Rev. Lett. **47**, 1121 (1981).

[13] W. D. Knight, K. Clemenger, W. A. de Heer, W. A. Saunders, M. Y. Chou, and M. L. Cohen, Phys. Rev. Lett. **52**, 2141 (1984).

[14] M. L. Cohen and M. Y. Chou, Phys. Lett. **113**, 420 (1986).

[15] P. Atkins and J. de Paula, *Physical chemistry* (Oxford university press, New York, 2002).

[16] J. Harnes, Master's thesis, University of Bergen (2006).

[17] F. Mandl, *Statistical Physics* (Oxford University Press, 1988), 2nd ed.

[18] D. Reguera and H. Reiss, Phys. Rev. Lett. **93**, 165701 (pages 4) (2004), URL `http://link.aps.org/abstract/PRL/v93/e165701`.

[19] J. Wedekind, J. Wölk, D. Reguera, and R. Strey, J. Chem. Phys. **127**, 154515 (pages 11) (2007).

[20] J. Farges, M. F. D. Feraudy, B. Raoult, and G. Torchet, J. Chem. Phys. **84**, 3491 (1986).

[21] G. Voet, Master's thesis, Uppsala University (2004).

[22] R. Karnbach, M. Joppien, J. Stapelfeldt, J. Wörmer, and T. Möller, Rev. Sci. Instrum. **64**, 2838 (1993).

[23] U. Buck and R. Krohne, J. Chem. Phys **105**, 5408 (1996).

[24] O. Hagena, Z. Phys. D. **4**, 291 (1987).

[25] F. Baletto and R. Ferrando, Rev. Mod. Phys. **77**, 371 (2005).

[26] J. Xie, J. A. Northby, D. L. Freeman, and J. D. Doll, J. Chem. Phys. **91**, 612 (1989).

[27] C. Kittel, *Introduction to Solid State Physics* (Wiley, New York, 1996), seventh ed.

[28] J. Farges, M. F. de Feraudy, B. Raoult, and G. Torchet, J. Chem. Phys. **84**, 3491 (1986).

[29] S. Kakar, O. Björneholm, J. Weigelt, A. R. B. de Castro, L. Tröger, and T. Möller, Phys. Rev. Lett. **78**, 1675 (1997).

[30] B. W. van de Waal, G. Torchet, and M. F. de Feraudy, Chem. Phys. Lett. **331**, 57 (2000).

[31] R. Eisenschitz and F. London, Z. Phys. **60**, 491 (1930).

[32] F. London, Z. Phys. **63**, 245 (1930).

[33] R. L. DeKock and H. B. Gray, *Chemical structure and bonding* (The Benjamin / Cummings Publishing Company, Menlo Park, California, 1980).

[34] J. E. Lennard-Jones, Proc. Phys. Soc. **43**, 461 (1931).

[35] H. Vach, Phys. Rev. B **59**, 13413 (1999).

[36] J. Delhommelle and P. Millié, Mol. Phys. **99** (2001).

[37] K. T. Tang and J. P. Toennies, J. Chem. Phys. **118**, 4976 (2003).

[38] J. Bzowski, E. A. Mason, and J. Kestin, Int. J. Thermophys. **9** (1988).

[39] F. Y. Naumkin and F. R. W. McCourt, Mol. Phys. **102**, 37 (2004).

[40] R. Fraenkel and Y. Haas, J. Chem. Phys. **100**, 4324 (1994).

[41] A. S. Clarke, R. Kapral, and G. N. Patey, J. Chem. Phys. **101**, 2432 (1994).

[42] M. Tchaplyguine, M. Lundwall, M. Gisselbrecht, G. Öhrwall, R. Feifel, S. L. Sorensen, S. Svensson, N. Mårtensson, and O. Björneholm, Phys. Rev. A **69**, 031210(R) (2004).

[43] H. Kragh, *Quantum generations* (Princeton Univ. Press, 1999), 1st ed.

[44] L. Karlsson, *Atomic Physics* (Repro fysikum, 2002), 2nd ed.

[45] A. Einstein, Ann. d. Physik **IV**, 132 (1905).

[46] O. Björneholm, F. Federmann, F. Fössing, T. Möller, and P. Stampfli, J. Chem. Phys. **104**, 1846 (1996).

[47] M. Lundwall, M. Tchaplyguine, G. Öhrwall, A. Lindblad, S. Peredkov, T. Rander, S. Svensson, and O. Björneholm, Surf. Sci. **594**, 12 (2005).

[48] M. Lundwall, A. Lindblad, H. Bergersen, T. Rander, G. Öhrwall, M. Tchaplyguine, S. Svensson, and O. Björneholm, J. Chem. Phys. **125**, 014305 (pages 7) (2006).

[49] H. Bergersen, Master's thesis, Uppsala University (2004).

[50] M. Tchaplyguine, R. R. Marinho, M. Gisselbrecht, J. Schulz, N. Mårtensson, S. L. Sörensen, A. N. de Brito, R. Feifel, G. Öhrwall, M. Lundwall, et al., J. Chem. Phys **120**, 345 (2004).

[51] P. van der Straten, R. Morgenstern, and A. Niehaus, Z. Phys. D. **8**, 35 (1988).

[52] A. Russek and W. Mehlhorn, J. Phys. B **19**, 911 (1986).

[53] J. Cooper and R. N. Zare, J. Chem. Phys **48**, 942 (1968).

[54] J. Tulkki, G. B. Armen, T. Åberg, B. Crasemann, and M. Chen, Z. Phys. D. **5**, 241 (1987).

[55] G. B. Armen, J. Tulkki, T. Åberg, and B. Crasemann, Phys. Rev. A **36**, 5606 (1987).

[56] G. B. Armen and J. C. Levin, Phys. Rev. A **56**, 3734 (1997).

[57] T. Åberg and G. Howat, in *Encyclopedia of Physics*, edited by W. Mehlhorn (Springer Verlag, 1981), xxxi ed.

[58] G. B. Armen, J. C. Levin, and I. A. Sellin, Phys. Rev. A **56**, 772 (1996).

[59] J. Tulkki, T. Åberg, S. B. Whitfield, and B. Crasemann, Phys. Rev. A **41**, 181 (1990).

[60] L. S. Cederbaum, J. Zobeley, and F. Tarantelli, Phys. Rev. Lett. **79**, 4778 (1997).

[61] J. Zobeley, L. S. Cederbaum, and F. Tarantelli, J. Chem. Phys. **108**, 9737 (1998).

[62] R. Santra, J. Zobeley, L. S. Cederbaum, and N. Moiseyev, Phys. Rev. Lett. **85**, 4493 (2000).

[63] J. Zobeley, R. Santra, and L. S. Cederbaum, **115**, 5076 (2001).

[64] S. Marburger, O. Kugeler, U. Hergenhahn, and T. Möller, Phys. Rev. Lett. **90**, 203401 (pages 4) (2003).

[65] F. Elder, A. M. Gurewitsch, R. V. Langmuir, and H. C. Pollock, Phys. Rev. **71**, 829 (1947).

[66] J. Schwinger, Physical review **75**, 1912 (1949).

[67] M. Bässler, J.-O. Forsell, O. Björneholm, R. Feifel, M. Jurvansuu, S. Aksela, S. Sundin, S. L. Sorensen, R. Nyholm, A. Ausmees, et al., J. Elect. Spectrosc. Rel. Phenom. **101-103**, 953 (1999).

[68] M. Bässler, A. Ausmees, M. Jurvansuu, R. Feifel, J. O. Forsell, P. de Tarso Fonseca, A. Kivimäki, S. Sundin, S. L. Sörensen, R. Nyholm, et al., Nucl. Instr. and Meth. A **469**, 382 (2001).

[69] B. Wannberg, U. Gelius, and K. Siegbahn, J. Phys E **7**, 149 (1974).

[70] M. Tchaplyguine, R. Feifel, R. R. T. Marinho, M. Gisselbrecht, S. L. Sörensen, A. N. de Brito, N. Mårtensson, S. Svensson, and O. Björneholm, Chem. Phys. **289**, 3 (2003).

[71] H. Bergersen, R. R. T. Marinho, W. Pokapanich, L. J. S. A. Lindblad, O. Björneholm, and G. Öhrwall, J. Phys.: Cond. Matt.. **19**, 326101 (2007).

[72] S. Peredkov, *Free clusters studied by synchrotron-based x-ray spectroscopy: from rare gases to metals* (Lund University, Sweden, 2007), Ph. D. thesis.

[73] M. Lengen, M. Joppien, R. Müller, J. Wörmer, and T. Möller, Phys. Rev. Lett. **68**, 2362 (1992).

[74] O. G. Danylchenko, Y. S. Doronin, S. I. Kovalenko, and V. N. Samovarov, JETP Lett. **84**, 324 (2006).

[75] O. G. Danylchenko, S. I. Kovalenko, and V. N. Samovarov, Low Temp. Phys. **32**, 1182 (2006).

[76] M. Rutzen, S. Kakar, C. Rienecker, R. von Pietrowski, and T. Möller, Z. Phys D **38**, 89 (1996).

[77] M. Lundwall, H. Bergersen, A. Lindblad, G. Öhrwall, M. Tchaplyguine, S. Svensson, and O. Björneholm, Phys. Rev. A **74**, 043206 (2006).

[78] H. Vach, J. Chem. Phys **113**, 1097 (2000).

[79] S. Marburger, *Experimentelle Untersuchungen zum Interatomaren Coulomb Zerfall an Neon Clustern: Nachweis eines ultraschnellen nichtlokalen Zerfallskanals* (Technischen Universität Berlin, 2004), Ph.D. Thesis.

[80] P. Lablanquie, F. Penent, R. I. Hall, J. H. D. Eland, P. Bolognesi, D. Cooper, G. C. King, L. Avaldi, R. Camilloni, S. Stranges, et al., Phys. Rev. Lett. **84**, 431 (2000).

[81] R. Santra, J. Zobeley, and L. S. Cederbaum, Phys. Rev. B **64**, 245104 (2001).

[82] N. Vaval and L. S. Cederbaum, J. Chem. Phys. **126**, 164110 (2007).

[83] S. Barth, *Untersuchung des Interatomaren Coulomb-Zerfalls in schwach gebundenen Systemen* (Max-Planck-Institut für Plasmaphysik, 2007), Ph. D. thesis.

[84] U. Hergenhahn, A. Kolmakov, M. Riedler, A. R. B. de Castro, O. Löfken, and T. Möller, Chem. Phys. Lett. **351**, 235 (2002).

[85] P. Wiethoff, H.-U. Ehrke, D. Menzel, and P. Feulner, Phys. Rev. Lett. **74**, 3792 (1995).

[86] K. Schulz, M. Domke, R. Püttner, A. Gutiérrez, G. Kaindl, G. Miecznik, and C. H. Greene, Phys. Rev. A **54**, 3095 (1996).

[87] M. Joppien, *Lumineszenzspektroskopische Untersuchung der elektronischen Anregungen von Helium- und Neon-Clustern* (Hamburg Universität, 1994), Ph.D. Thesis.

[88] V. Averbukh, I. B. Muller, and L. S. Cederbaum, Phys. Rev. Lett. **93**, 263002 (2004).

[89] S. Barth, S. Marburger, S. Joshi, V. Ulrich, O. Kugeler, and U. Hergenhahn, Phys. Chem. Chem. Phys. **8**, 3218 (2006).

[90] S. Scheit, V. Averbukh, H.-D. Meyer, J. Zobeley, and L. S. Cederbaum, J. Chem. Phys. **124**, 154305 (2006).

[91] G. Kaindl, T.-C. Chiang, D. E. Eastman, and F. J. Himpsel, Phys. Rev. Lett. **45**, 1808 (1980).

[92] M. Lundwall, M. Tchaplyguine, G. Öhrwall, A. Lindblad, S. Peredkov, T. Rander, S. Svensson, and O. Björneholm, Surf. Sci. **594**, 12 (2005).

[93] M. Lundwall, A. Lindblad, G. Öhrwall, M. Tchaplyguine, S. Svensson, and O. Björneholm, J. Phys. B: At. Mol. Opt. Phys. **126**, 214706 (2007).

[94] G. Öhrwall, R. F. Fink, M. Tchaplyguine, L. Ojamae, M. Lundwall, R. R. T. Marinho, A. N. de Brito, S. L. Sorensen, M. Gisselbrecht, R. Feifel, et al., J. Chem. Phys. **123**, 054310 (pages 10) (2005).

[95] F. P. Larkins and A. Lubenfeld, J. Elec. Spec. Rel. Phen. **15**, 137 (1979).

[96] C.-M. Liegener, Phys. Stat. Sol. (b) **156**, 441 (1989).

[97] C.-M. Liegener and R. Chen, J. Chem. Phys. **88**, 2618 (1988).

[98] W. Pokapanich, H. Bergersen, R. R. T. Marinho, A. Lindblad, I. Bradeanu, S. Legendre, A. Rosso, M. Tchaplyguine, S. Svensson, O. Björneholm, et al. (2008), *in manuscript*.

[99] G. Elert, *The physics factbook* (2002), URL `http://hypertextbook.com/facts/AngieYee.shtml`.

[100] S. D. Stoychev, A. I. Kuleff, F. Tarantelli, and L. S. Cederbaum, J. Chem. Phys. **128**, 014307 (2008).

[101] J. Farges, M. F. de Feraudy, B. Raoult, and G. Torchet, Surf. Sci. **106**, 95 (1981).

[102] J. Farges, M. F. de Feraudy, B. Raoult, and G. Torchet, J. Chem. Phys. **78**, 5067 (1983).

[103] J. H. Fendler, Chem. Mater. **13** (2001).

[104] A. Venkateshan, R. Singh, and K. F. Poole, Advanced Thermal Processing of Semiconductors, RTP 2007. 15th International Conference on pp. 65–69 (2007).

[105] A. C. Templeton, W. P. Wuelfing, and R. W. Murray, Acc. Chem. Res. **33**, 27 (2000).

[106] H. Wabnitz, L. Bittner, A. R. B. de Castro, R. Dohrmann, P. Gurtler, T. Laarmann, W. Laasch, J. Schulz, A. Swiderski, K. von Haeften, et al., Nature **420**, 482 (2002).

[107] I. Last and J. Jortner, **106**, 10877 (2002).

[108] M. Lundwall, *Rare-gas clusters studied by electron spectroscopy – structure of heterogeneous clusters and effects of electron scattering on auger decay*, Acta Universitatis Upsaliensis, Uppsala (2007), Ph. D. Thesis.

[109] P. A. Brühwiler, O. Karis, and N. Mårtensson, Rev. Mod. Phys. **74**, 703 (2002).

[110] J. Schnadt, A. P. Brühwiler, L. Patthey, J. N. O'Shea, S. Södergren, M. Odelius, R. Ahuja, O. Karis, M. Bässler, P. Persson, et al., Nature **418**, 620 (2002).

[111] A. Föhlisch, P. Feulner, F. Hennies, A. Fink, D. Menzel, D. Sanchez-Portal, P. M. Echenique, and W. Wurth, Nature **436**, 373 (2005).

Acta Universitatis Upsaliensis

Digital Comprehensive Summaries of Uppsala Dissertations from the Faculty of Science and Technology 393

Editor: The Dean of the Faculty of Science and Technology

A doctoral dissertation from the Faculty of Science and Technology, Uppsala University, is usually a summary of a number of papers. A few copies of the complete dissertation are kept at major Swedish research libraries, while the summary alone is distributed internationally through the series Digital Comprehensive Summaries of Uppsala Dissertations from the Faculty of Science and Technology. (Prior to January, 2005, the series was published under the title "Comprehensive Summaries of Uppsala Dissertations from the Faculty of Science and Technology".)

Distribution: publications.uu.se
urn:nbn:se:uu:diva-8463

ACTA
UNIVERSITATIS
UPSALIENSIS
UPPSALA
2008